Rheological Studies, Time Dependency and Orientation of Nematic Lyotropic Liquid Crystal Gels

Von der Fakultät Chemie der Universität Stuttgart

zur Erlangung der Würde eines Doktors der

Naturwissenschaften (Dr. rer. nat.) genehmigte Abhandlung

Vorgelegt von

Max Dombrowski

Aus Rosenheim

Hauptberichter:	Prof. Dr. Cosima Stubenrauch
Mitberichter:	Prof. Dr. Claudia Schmidt
Prüfungsvorsitzender:	Prof. Dr. Jens Brockmeyer

Tag der mündlichen Prüfung

15.07.2025

Institut für Physikalische Chemie

der Universität Stuttgart

2025

Acknowledgement

First and foremost, I would like to express my deepest gratitude to my supervisor, Prof. Dr. Cosima Stubenrauch, for the opportunity to pursue this PhD thesis under her guidance. Her insightful supervision, continuous support, encouragement and the opportunity to participate in numerous national and international conferences have been instrumental to my academic and personal development.

I am also thankful to Prof. Dr. Claudia Schmidt for serving as the second examiner of my thesis, and to Prof. Dr. Jens Brockmeyer for kindly assuming the role of chair during my defense.

I would like to extend my sincere thanks to Dr. Philippe J. Mésini for his generous provision of the gelators used in this work and for his kind hospitality during my research stays in Strasbourg.

I am especially grateful to Michael Herbst for his close collaboration throughout the course of this research. My thanks also go to Diana Sottmann for her consistent support in the laboratory, and to Dr. Natalie Preisig for recording the FFEM images.

Finally, I would like to thank all the members of the Stubenrauch, Sottmann and Gießelmann groups for the enjoyable times and supportive environment.

Above all, I am grateful to my mother for her support during my studies and PhD thesis.

Table of Contents

Abbreviations and Symbols

Numerical and Latin

12-HOA	12-hydroxy-octadecanoic acid
1D	one dimensional
3D	three dimensional
A	area
a_0	effective head group area
a_C	area of the hydrophobic part
BHPB-10	3,5-bis-(5-hexylcarbamoyl-pentoxy)-benzoate acid decyl ester
BHPB-13	3,5-bis-(5-hexylcarbamoyl-pentoxy)-benzoate acid tridecyl ester
BHPB-6	3,5-bis-(5-hexylcarbamoyl-pentoxy)-benzoate acid hexyl ester
BHPB-*n*	3,5-bis-(5-hexylcarbamoyl-pentoxy)-benzoate acid *n*-alkyl ester
$C_{10}E_4$	tetraethylene glycol monodecyl ether
$C_{12}E_7$	heptaethylene glycol monododecyl ether
$C_{12}E_8$	octaethylene glycol monododecyl ether
$C_{12}G_1$	lauryl glucoside
C_{14}TAB	*N*,*N*,*N*-trimethyl-1-tetradecylammonium bromide
CAPB	cocamidopropyl betaine
CDEAB	*N*,*N*-dimethyl-*N*-ethyl-1-hexadecylammonium bromide
cmc	critical micelle concentration
d	days
D_2O	deuterated water
DBC	*N*,*N´*-dibenzoyl-L-cystine
DBS	1,3:2,4-dibenzylidene-D-sorbitol

d*t*	time
d*x*	displacement
F	force
FFEM	freeze fracture electron microscopy
G	shear modulus
$G^{'}$	storage modulus
$G^{''}$	loss modulus
G^{*}	complex shear modulus
h	(a) distance between the two plates; (b) hour
H_2O	water
HG1	tris-amido-cyclohexane derivative
I_1	cubic phase
I_2	inverse cubic phase
L_1	micellar isotropic phase
l_C	length of the hydrocarbon chain
LCE	liquid crystal elastomer
LLC	lyotropic liquid crystal
LMWG	low molecular weight gelator
LVE	linear viscoelastic region
L_α	lamellar phase
m	mass
n	direction of the applied magnetic field
N_C	calamitic nematic phase
N_D	discotic nematic phase

P	(a) packing parameter; (b) polarizer
POM	polarized optical microscopy
S	order parameter
SaFiNs	self-assembled fibrillar networks
SDS	sodium dodecyl sulfate
t	time
T	temperature
T_{Cl}	clearing temperature
$T_{nem\text{-}iso}$	nematic to isotropic transition temperature
$T_{sol\text{-}gel}$	sol-gel transition temperature
v	velocity of the sample
V_1	bicontinuous phase
wt%	weight percent

Greek

γ	shear strain
$\dot{\gamma}$	shear rate
γ_l	limiting strain amplitude
γ_{max}	shear strain amplitude
δ	phase shift
η	(a) shear viscosity; (b) gelator mass fraction
μ	surfactant mass fraction
μ_{bin}	surfactant mass fraction of the binary CDEAB system
μ_{ter}	surfactant mass fraction of the ternary C_{14}TAB system
σ	surfactant-to-cosurfactant ratio

τ	shear stress
τ_{max}	shear stress amplitude
φ	deflection angle

Abstract

Lyotropic liquid crystal gels (LLC gels) are versatile materials combining the anisotropy of a lyotropic liquid crystal (LLC) with the rigidity of a gel. In this work, we studied the calamitic nematic N_C phase of two LLC systems, namely of the binary system H_2O – *N*,*N*-dimethyl-*N*-ethyl-1-hexadecylammonium bromide (CDEAB) and of the ternary system H_2O – *N*,*N*,*N*-trimethyl-1-tetradecylammonium bromide (C_{14}TAB) – *n*-decanol. We gelled the N_C phases using the low molecular weight gelator (LMWG) 3,5-bis-(5-hexylcarbamoyl-pentoxy)-benzoate acid *n*-alkyl ester (BHPB-*n*, *n* = 6, 10, 13). The two systems were chosen because of the similarities of the two surfactants, one of which requires the cosurfactant *n*-decanol to form the N_C phase.

In preliminary studies, we measured the phase diagram of the ternary C_{14}TAB system to determine the boundaries of the N_C phase and to select an optimal surfactant-to-cosurfactant ratio. In addition, we tested the three gelators for compatibility with our N_C phases and selected BHPB-6 for the following studies. The gelator was synthesized in multiple batches. We observed non-negligible, batch-dependent differences of the gelator's properties: we used rheology to compare the batches. By studying the gelation process of the LLC gels, we discovered that the gelation occurs on several time scales. Firstly, the initial gelation process, which occurs within the first 20 h, and secondly, a longer gelation process that can take up to 30 d. Additionally, the two LLC systems behave differently during gelation. Freeze fracture electron microscopy (FFEM) was used to observe the structure of the gel fibers at different stages of the gelation process. The addition of the cosurfactant *n*-decanol, which is a good solvent for the gelator, in the ternary C_{14}TAB system causes the gel to form much more slowly than in the binary CDEAB system. The development of the N_C phase is also hindered because the cosurfactant needed to form the N_C phase is used to solubilize the gelator. Oriented samples of the two LLC gels were prepared by cooling the samples to room temperature in a magnetic field. The orientation of the N_C phases was confirmed by polarized optical microscopy (POM). The alignment of the gel network was also studied using microscopy. Finally, we investigated the templating effect of the aligned gel networks of the LLC gels by inducing a reversible phase transition from the nematic N_C phase to the isotropic L_1 phase and back while not destroying the gel. We found that the N_C phase was restored in the same orientation as before, proving that the aligned gel network is capable of acting as a template.

Zusammenfassung

Lyotrope Flüssigkristallgele sind vielseitige Materialien, die die Anisotropie eines lyotropen Flüssigkristalls (LLC) mit der Steifigkeit eines Gels kombinieren. In dieser Arbeit haben wir die kalamitisch nematische N_C-Phase von zwei LLC-Systemen untersucht, nämlich des binären Systems H_2O - *N*,*N*-Dimethyl-*N*-ethyl-1-hexadecylammoniumbromid (CDEAB) und des ternären Systems H_2O - *N*,*N*,*N*-Trimethyl-1-tetradecylammoniumbromid (C_{14}TAB) - *n*-Decanol. Wir gelierten die N_C-Phasen mit dem niedermolekularen Gelator (LMWG) 3,5-Bis-(5-hexylcarbamoyl-pentoxy)-benzoat-säure-*n*-alkylester (BHPB-*n*, *n* = 6, 10, 13). Die beiden Systeme wurden aufgrund der Ähnlichkeiten der beiden Tenside ausgewählt, von denen eines das Cotensid *n*-Decanol zur Bildung der N_C-Phase benötigt.

In Vorstudien haben wir das Phasendiagramm des ternären C_{14}TAB-Systems gemessen, um die Grenzen der N_C-Phase zu bestimmen und ein optimales Verhältnis von Tensid zu Cotensid auszuwählen. Darüber hinaus testeten wir die drei Gelatoren auf ihre Kompatibilität mit unseren N_C-Phasen und wählten BHPB-6 für die folgenden Studien aus. Der Gelator wurde in mehreren Chargen synthetisiert. Wir beobachteten nicht vernachlässigbare, chargenabhängige Unterschiede in den Eigenschaften des Gelators: Wir verwendeten Rheologie, um die Chargen zu vergleichen. Bei der Untersuchung des Gelierungsprozesses der LLC-Gele stellten wir fest, dass die Gelierung auf mehreren Zeitskalen erfolgt. Erstens der anfängliche Gelierungsprozess, der innerhalb der ersten 20 Stunden stattfindet, und zweitens ein längerer Gelierungsprozess, der bis zu 30 Tage dauern kann. Mit Hilfe der Gefrierbruch-Elektronenmikroskopie (FFEM) wurde die Struktur der Gelfasern in verschiedenen Stadien des Gelierungsprozesses beobachtet. Die Zugabe des Cotensids *n*-Decanol, dass ein gutes Lösungsmittel für den Gelator ist, führt im ternären C_{14}TAB-System zu einer wesentlich langsameren Gelbildung als im binären CDEAB-System. Die Entwicklung der N_C-Phase wird auch dadurch behindert, dass das zur Bildung der N_C-Phase benötigte Cotensid zur Solubilisierung des Gelators verwendet wird. Orientierte Proben der beiden LLC-Gele wurden durch Abkühlen der Proben auf Raumtemperatur in einem Magnetfeld hergestellt. Die Orientierung der N_C-Phasen wurde durch polarisierte optische Mikroskopie (POM) bestätigt. Die Ausrichtung des Gelnetzwerks wurde auch mit Hilfe der Mikroskopie untersucht. Schließlich untersuchten wir den Template-Effekt der ausgerichteten Gel-Netzwerke der LLC-Gele, indem wir einen reversiblen Phasenübergang von der nematischen N_C-Phase zur isotropen L_1-Phase und zurück herbeiführten, ohne das Gel zu zerstören. Wir fanden heraus, dass die N_C-Phase in der gleichen Orientierung wie zuvor

wiederhergestellt wurde, was beweist, dass das ausgerichtete Gel-Netzwerk in der Lage ist, als Vorlage zu dienen.

1 Introduction

1.1 Motivation

Orthogonal and non-orthogonal self-assembly

Orthogonal self-assembly refers to the simultaneous formation and coexistence of two distinct self-assembled structures. The term was introduced by Laibinis *et al*. who used it to describe the selective adsorption of two different adsorbates in the same solution onto a substrate with two different materials at the surface [Lai89]. Orthogonal self-assembly, however, is not limited to the surface but was observed in bulk systems as well [Hu14, Kum14]. Perhaps the most well-known orthogonally self-assembled system is the cell. The self-assembled phospholipid bilayer of the cell surrounds other self-assembled structures such as the cytoskeleton, which is a three-dimensional scaffold providing the mechanical stability. In biological systems self-assembly occurs on highly selective non-covalent binding sites which do not interfere with each other directly [Hof05]. When it comes to gelling complex fluids in general or liquid crystals in particular it is important to know that orthogonal self-assembly describes a very special case with most systems not belonging to this type of structure. Note that throughout this thesis the term orthogonal self-assembly is not reserved for systems with no interaction between their self-assembling entities but is also used for systems with weak interactions if these interactions do not change the general pattern. Stubenrauch and Gießelmann presented in a review article examples of several gelled complex fluids, their applications and whether or not they form via orthogonal self-assembly [Stu16]. In the following three examples of orthogonal and non-orthogonal self-assembled systems which contain a surfactant and a gelator as self-assembling entities are discussed. (1) Laupheimer *et al.* investigated the microstructure of the bicontinuous microemulsion H_2O – tetraethylene glycol monodecyl ether ($C_{10}E_4$) – *n*-decane gelled with 12-hydroxy-octadecanoic acid (12-HOA). Since the microemulsion coexisted with the gel fibers of 12-HOA without significant interference the system was described as orthogonal self-assembled system [Lau14]. (2) Xu *et al*. observed that the introduction of 12-HOA to a lamellar L_α phase of D_2O – $C_{10}E_4$ – *n*-decane shifts the phase boundaries of the lyotropic liquid crystal to lower temperatures but does not change the general pattern. However, the gelfibers experience changes, with their shape changing from twisted (in a binary gel with *n*-decane) to not twisted in the L_α phase. Because of this change it is questionable whether this lyotropic liquid crystal gel can be referred to as orthogonally self-assembled [Xu15]. (3) The gelation of the L_α phase and the hexagonal H_1 phase of H_2O – heptaethylene glycol monododecyl

ether ($C_{12}E_7$) by Steck *et al*. with the gelator 12-HOA is a good example of non-orthogonal self-assembly, *i.e.* of how one self-assembled system influences another. 12-HOA strongly influences the phase behavior which indicates that it functions as a cosurfactant in this system: 12-HOA destabilizes the H_1 phase, while the L_α phase is stabilized [Ste18]. It is noteworthy that in all systems the gelator 12-HOA was used which shows how different the interactions between the gelator and the complex fluid can be.

Lyotropic liquid crystals

Lyotropic liquid crystals are mixtures of surfactants and solvents, most often water, which form in specific temperature and concentration ranges. The surfactant molecules can self-assemble into anisotropic micelles, which are the basic unit of the birefringent mesophases. If the basic unit is isotropic, the resulting phase is referred to as plastic crystal instead. The most common lyotropic liquid crystal mesophases are (a) the H_1 phase, characterized by its cylindrical micelles, two-dimensional positional order, and high viscosity and (b) the L_α phase which is characterized by its surfactant bilayers, one-dimensional positional order and a lower viscosity than the H_1 phase. Less known lyotropic liquid crystals are the columnar nematic N_C phase and the discotic nematic N_D phase which possess only an orientational order and no positional order. Nematic phases can be viewed as intermediates between the structured H_1 and L_α phase and the micellar L_1 phase [Hen84]. Nematic phases are interesting candidates for lyotropic liquid crystal gels as they possess an orientational order as well as the fluidity of a liquid. We will come back to this point further below.

Gels

The term ‘gel’ has been used for a wide variety of systems not all of which being gels [Alm93]. Gels can be defined as cross-linked diluted systems which exhibit no flow in the steady-state [Fer80]. The solvent is the major component with up to, and in some cases even above, 99 wt% with the gelator taking up the rest. Gelators can be subdivided into many categories depending on the nature of the gelling process or the type of solvent. Gels can be classified into physical and chemical gels. In physical gels the gelator forms one- to three-dimensional structures via non-covalent interactions, *i.e.* hydrogen bonding, π-π stacking, van der Waals interactions etc., and the formation of physical gels is reversible. In chemical gels the gel is obtained via the crosslinking of polymer chains or polymerization of monomers. The second way to divide gelators is into hydro- and organogelators. Hydrogelators gel aqueous solutions, while organogelators gel organic solvents [Wei06, Du15].

Lyotropic liquid crystal gels

Lyotropic liquid crystal gels is a new class of gels. Lyotropic liquid crystals are complex fluids and thus the resulting gel cannot be classified as hydrogel or organogel. The difficulty one encounters if one wants to gel an LLC lie in the fact that the interactions between gelators and surfactants are unknown and thus unpredictable, e.g. gelators that orthogonally self-assemble in one solvent may be unable to do so in another. In the gelation of the L_α phase and the H_1 phase of the system H_2O – $C_{12}E_7$ with the gelator 12-hydroxyoctadecanoic acid (12-HOA), the gelator also acts as a cosurfactant. The addition of 12-HOA results in the transition of the H_1 phase to the L_α phase, while the L_α phase required more gelator to form a gel [Ste18]. Using the same gelator one obtains similar results for the gelation of the N_C, N_D, H_1, and L_α phases of the ternary system H_2O – sodium dodecyl sulfate (SDS) – *n*-decanol by Dieterich *et al*. The gelator 12-HOA, functioning as a cosurfactant, transforms both nematic phases to a lamellar phase, while the hexagonal phase becomes an isotropic phase [Die19a]. However, there are examples of a successful gelation of lyotropic liquid crystals. Steck *et al*. were able to gel the L_α phase and the H_1 phase of the system H_2O – $C_{12}E_7$ with 1,3:2,4-dibenzylidene-D-sorbitol (DBS). The phase boundaries are only slightly different compared to the ungelled system, and rheological studies showed the solid-like viscoelastic behavior expected for a gel [Ste19a]. The gelation of a nematic phase was reported soon after by Dieterich *et al*. [Die21]. They successfully gelled the nematic N_C and N_D phases of the binary system H_2O – *N*,*N*-dimethyl-*N*-ethyl-1-hexadecylammonium bromide (CDEAB) and of the ternary systems H_2O – CDEAB – *n*-decanol and H_2O – SDS – *n*-decanol. They used the gelators DBS, tris-amido-cyclohexane derivative (HG1), and *N*,*N´*-dibenzoyl-L-cystine (DBC), respectively. The gelation of lyotropic nematic phases opens up broad new avenues to stimuli-responsive water-based materials. Gelled lyotropic nematic phases could possibly be used analogous to thermotropic liquid crystal elastomers (LCE) as stimuli responsive actuators. For example, weakly crosslinked LCE particles synthesized by Ohm *et al*. were able to undergo a reversible change in shape during the phase transition from nematic to isotropic [Ohm11]. The LCE particles became anisotropic after flow-alignment during microfluidic synthesis, and since the anisotropy of the polymer network was coupled to the anisotropy of the liquid crystal mesogen, the phase transition of the liquid crystal induced a change in the macroscopic shape of the particle. The alignment of the gel network in the liquid crystal state is crucially important for the shape response. Lyotropic liquid crystal gels are expected to respond to changes in the liquid crystal order similarly to their thermotropic LCE counterparts. Since the order of lyotropic liquid crystals can be triggered by more external stimuli compared to thermotropic liquid crystals, the macroscopic

shape of the LLC gel should be responsive to any stimulus that can modify or destroy the liquid crystalline order, *e.g.* temperature, concentration, pH-value or solvent composition.

1.2 Task Description

To obtain and characterize aligned nematic LLC gels the work is divided into three principal tasks, namely the formulation and characterization of nematic LLC gels (Section 3.1), the influence of time on the structure and properties of the gel network (Section 3.3), and the orientation of the gelled nematic LLC gels (Section 3.4).

The first task deals with the formulation of tailored nematic LLC gels where the fiber network forms in an anisotropic matrix provided by the nematic liquid . To begin with, a nematic lyotropic liquid crystal was selected with a nematic to isotropic transition temperature of $T_{\text{nem-iso}} \geq 30°C$. The lyotropic liquid crystal systems selected were H_2O – *N*,*N*-dimethyl-*N*-ethyl-1-hexadecylammonium bromide (CDEAB) and H_2O – *N*,*N*,*N*-trimethyl-1-tetradecylammonium bromide (C_{14}TAB) – *n*-decanol, a binary and ternary system, respectively. Both systems can form nematic N_C and N_D phases. The columnar nematic N_C phase, which this thesis focusses on, is bordered by the isotropic L_1 phase at lower surfactant concentrations and by the H_1 phase at higher surfactant concentrations. With increasing temperature, the N_C phase transforms into the L_1 phase at lower and into the H_1 phase at higher surfactant concentrations. The organogelators 3,5-bis-(5-hexylcarbamoyl-pentoxy)-benzoate acid *n*-alkyl ester BHPB-*n* (*n* = 6, 10, 13) were selected and the optimum concentration was to be determined. The influence of the gelator on the phase behavior was to be studied via visual inspection and polarized optical microscopy (POM). Freeze fracture electron microscopy (FFEM) was to be used to study the size, shape and alignment of the gel fibers within the LLC gels. The rheology of the nematic LLC gels was to be studied to determine the amount of gelator necessary to form a gel and to quantify the mechanical strength of the LLC gel. In order to obtain a macroscopically aligned LLC gel, the alignment of the LLC needs to be completed before the gelation has progressed significantly, so that the LLC serves as soft template for the formation of an anisotropic gel network. The preferred methods to align liquid crystals are the use of a magnetic or an electric field. The degree of alignment was to be determined via POM and FFEM studies. Finally, the memory effect of the aligned samples was to be tested. Firstly, by inducing a reversible phase transition of a nematic LLC to an isotropic LLC and back in a sample with an aligned gel network and initially aligned LLC phase it was to be determined whether the reforming nematic LLC retains its alignment after the phase transition. Secondly, the influence

of the isotropic LLC phase on the aligned gel network and whether the gel network retains its alignment throughout the phase transitions was to be determined.

2 Theoretical Background

In this chapter the two parent systems of the LLC gel, namely lyotropic liquid crystals and molecular gels, will be introduced, beginning with an overview of lyotropic liquid crystals in Section 2.1, molecular gels in Section 2.2 and rheology of gels in Section 2.3.

2.1 Lyotropic Liquid Crystals

Liquid Crystals

Liquid crystals were accidentally discovered by the Austrian botanist and chemist Friedrich Reinitzer [DiL19]. While studying cholesterols extracted from plants he observed that cholesteryl benzoate exhibited two melting points that were associated with birefringence and vivid iridescent color changes. Otto Lehmann, who studied similar materials and was the first to combine the hot stage with a polarized optical microscope, referred to them as “fliessende Krystalle” (*i.e.* flowing crystal) in a paper in 1889 [DiL19]. This opened a new chapter in research on materials that are now known as liquid crystals. Liquid crystals can be seen as an intermediate phase that exhibits properties of both a liquid and a crystal [Net05]. The differences between a liquid and a crystal can be most accurately described by the degree of order with which the molecules are arranged. The degrees of order can be subdivided into positional and orientational order [Moh03]. Positional order refers to the extent to which molecules or groups of molecules, on average, show translational symmetry. Orientational order refers to the extent to which the molecules or groups of molecules align along a specific direction on a long-range basis. Crystals possess an orientational order as well as a three-dimensional positional order, whereas a regular liquid possesses neither orientational nor positional order. Liquid crystals, however, possess at least an orientational order and specific mesophases also possess positional order (Figure 2.1).

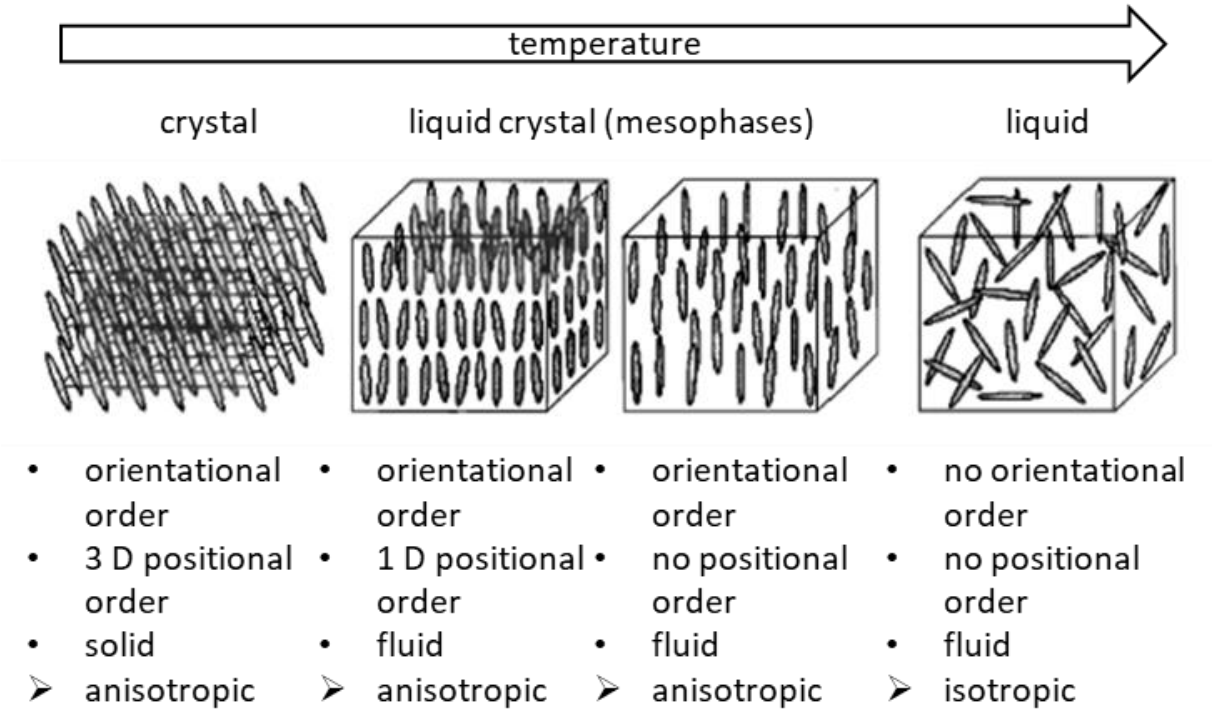

Figure 2.1: Schematic drawings of the positional and orientational order of a crystal (left), a smectic liquid crystal (center left), a nematic liquid crystal (center right), and an isotropic liquid (right) [Moh03]. Reproduced with permission from Springer Nature.

All liquid crystal phases have long-range orientational order, the degree of which can be quantified by the orientational order parameter S [Die19b]. Even in phases that possess an orientational order along a preferred direction, such as the nematic and the smectic phase, the molecules or aggregates will not be oriented perfectly parallel to the director, but have certain tilt angles θ. The order parameter for cylindrically symmetric molecules is defined as

$$S = \frac{1}{2}\langle 3cos^2\theta - 1\rangle. \qquad (2.1)$$

Liquid crystals can be divided into two categories, namely thermotropic and lyotropic liquid crystals, which have different building blocks, more commonly referred to as mesogens [Die19b]. In thermotropic liquid crystals the mesogens are single molecules that are either cylindrical or disk-like. In lyotropic liquid crystals the mesogens are micelles formed by the self-aggregation of surfactants. Depending on the surfactant concentration and the temperature, anisotropic cylindrical or disk-like micelles as well as bilayers can form [Net05] (Figure 2.2).

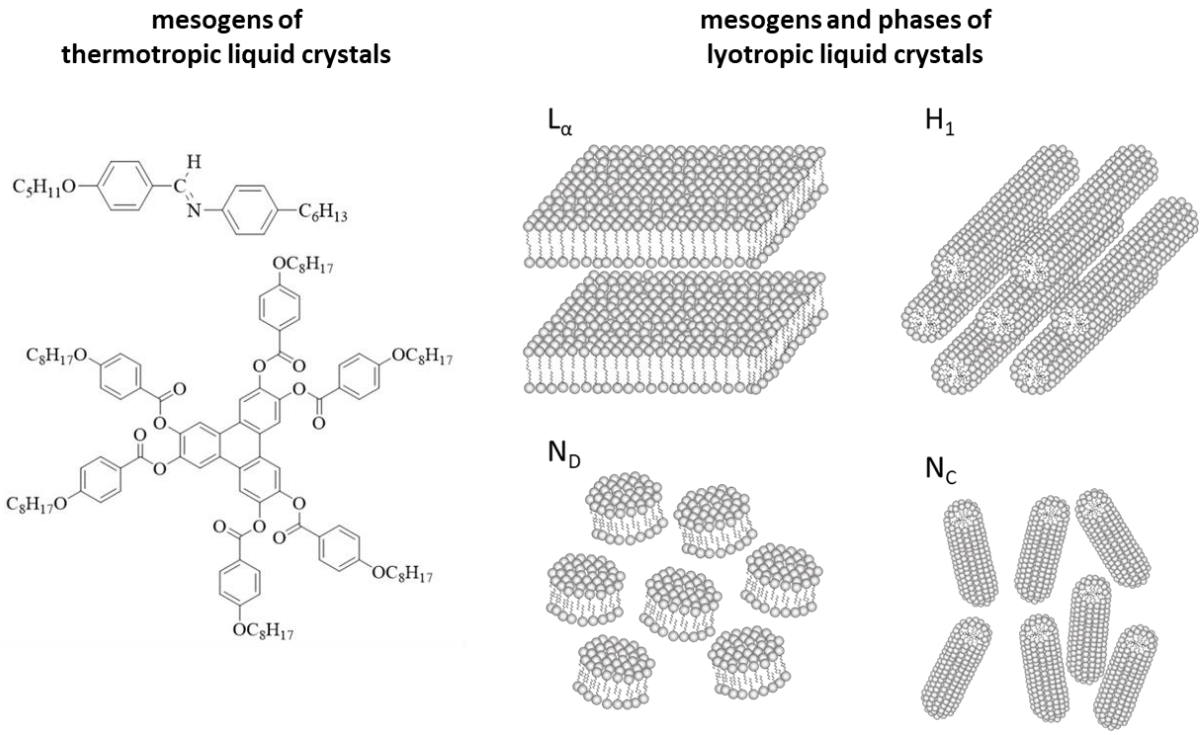

Figure 2.2: Mesogens of thermotropic liquid crystals (left) and lyotropic liquid crystals (right). For thermotropic liquid crystals, the mesogens consist of molecules that are shaped anisotropically, mostly rod-like or disk-like. For lyotropic liquid crystals, the mesogens are formed by the self-aggregation of surfactants. The three-dimensional arrangement of the mesogens leads to the respective mesophases. Depicted are the lamellar L_α phase, the hexagonal H_1 phase, the discotic nematic N_D phase, and the columnar nematic N_C phase.

In both thermotropic and lyotropic liquid crystals the mesogen must be anisotropic. Isotropic refers to materials that show uniform behavior in all directions, while anisotropic refers to materials that exhibit direction-dependent properties. In thermotropic liquid crystals the phase transitions are induced by temperature. In lyotropic liquid crystals on the other hand, while also undergoing temperature induced phase transitions, the phase transitions are dependent on the solvent concentration (from Greek, lyo = to dissolve) [Net05].

Lyotropic Liquid Crystals

Lyotropic liquid crystals can form in either binary mixtures of surfactant and water or ternary mixtures. In the latter case the system consists of surfactant, cosurfactant and water or of surfactant, oil and water. In this work only binary systems and ternary systems consisting of surfactant, cosurfactant and water will be studied. Surfactants, which is an acronym for surface active agents, consist of a non-polar hydrophobic part (tail) and a polar hydrophilic part (head group). Surfactants are divided into four categories, namely non-ionic, zwitterionic, anionic, and cationic depending on the charge of their head group [Net05]. Non-ionic surfactants have

head groups such as sugars (*e.g.* lauryl glucoside $C_{12}G_1$) or polyethylene oxides (*e.g.* octaethylene glycol monododecyl ether $C_{12}E_8$). The head groups of zwitterionic surfactants have both negatively and positively charged functional groups. An example of a zwitterionic surfactant is cocamidopropyl betaine (CAPB). For anionic surfactants the head group can be comprised of a sulfate, sulfonate, phosphate, carboxylate, etc. The most prominent anionic surfactant is sodium dodecyl sulfate (SDS) which is used in many industrial and home applications. The head group of cationic surfactants consist *e.g.* of amines or quaternary ammonium cations. An example of cationic surfactant which is used within this work is *N*,*N*,*N*-trimethyl-1-tetradecylammonium bromide (C_{14}TAB). Listed below are the examples of each category (Figure 2.3).

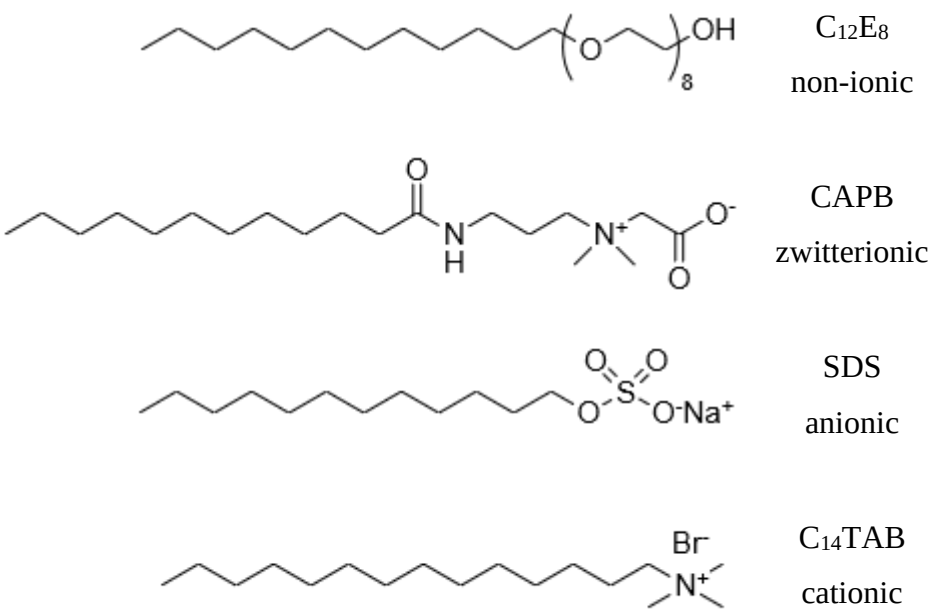

Figure 2.3: Classifications of different surfactants according to their head group with examples. Non-ionic surfactant: Octaethylene glycol monododecyl ether ($C_{12}E_8$), zwitterionic surfactant: cocamidopropyl betaine (CAPB), anionic surfactant: sodium dodecyl sulfate (SDS), cationic surfactant: *N*,*N*,*N*-trimethyl-1-tetradecylammonium bromide (C_{14}TAB).

As the acronym surface active agent suggests, surfactants accumulate at the surface if added to water. In low concentrations the surfactants accumulate at the water/air interface with the hydrophilic head group being oriented towards water and the hydrophobic tail towards air. Increasing the surfactant concentration saturates the water/air interface and above a certain concentration, the critical micelle concentration (cmc), the surfactant molecules self-aggregate into micelles. The hydrophobic tail point towards the center and the head groups form the outside of the initially spherical micelle. Micelles form due to the hydrophobic effect caused

by the aggregation of non-polar compounds in water. While aggregation is unfavorably from an entropic standpoint it is counterbalanced by the increase of entropy caused by the release of the solvation shell around the hydrophobic tail. The shape of the micelle is determined by two factors, namely the shape of the surfactant and the hydration of the head group. Beginning with the shape of the surfactant, Israelachvili *et al*. introduced the packing parameter *P* in order to predict the shape of micelles [Isr76]

$$P = \frac{v}{a_0 \cdot l_c} = \frac{a_c}{a_0}, \tag{2.2}$$

with ν being the volume of the hydrocarbon chain, a_0 the effective head group area, and l_c the length of the hydrocarbon chain. The packing parameter *P* can be understood as the ratio of the area of the chain to the area of the head group. In case of the head group, the hydration shell must also be considered. At low packing parameters *P* of ≤ 1/3, the surfactant can be seen as a cone which causes the micelle shape to be round. If the packing parameter increases to $1/3 \leq P \geq ½$ the shape of the surfactant is still cone-like but with a smaller difference in effective areas of the chain and the head group. The resulting micelle is cylindrical. If the packing parameter $P = 1$, *i.e.* the surfactant is shaped cylindrically, the surfactants form bilayers. At packing parameters $P > 1$ inverse structures form with the head groups pointing inwards (Figure 2.4).

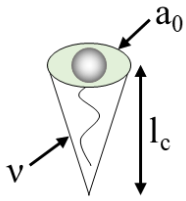

$$P = \frac{v}{a_0 \cdot l_c}$$

Packing parameter P	Surfactant shape	Micelle shape
< 1/3	Cone	Spherical micelle
1/3 – ½	Truncated cone	Cylindrical micelle
½ - 1	Truncated cone	Flexible bilayers, vesicles
~ 1	Cylinder	Planar bilayers
> 1	Inverted cone	Inverted micelles

Figure 2.4: Critical packing parameters *P* of differently shaped molecules and the shape of the respective micelles, with ν being the volume of the hydrocarbon chain, a_0 the effective head group area, and l_c the length of the hydrocarbon chain. Redrawn from [Dut17].

The other factor that influences the shape of the micelle is the surfactant concentration. Above the cmc many phases can be formed such as the cubic I_1, hexagonal H_1, bicontinuous V_1 and lamellar L_α [Net05, Bal69]. At even higher surfactant concentrations inverse structures can form. Lyotropic liquid crystalline structures with index 1 are regular structures with water as

continuous phase, whereas index 2 indicates inverse structures. At high temperatures the lyotropic liquid crystal phases melt into the isotropic L_1 phase. When transitioning into the L_1 phase the system passes a two-phase region where both phases exist simultaneously, except at the critical point where the phase transition is instant. Between two lyotropic liquid crystalline phases are also two-phase regions and at a certain temperature where both lyotropic liquid crystalline phases start the transition into the isotropic L_1 phase there exists a line where all three phases coexist simultaneously called the triple line.

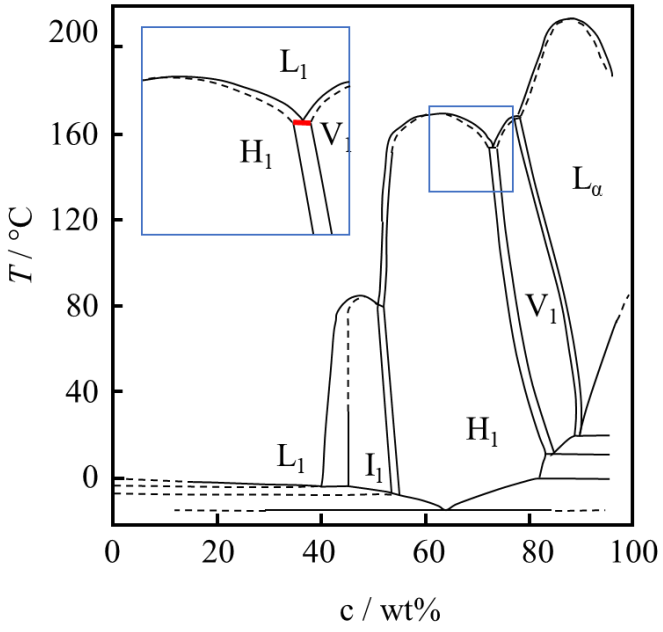

Figure 2.5: Schematic phase diagram of a binary water – surfactant system. The different lyotropic liquid crystalline phases cubic I_1, hexagonal H_1, bicontinuous V_1, and lamellar L_α are depicted at the respective surfactant concentrations and temperatures. One region containing a triple line (red) is highlighted.

A schematic drawing of the cubic I_1 phase, hexagonal H_1 phase, bicontinuous V_1 phase, and the lamellar L_α phase is depicted in Figure 2.5. The cubic I_1 phase is placed between the micellar phase and the hexagonal H_1 phase and consists of spherical micelles which are arranged in a cubic lattice. High viscosity and optical isotropy are characteristic for the cubic I_1 phase. The cubic arrangement is due to the high number of spherical micelles which leads to repulsive forces between the micelles. At higher surfactant concentration the hexagonal H_1 phase forms. It consists of cylindrical micelles with indefinite length that are arranged into a hexagonal lattice. Similar to the cubic I_1 phase, the hexagonal H_1 phase is highly viscous. However, unlike the cubic I_1 phase, it is anisotropic. At higher surfactant concentrations the bicontinuous cubic V_1 phase might be formed, which has two continuous domains one consisting of water and the

other of surfactants aggregated into extended surfactant bilayers. Lastly there is the lamellar L_α phase which forms at higher surfactant concentrations and is characterized by its optical anisotropy and the formation of bilayers separated by water. Nematic N_C and N_D phases are very rare and thus not depicted in Figure 2.5. These phases are present in some binary systems such as H_2O – *N*,*N*-dimethyl-*N*-ethyl-1-hexadecylammonium bromide (CDEAB) (Figure 2.6 left), but they mainly appear in ternary systems consisting of H_2O – surfactant – cosurfactant. Two examples are given in Figure 2.6 (right) and Figure 2.7. In the field of lyotropic liquid crystals the most commonly used cosurfactants are single-chain alcohols. The incorporation of cosurfactants leads to an increase of the average packing parameter and thus to a decrease of the micelles' curvature.

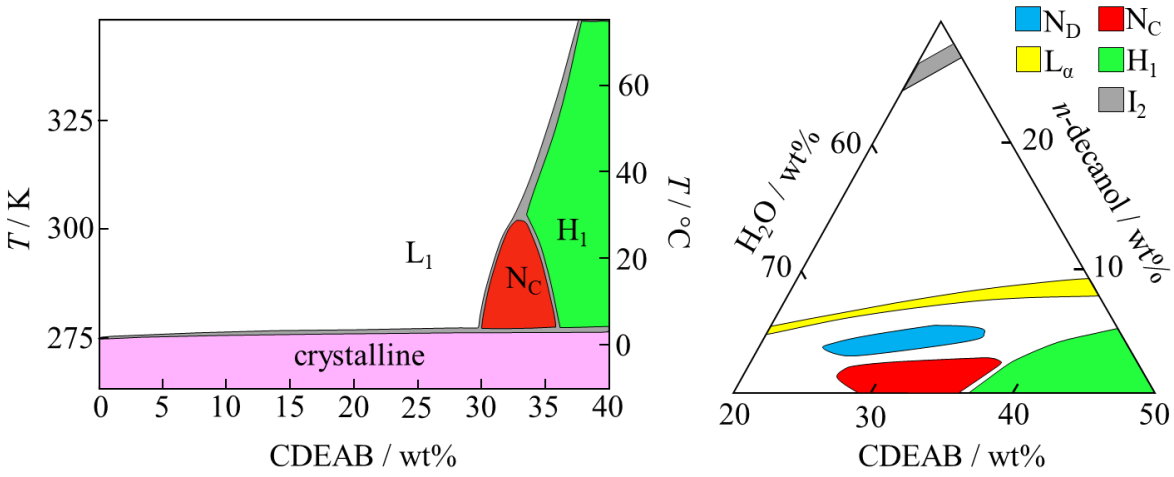

Figure 2.6: Partial phase diagram of the binary system H_2O – CDEAB with the nematic N_C phase between the isotropic L_1 phase and the hexagonal H_1 phase (left), schematically redrawn from [Sch15]. Partial phase diagram of the ternary system H_2O – CDEAB – *n*-decanol recorded at 298 K with the nematic N_C and N_D phases, the lamellar L_α phase, the hexagonal H_1 phase and the inverse cubic I_2 phase, schematically redrawn from [Gör96].

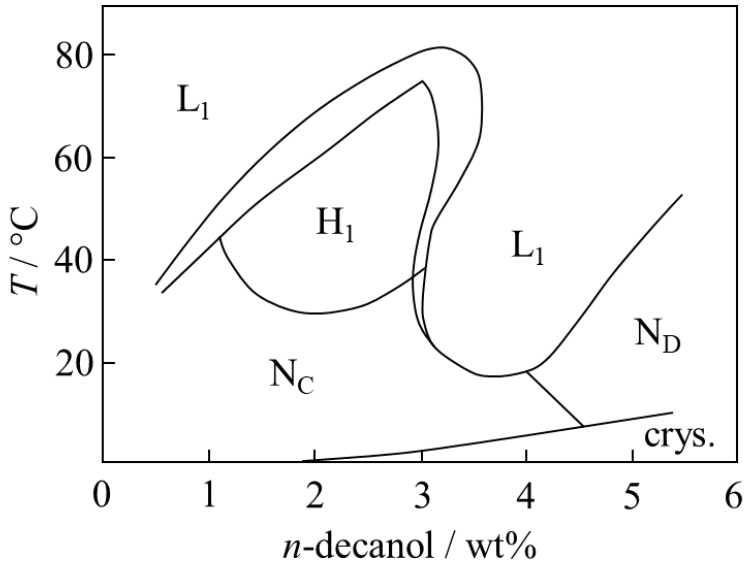

Figure 2.7: Section of the D_2O – $C_{14}TAB$ – *n*-decanol phase diagram with a constant mass ratio of $C_{14}TAB$ (33.85 wt%) and varying amounts of *n*-decanol. Schematically redrawn from [Sau91].

The lyotropic nematic phases consist of micelles with long range orientational order and can be viewed as intermediate phases between the lamellar L_α phase, hexagonal H_1 phase, and the isotropic micellar L_1 phase. They are the result of disruption of phases with translational order by defects, such as breaks in the bilayers of the lamellar Lα phase or breaks in the infinite cylinders of the hexagonal H_1 phase (Figure 2.2). In either case an anisotropic micelle is formed, an oblate disk in the former and a prolate rod in the latter case [Hen84]. The disk-like or discotic nematic N_D phase as well as the rod-like or columnar nematic N_C phase are the lyotropic counterparts to the respective thermotropic nematic phases.

2.2 Molecular Gels

Formation and Structure

The term gel has been historically used to describe a wide variety of systems including inorganic clays, lamellar mesophases, vanadium pentoxide gels, phospholipids, three-dimensional or network polymers and more [Flo74]. The term gel was used to describe characteristics of materials that have gelatinous properties, rather than to substances with set phenomenological characteristics. According to Kramer *et al*. a gel is a soft, solid or solid-like material which consists of two or more components one of which is a liquid that is present in substantial quantity [Alm93]. Gels consist of two continuous phases one of which is a liquid

which is immobilized by the gel network via surface tension and capillary forces [Dra17]. The solvent is the major component with up to 99 wt% of the gel, though the amount varies depending on the solvent and gelator, with some gels requiring only 0.01 wt% gelator while others require 2 wt% or more [Wan10]. The gelator can be small molecules, polymers, inorganic particles or colloidal particle, which aggregate via covalent or non-covalent interactions and form one- to three-dimensional structures. Gels are commonly divided into two categories, depending on the type of interaction responsible for the gel formation, namely chemical and physical gels. Chemical gels are irreversibly crosslinked networks formed via covalent interactions of the gelators. Examples include the polymerization of acrylamides to stabilize lamellar phases [Ily17], and light crosslinking of long chain polymeric gelators [Zha18]. Physical gels are formed via weak interactions such as π-π stacking, van der Waals interactions and hydrogen bond interactions. Examples of physical gels are gels formed by low molecular weight gelators such as 1,3:2,4-dibenzylidene-D-sorbitol (DBS) [San10] or gels formed by natural polymers such as gelatin and agarose [Dja16]. Additionally, gels can also be divided into hydrogels and organogels, depending on whether the solvent is aqueous or organic in nature.

Molecular gels which are formed by low molecular weight gelators (LMWG) have gained increasing interest over the years [Wei06]. These gels form via the self-assembly of LMWGs into so-called self-assembled fibrillar networks. The interactions between the LMWGs are non-covalent in nature, *i.e.* London dispersion forces, π-π stacking and hydrogen bond interactions drive the fiber formation. The solvent of the gel is also very important, since it either promotes or discourages certain interactions of the LMWGs [Wei06]. Above the minimum gelator concentration the fibers entangle which leads to the formation of a network that can immobilize the solvent through surface tension and capillary forces [Dra17]. Unlike for chemical gels, the gelation process in physical gels is reversible *e.g.* by heating. The preparation of molecular gels consists of dissolving the LMWG, generally at concentrations below 2 wt%, heating, and subsequently cooling the solution. Below the sol-gel transition temperature $T_{\text{sol-gel}}$ the gel is formed. $T_{\text{sol-gel}}$ is influenced by the solvent, the type of gelator, and the gelator concentration. With increasing gelator concentration $T_{\text{sol-gel}}$ also increases until it reaches a plateau (Figure 2.8). Christ *et al*. studied the gelator BHPB-10 (Table 2.1) in trans-decalin and showed that while initially transitioning from a gel to a liquid after passing $T_{\text{sol-gel}}$, at sufficiently high gelator concentration a two-phase region occurs between the gel and liquid state [Chr16].

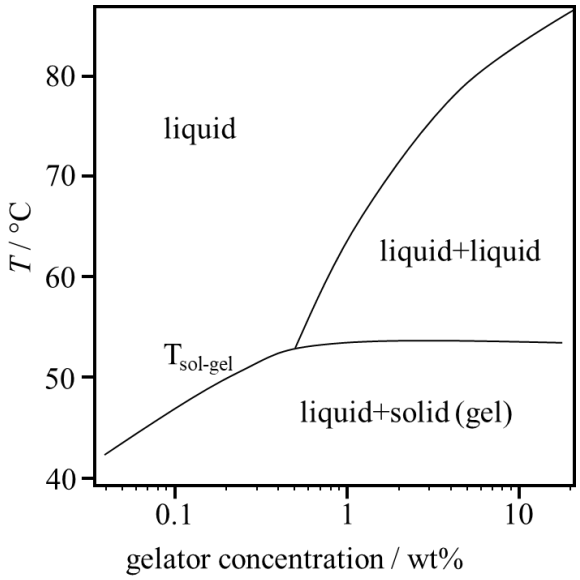

Figure 2.8: Schematic redrawing of the sol-gel transition temperature $T_{sol\text{-}gel}$ of BHPB-10 in trans-decalin as a function of the gelator concentration. Above a certain gelator concentration, the gelator is no longer solubilized in the solvent but phase separates into two liquid phases [Chr16].

The gel formation process can be viewed as a microscopic phase separation, as opposed to a macroscopic phase separation, *i.e.* crystallization. The gelator molecules self-assemble via highly specific interactions that allow for preferential one-dimensional growth. The resulting fibers can have many shapes including tapes, twisted ribbons and tubes. The properties of a gel are dependent on many factors such as the method of gel formation, the temperature it is kept at, the cooling rate, the liquid type, the gelator concentration and the age of the gel [Wei06]. Many molecular gels are not thermodynamically stable and undergo phase separation or changes in the gel network over time.

Examples of LMWGs and the type of fibers they form are shown in Table 2.1. The gelators DBS, 12-hydroxy-octadecanoic acid (12-HOA), and the tris-amido-cyclohexane derivative (HG1) have been used to successfully gel surfactant-based lyotropic liquid crystals [Ste20].

Table 2.1: LMWGs used to gel lyotropic liquid crystals, with schematic drawings of the fiber structure of 12-HOA, DBS, and HG1 and a FFEM image of BHPB-10 in cyclohexane.

LMWG	Molecular structure	Fiber structure	Ref.
12-HOA, 12-hydroxy-octadecanoic acid	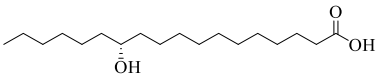	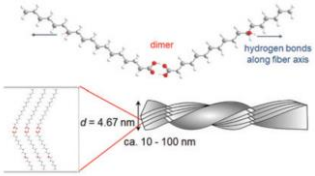	[Ste20]
DBS, 1,3:2,4-dibenzylidene-D-sorbitol	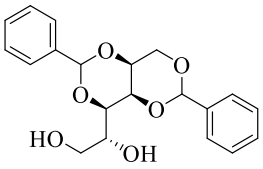		[Ste20]
HG1, tris-amido-cyclohexane derivative	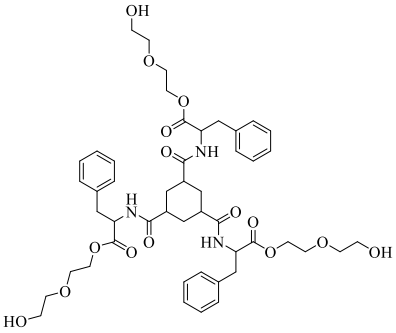	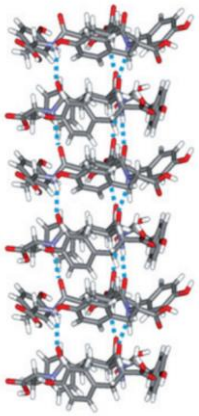	[Bri09]
BHPB-10, 3,5-bis-(5-hexylcarbamoyl-pentoxy)-benzoate acid decyl ester	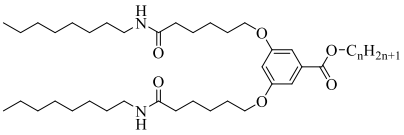	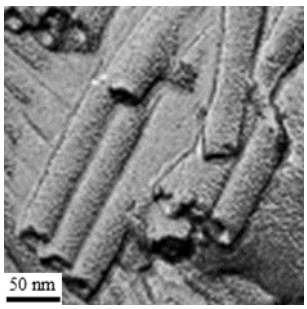	[Sim13]

12-HOA self-assembles into twisted fibers in organic solvents. The interactions between two carboxylic head groups leads to the formation of dimers which, in turn, form the gel fiber via hydrogen bonds between the hydroxy groups. Due to the chirality of 12-HOA the fibers are

twisted. DBS is another organogelator which self-assembles via hydrogen bonds of the hydroxyl groups or via π-π stacking of the phenyl moiety [Ste20]. HG1 is a hydrogelator which self-assembles using hydrogen bonds and hydrophobic interactions. Finally, BHPB-10 is an organogelator which self-assembles into hollow tubes. It contains a phenyl moiety that is capable of π-π-stacking and two amide moieties capable of forming hydrogen bonds. Varying the alkyl chain length of the benzoate acid ester leads to other fiber shapes such as flat ribbons and twisted ribbons [Sim13].

Aging Effects

Gels, in particular supramolecular gels formed by low molecular weight gelators, cannot be considered the simple result of a system that is either present in the sol state or the gel state depending on the conditions [Smi24]. The gel can undergo changes long after the "gel" state is reached. This is due to the kinetically dominated formation of the gel network, which may only occupy a local energetic minimum as opposed to a thermodynamic stable minimum [Yil23, Tan16]. The gel state can thus be considered metastable, i.e. that changes into a more energetically favorable state are possible. This allows the gel to change between multiple states in search of a lower energetic state. These transitions can either be a crystallization of the gelator or a structural change of the gel.

In the former case, the energetically unfavorable gel state makes way for the energetically more favorable crystalline state. In the initially formed fiber network small crystals begin to appear which continue to grow causing the gel network to collapse and to release the liquid. An example of this can be found in the work of Xu *et al*. who gelled o-xylene with an amino alcohol which remained stable for only two days before crystallization occurred and the gel collapsed [Xu12]. In some cases, this transformation occurs at times that are not reproducible, ranging from a few days to several months, as was observed in the gel studied by Andrews *et al*. [And18]. However, it can be accelerated by agitation, such as shaking, cutting, stirring or oscillatory shearing. It should be noted that this process is irreversible; a system that has formed crystals can only be returned to a gel state by melting the crystals (sol) before cooling (gel).

In the latter case, the initially formed gel network transforms into a more energetically favored network which is visible by the appearance of a Bragg peak or by the transformation from thin fibers into thicker fibers. Such a transition was observed in the gel studied by Baral *et al.* where the formation of a sharp Bragg peak alongside a visual change from clear to turbid was observed in the gel [Bar15]. Draper *et al.*, however, observed a change from an initially turbid to clear

gel [Dra15]. The mechanism is similar to that of the gel to crystal transition albeit with the initially formed metastable gel transforming into a more stable gel as opposed to a crystal.

The change of structure is in line with Ostwald's rule which states that less stable polymorphs form before the thermodynamically stable form under the same conditions. In the case of supramolecular gels, the initially formed gel network can be considered as the kinetically favored polymorph which can then undergo changes into a more stable gel or into a crystal. There can be multiple local minima of a gel network which can be formed simultaneously or change from one to the other. Furthermore, Díaz-Oltra *et al.* showed that small changes in the gelation conditions led to specific polymorphs [Dia15].

2.3 Rheology of Gels

Rheology (from the Greek rheo (flow) and logia (study of)) is the science of liquid flow and of the deformation behavior of solids. The shear behavior of all materials can be seen as an intermediate between two extremes: the flow of ideal viscous fluids and the deformation of ideal elastic solids. The combination of viscous and elastic properties is referred to as viscoelastic. Viscoelastic materials can be further divided into viscoelastic liquids such as wallpaper paste and viscoelastic solids such as gels. The relevant theory was taken from [Mez06, www01, www02].

Fundamentals

The two-plates model will be used to define some fundamental rheological parameters (Figure 2.9).

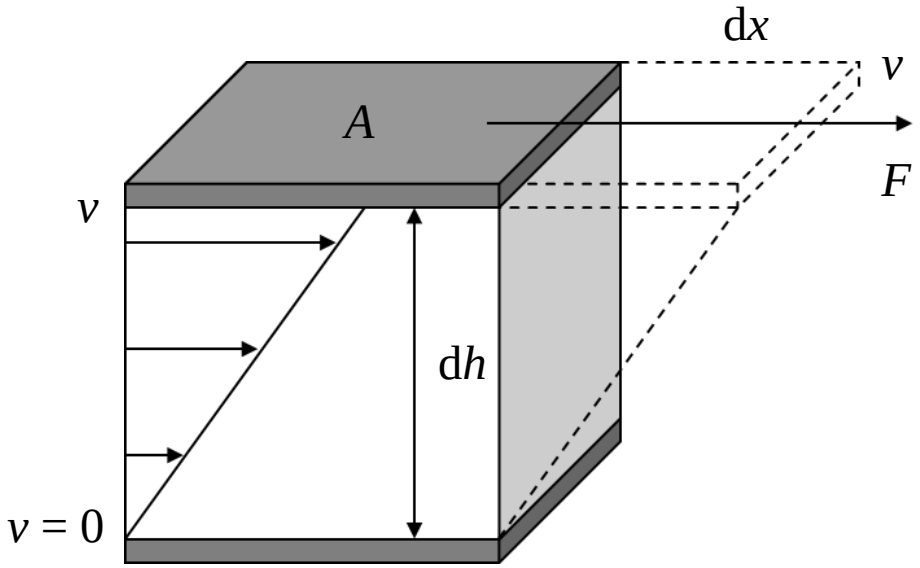

Figure 1.9: Schematic drawing of the two-plates model with an area *A*, distance between the two plates *h*, displacement d*x*, force *F* and velocity of the sample *v*. The force is applied on the upper plate, while the lower plate is fixed.

Two conditions must be met for the accurate calculation of rheological parameters. Firstly, the sample must adhere to both plates and must not slide along them. Secondly, there must be laminar flow conditions, i.e. no turbulent flow such as vortices. The upper plate with the shear area *A* is set in motion with a force *F*, while the lower plate remains stationary and the resulting velocity *v* of the upper plate is measured. The distance *h* between the two plates is referred to as the shear gap. The sample is between the two plates.

By dividing the force applied to the plate by its area one obtains the shear stress

$$\tau = \frac{F}{A}. \tag{2.3}$$

The shear strain γ is obtained by dividing the distance of deflection d*x* by the distance between the plates *h*. It holds

$$\gamma = \frac{dx}{dh}. \tag{2.4}$$

Dividing the shear strain γ by the time d*t*, or dividing the velocity *v* by the distance h between the plates, one obtains the shear rate

$$\dot{\gamma} = \frac{d\gamma}{dt} = \frac{d}{dh}\left(\frac{dx}{dt}\right) = \frac{dv}{dh}. \tag{2.5}$$

Viscoelastic Behavior

As already explained, the behavior of any material can be explained by a combination of ideal viscous and ideal elastic behavior. The difference can be illustrated with the dashpot model for an ideal viscous or Newtonian liquid (Figure 2.10 left), and the spring model for the ideal elastic solid (Figure 2.10 right), respectively.

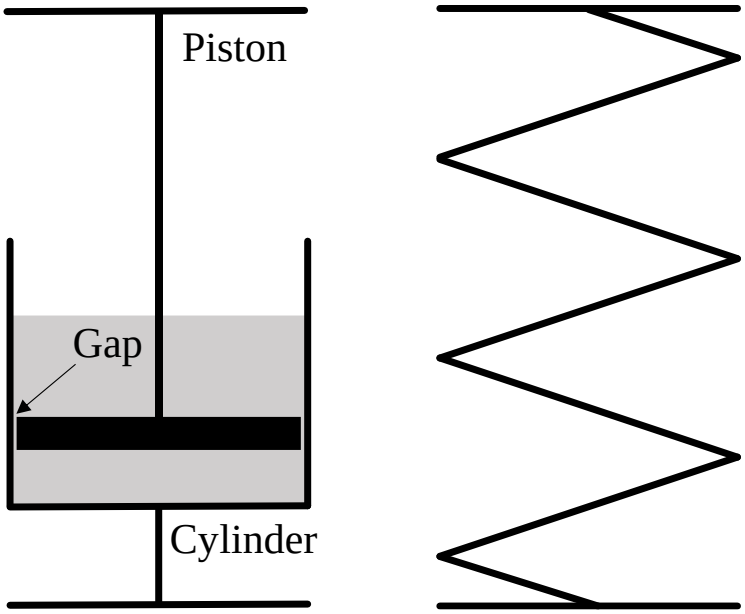

Figure 2.10: Schematic drawing of (left) the dashpot model for ideal viscous liquids and (right) the spring model for ideal elastic solids.

In the case of the dashpot model one applies a constant shear force and the piston moves continuously through the cylinder pressing the fluid through the tiny gap between the piston and the cylinder wall. Once the shear force is removed, the piston stops and remains in its last position. The applied force is proportional to the resulting speed of the piston and depends on the viscosity of the fluid. The shear viscosity of the fluid is defined as

$$\eta = \frac{\tau}{\dot{\gamma}}. \tag{2.6}$$

For ideal viscous liquids the shear viscosity is constant, however, in real liquids this is only the case for low shear rates. At higher shear rates, shear thickening and shear thinning, such as in starch solutions or ketchup, respectively, can be observed.

For ideal elastic materials, the spring model is often used as an illustration. Upon exercising a force on the spring, it immediately is deformed, holding that deformation as long as the force remains applied. Once the force is removed, the spring returns to its original position and no

permanent deformation occurs as opposed to the dashpot model for ideal viscous fluids. The deformation applied to the object is, according to Hooke's Law, linear to the force applied. For ideal elastic solids one obtains the shear modulus

$$G = \frac{\tau}{\gamma} \tag{2.7}$$

as a proportionality constant of the shear stress τ and the shear strain γ.

The main differences between ideal viscous and ideal elastic systems is their response to a deformation. The ideal viscous system deforms irreversibly, whereas the deformation of the ideal solid system is fully reversible. Many materials, however, have both viscous and elastic properties and thus neither model can describe their behavior. For viscoelastic materials, more complex models such as the Kelvin-Voigt model and the Maxwell model, which combine the dashpot and spring model, can be used.

The properties of fluids, such as viscosity, can be measured via rotational measurements. However, in the case of materials that break irreversibly under high deformations, oscillatory measurements are performed. Oscillatory measurements can also be explained by the two-plates model (Figure 2.11).

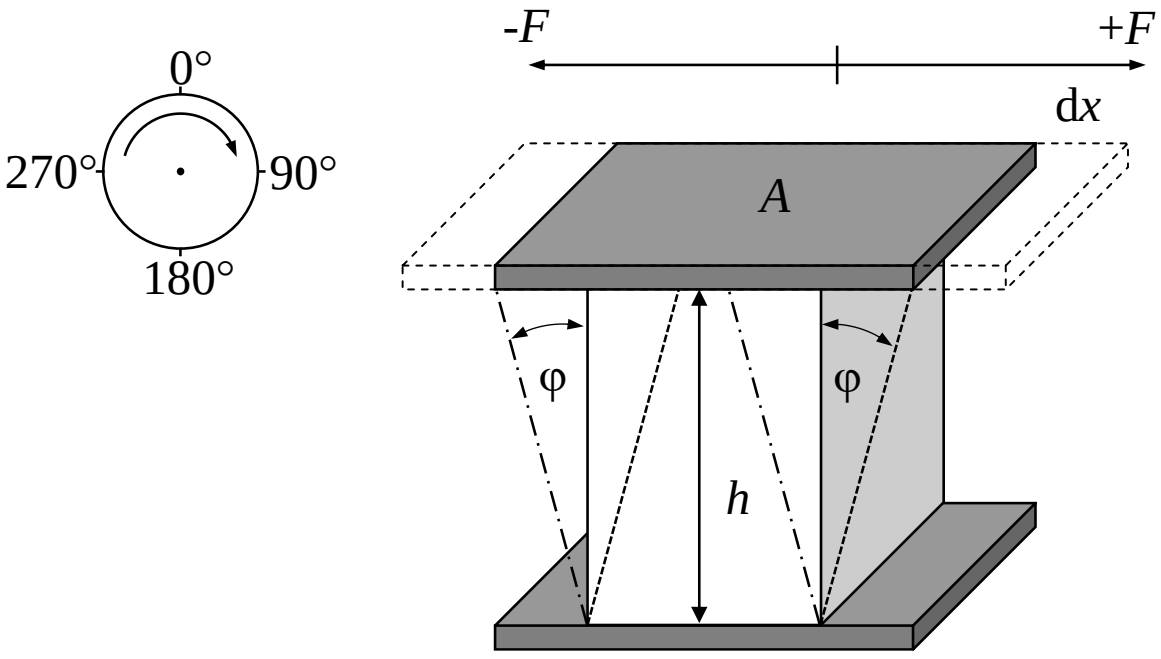

Figure 2.11: Schematic drawing of the two-plates model with an area *A*, height between the two plates *h*, displacement d*x*, force *F* and deflection angle φ. The force is applied on the upper plate, while the lower plate is fixed.

The oscillatory movement of the plates create a sinusoidal shear strain and shear stress with the respective amplitudes γ_{max} and τ_{max}. In the case of ideal elastic materials, the stress response to an applied strain is immediate. The sine curves of the shear strain and shear stress are thus completely in phase $\delta = 0°$. In the case of ideal viscous materials, the shear stress is in phase to the shear rate which reaches its highest value at the lowest deflection and thus at a shear strain $\gamma = 0$. The sine curves of τ and γ are thus out of phase by $\delta = 90°$. For viscoelastic materials whose properties lie in between these two extremes, the phase difference between τ and γ is $0° < \delta < 90°$. The phase angle does not exceed 90° as above this angle the plate would turn in the opposite direction. The sine curves of τ and γ as well as their phase angle are shown in Figure 2.12.

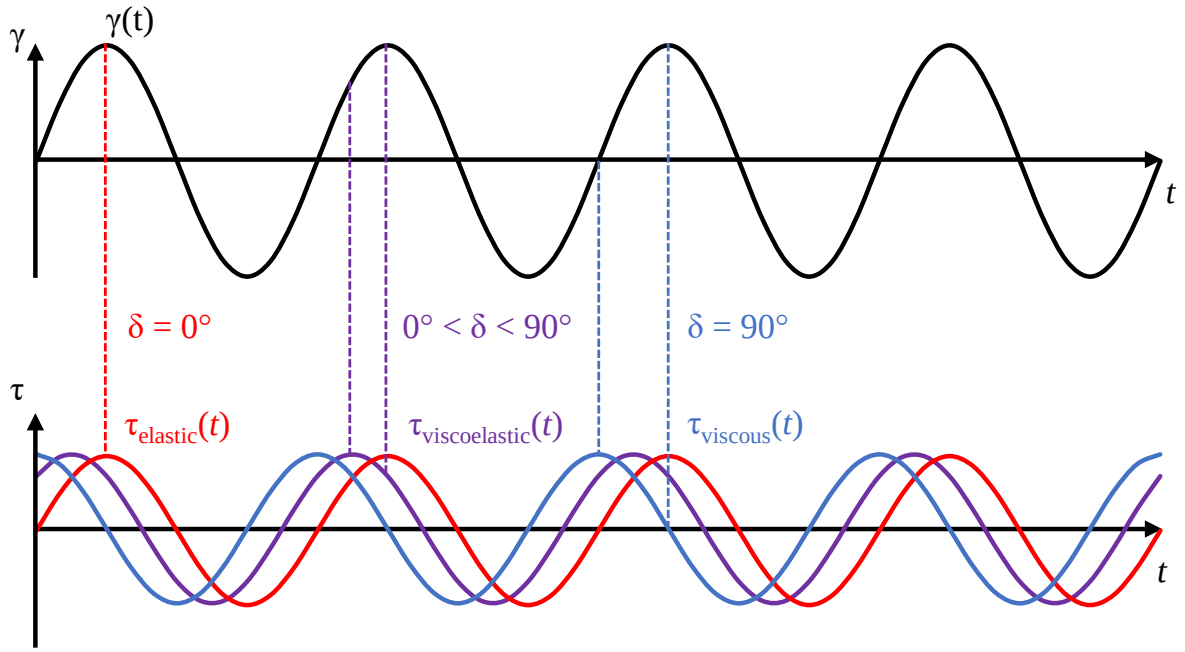

Figure 2.12: The time-dependent sine function of the shear strain γ(t) (black) and the corresponding time-dependent shear stress functions τ(*t*) of an elastic (red), viscous (blue) and viscoelastic (purple) material as well as the phase angle δ of each case.

The ratio of the shear stress amplitude τ_{max} and shear strain amplitude γ_{max} is the complex shear modulus

$$|G^*| = \frac{\tau_{max}}{\gamma_{max}}. \tag{2.8}$$

The complex shear modulus G^* is not to be confused with the shear modulus G (Equation 2.7) which is determined under steady shear conditions and not oscillatory measurements. G^* describes the resistance of a sample against deformation. Furthermore, G^* can be divided into an elastic component, the storage modulus G', and a viscous component, the loss modulus G''.

$$G^* = G' + iG''. \tag{2.9}$$

The storage modulus G' is a measure for the stored deformation energy. After the applied acting force is removed, this energy restores the sample to its original state. The loss modulus G'', however, is a measure for the deformation energy that is lost during the shear process. Using the complex shear modulus G^* and the phase angle δ, the storage modulus G' and loss modulus G'' can be determined with a vector diagram, with G' being plotted on the x-axis and G'' on the y-axis (Figure 2.13).

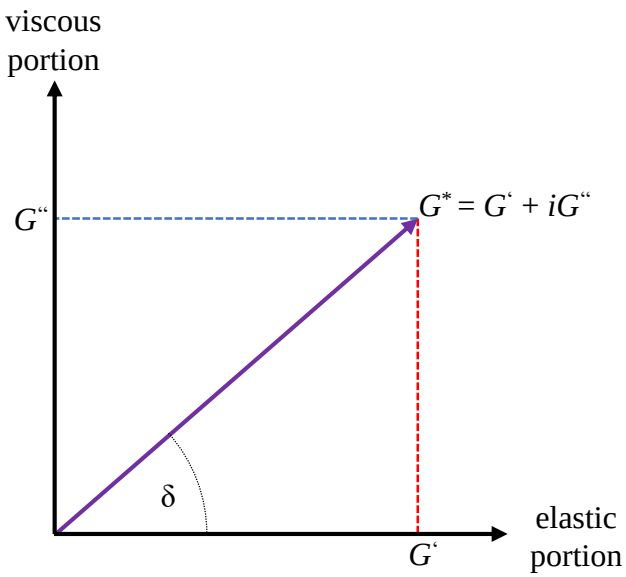

Figure 2.13: Illustration of the relations of the shear modulus G^*, storage modulus G', loss modulus G'' and phase angle δ.

It thus holds for the storage and loss modulus:

$$G' = |G^*|cos\delta$$

and (2.10)

$$G'' = |G^*|sin\delta.$$

The relation between G' and G'' can be used to characterize a material. If $G' > G''$ the material is considered to be a viscoelastic solid, whereas for $G'' > G'$ the material is considered to be a viscoelastic liquid.

Amplitude Sweeps

Amplitude sweeps determine the deformation behavior in the non-destructive deformation range as well as its upper limit. The oscillation frequency ω is kept constant while the shear strain amplitude γ_{max} is increased (Figure 2.14).

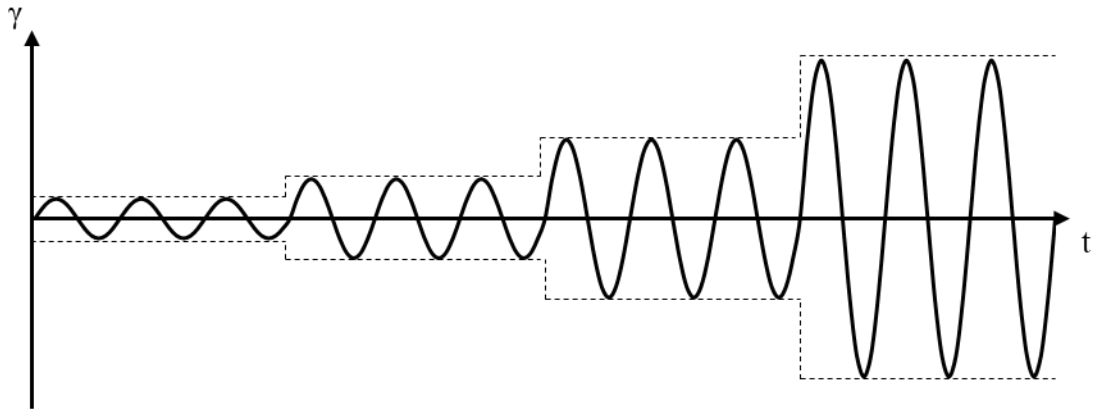

Figure 2.14: Illustration of an amplitude sweep. The shear strain amplitude γ_{max} is increased, while the frequency ω is kept constant.

The storage modulus G' and loss modulus G'' remain constant at low γ_{max}-values. This region is referred to as the linear viscoelastic (LVE) region. We can again differentiate whether a material is a viscoelastic solid $G' > G''$ or a viscoelastic liquid $G' < G''$, though for the determination of the LVE region mostly the G'-values are taken for analysis as they generally tend to leave the LVE region first. Above a certain strain amplitude γ_l (l = limiting value), the linearity of the LVE region is reached and the sample is damaged or destroyed (Figure 2.15).

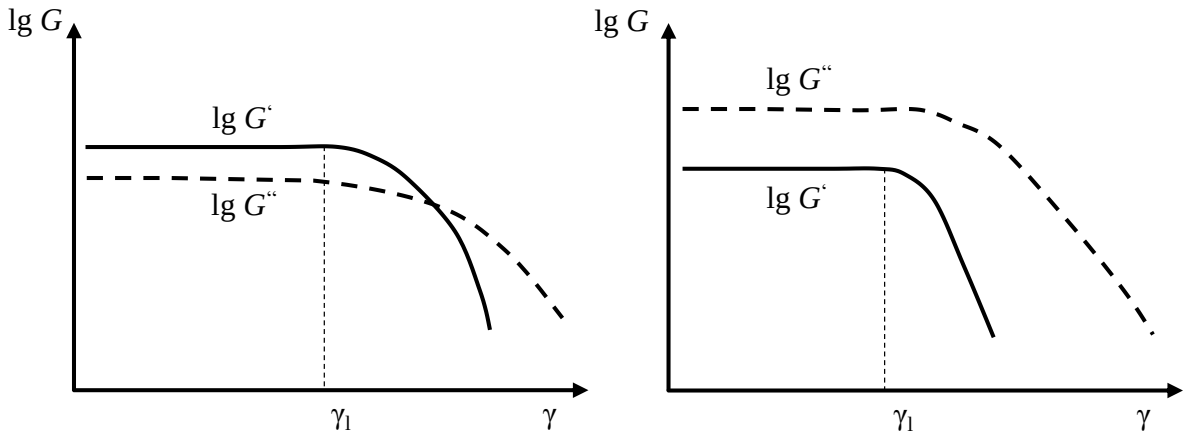

Figure 2.15: Schematic drawing of an amplitude sweep of (left) a gel like sample with $G' > G''$ and (right) a liquid sample with $G'' > G'$.

Amplitude sweeps are generally performed to determine the LVE region for subsequent frequency sweeps. The maximum value of the strain for the following measurements must be below the γ_l determined for the sample.

Frequency sweeps

Frequency sweeps investigate the time-dependent shear behavior of a sample. To that effect the amplitude of the strain γ_{max} is kept constant while the frequency is varied (Figure 2.16).

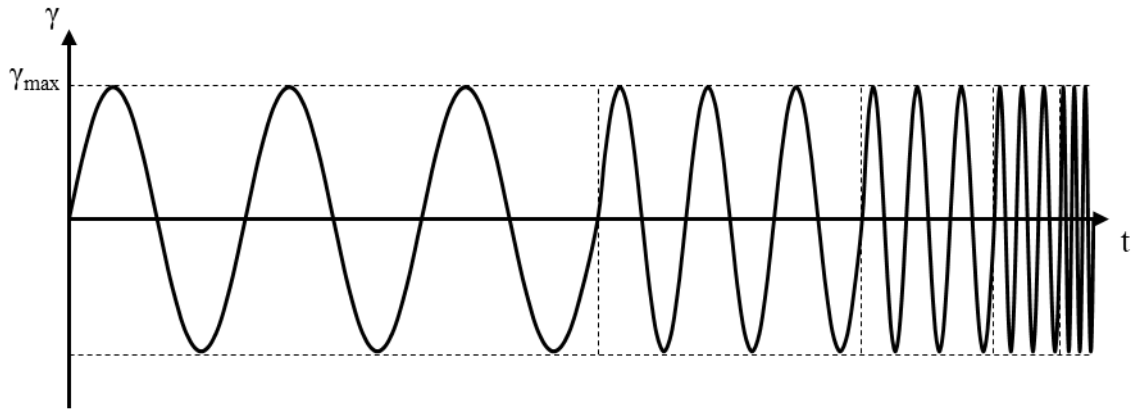

Figure 2.16: Illustration of a frequency sweep. The shear strain amplitude γ_{max} is kept constant while the frequency ω is increased.

The selected γ is determined by a preceeding amplitude sweep to ensure that the measurement takes place in the linear viscoelastic (LVE) region. Low frequencies represent here long times scales, whereas high frequencies correspond to short time scales.

3 Results and Discussion

3.1 Preliminary Studies

The lyotropic liquid crystal gels (LLC gels) in this work are obtained by adding a low molecular weight gelator (LMWG) to a lyotropic liquid crystal (LLC). Two LLC systems, one containing the surfactant *N*,*N*-dimethyl-*N*-ethyl-1-hexadecylammonium bromide (CDEAB) and the other containing the surfactant *N*,*N*,*N*-trimethyl-1-tetradecylammonium bromide (C_{14}TAB), were selected as they both form the calamitic nematic N_C phase. Given that the region in which the N_C phase forms is relatively small, the composition of water, surfactant and cosurfactant must be chosen carefully to avoid that small temperature or concentration changes induce a phase transition. A ternary phase diagram already existed for the CDEAB system [Gör96] (Figure 3.1 left), however, no such phase diagram was available for the C_{14}TAB system. To determine the ideal ratio of the components of the ternary LLC a ternary phase diagram was recorded (Figure 3.1 right) by observing the samples between crossed polarizers in a temperature-controlled water basin.

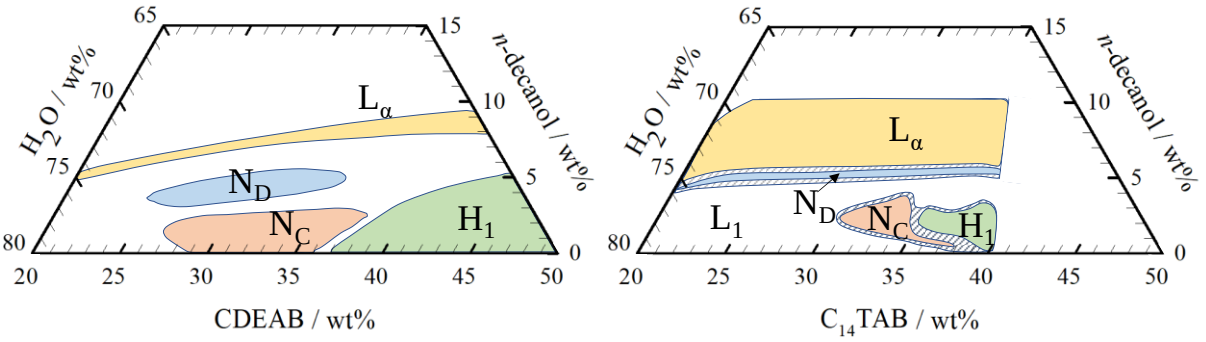

Figure 2.1: Ternary phase diagrams of (left) the binary LLC system H_2O – CDEAB recorded at T = 298 K [Gör96] and (right) the ternary LLC system H_2O – C_{14}TAB – *n*-decanol recorded at T = 293 K. The calamitic nematic N_C phase (orange), discotic nematic N_D phase (blue), hexagonal H_1 phase (green) and lamellar L_α phase (yellow) are indicated.

It can be seen that both systems possess a calamitic nematic N_C phase as well as a discotic nematic N_D phase. Towards higher surfactant concentrations the hexagonal H_1 phase forms, while higher cosurfactant concentrations favor the formation of the lamellar L_α phase. It can be seen that the CDEAB system is able to form an N_C phase with and without the cosurfactant *n*-decanol, while in the case of the C_{14}TAB system *n*-decanol is required to form the N_C phase. This difference is due to the increased hydrophobicity of CDEAB compared to C_{14}TAB. The longer chain length as well as the additional ethyl chain in its head group leads to a different

packing behavior when compared to C_{14}TAB. For C_{14}TAB to be able to form the N_C phase a cosurfactant has to be added to adjust the hydrophobic character of the surfactant. The water insoluble cosurfactant incorporates itself into the micelle and promotes the formation of anisotropic micelles. Given that the LLC system H_2O – CDEAB is able to form the nematic phase without the addition of the cosurfactant *n*-decanol, we decided to use it as a binary LLC referring to it henceforth as binary CDEAB system. In the case of the LLC system H_2O – C_{14}TAB – *n*-decanol, we will refer to it as ternary C_{14}TAB system.

For potential applications the LLC should remain stable over a large temperature range, to ensure that small uncontrolled temperature deviations do not induce a phase transition. To determine at which composition the clearing temperature T_{Cl} of the nematic phase is the highest, the temperature dependent phase diagrams of both systems are required. For the CDEAB system, a temperature dependent phase diagram already existed [Sch15] (Figure 3.3 left), while for the C_{14}TAB system the phase diagram was recorded using polarized optical microscopy (POM). The images can be seen in Figure 3.2. The surfactant-to-cosurfactant ratio was set at $\sigma = 0.93$ as at this ratio the extension of the nematic phase is the largest (see Figure 3.1 right).

The surfactant mass fraction μ_{bin} of the binary CDEAB system is given in wt% and calculated according to

$$\mu_{\mathrm{bin}} = \frac{m_{\mathrm{surfactant}}}{m_{\mathrm{surfactant}} + m_{\mathrm{H_2O}}} \cdot 100\%. \tag{3.1}$$

A surfactant mass fraction μ_{bin} of 31% was used for the subsequent experiments. For the ternary C_{14}TAB system the equation of the surfactant mass fraction μ_{ter} was modified to include the cosurfactant and is calculated according to

$$\mu_{\mathrm{ter}} = \frac{m_{\mathrm{surfactant}} + m_{\mathrm{cosurfactant}}}{m_{\mathrm{surfactant}} + m_{\mathrm{cosurfactant}} + m_{\mathrm{H_2O}}} \cdot 100\%. \tag{3.2}$$

A surfactant mass fraction μ_{ter} of 35% was used for the subsequent experiments. For the surfactant-to-cosurfactant ratio σ the value was selected so that the broadest region of the nematic N_C phase is covered. The surfactant to cosurfactant ratio σ was kept constant and is calculated according to

$$\sigma = \frac{m_{\mathrm{C_{14}TAB}}}{m_{\mathrm{C_{14}TAB}} + m_{n-\mathrm{decanol}}}. \tag{3.3}$$

Overall, two transitions from the N_C phase could be observed. Firstly, the transition from the N_C phase to the isotropic phase (Figure 3.2 top), and secondly, from the N_C phase to the hexagonal phase (Figure 3.2 bottom).

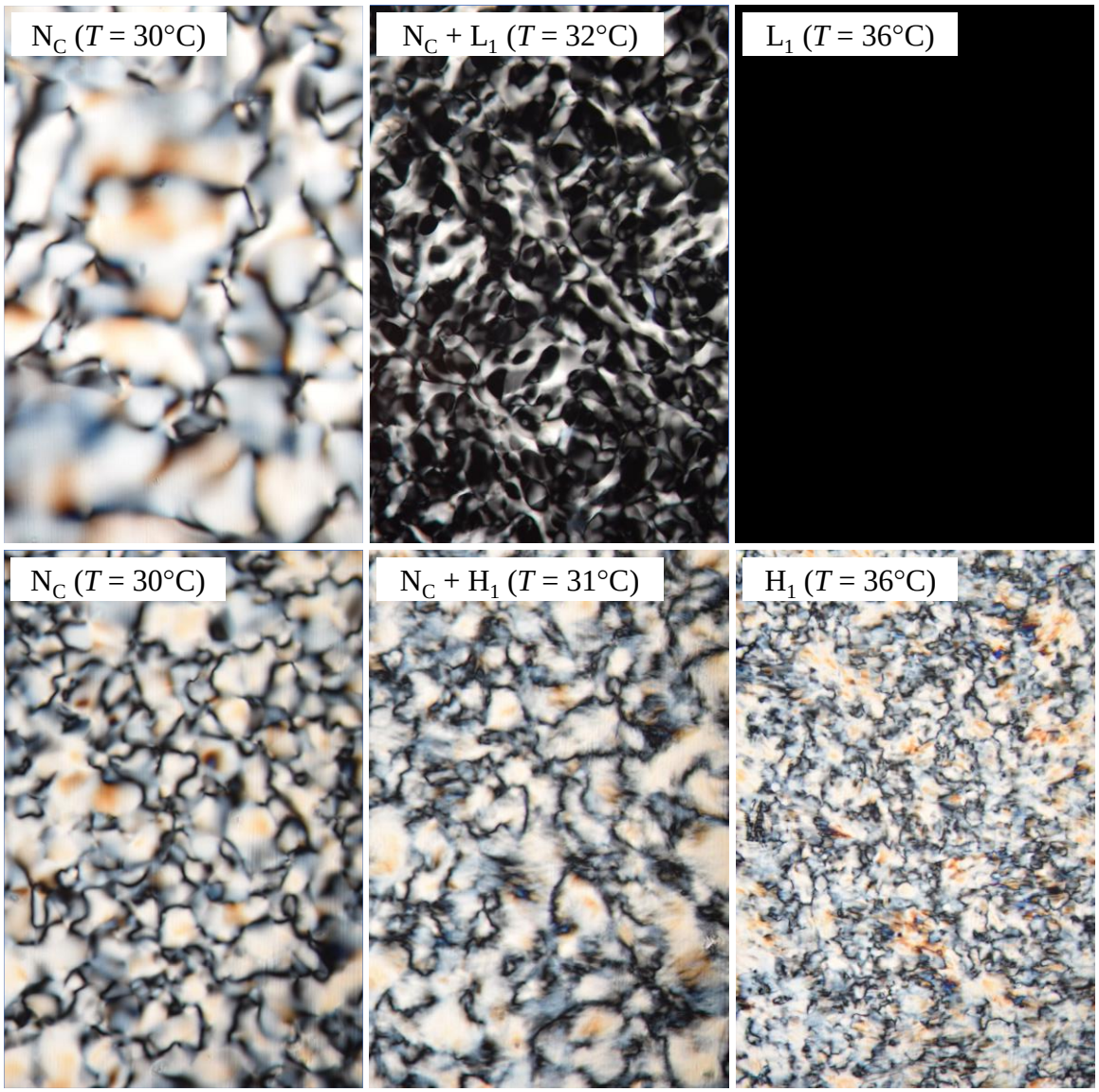

Figure 3.2: POM images between crossed polarizers recorded during the transition of (top) the nematic N_C phase to the isotropic L_1 phase and (bottom) the nematic N_C phase to the hexagonal H_1 phase. During heating the samples transition from the nematic N_C phase (left) to a two-phase region (center) to the isotropic L_1 phase or hexagonal H_1 phase (right). The isotropic L_1 phase possesses no birefringence.

The phase boundaries were determined visually by observing the changes in the texture of the sample between crossed polarizers. An initially nematic N_C sample undergoes one of two phase transitions, which can be visually followed upon heating. At lower total surfactant mass fractions, the nematic N_C phase transitions to the isotropic L_1 phase (Figure 3.2 top) which causes the birefringence of the sample to gradually disappear until the L_1 phase is fully developed. At higher total surfactant mass fractions, the nematic N_C phase transitions into the hexagonal H_1 phase (Figure 3.2 bottom) where the phase boundaries are much harder to spot as both phases show birefringence. Nevertheless, a small change in texture can be observed when entering the two-phase region allowing for the measurement of a temperature dependent phase diagram (Figure 3.3 right).

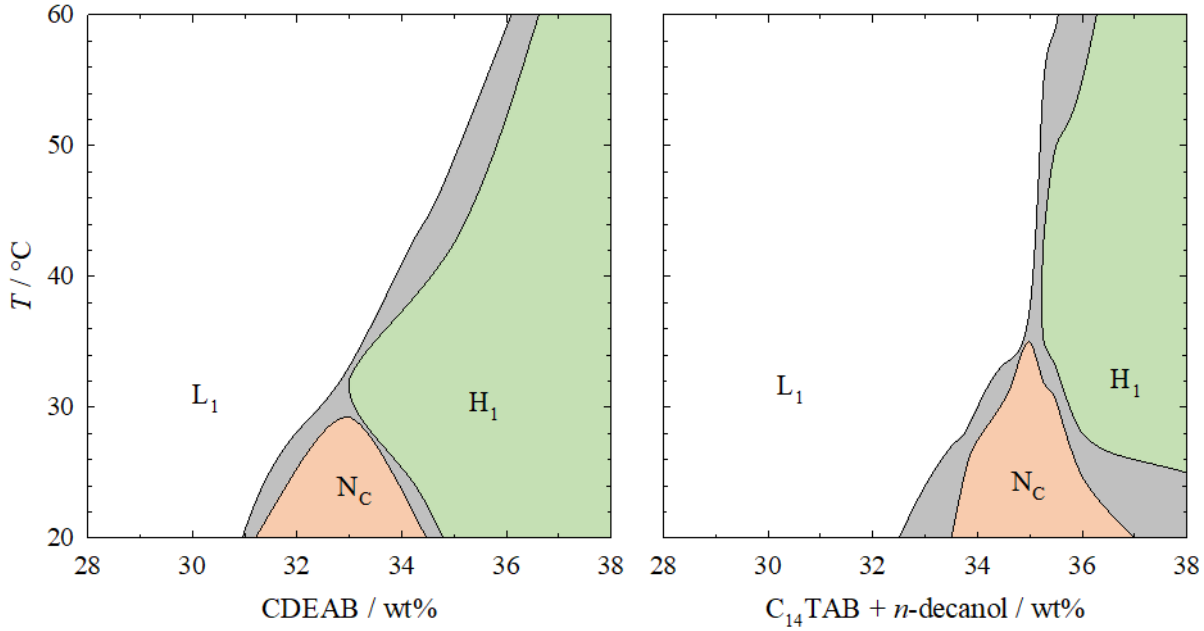

Figure 3.3: Phase diagrams of (left) the binary LLC system H_2O – CDEAB, schematically redrawn from [Sch15], and (right) the ternary LLC system H_2O – C_{14}TAB – *n*-decanol at a constant surfactant-to-cosurfactant ratio of $\sigma = 0.93$. The calamitic nematic N_C phase (orange), the micellar isotropic L_1 phase (white), the hexagonal H_1 phase (green) as well as the two-phase regions (gray), are indicated.

It can be seen that for both systems the N_C phase is bordered by the hexagonal H_1 phase at higher surfactant concentrations, and the micellar isotropic L_1 phase at lower surfactant concentration. The N_C phase forms at a surfactant concentration of $\mu_{bin} = 31$ - 35 wt% for the binary CDEAB system and at a combined surfactant and cosurfactant concentration of $\mu_{ter} = 33$ - 37 wt% for the ternary C_{14}TAB system. The highest clearing temperature observed was $T = 28$°C for $\mu_{bin} = 33$ wt% for the binary CDEAB system and $T = 35$°C for $\mu_{ter} = 35$ wt%

for the ternary C_{14}TAB system. For further experiments the surfactant mass ratios μ with the highest clearing temperatures were selected.

For gelling the nematic N_C phases three homologues of the low molecular weight gelator (LMWG) 3,5-bis-(5-hexylcarbamoyl-pentoxy)-benzoate acid *n*-alkyl ester BHPB-*n* (Figure 3.4) were tested.

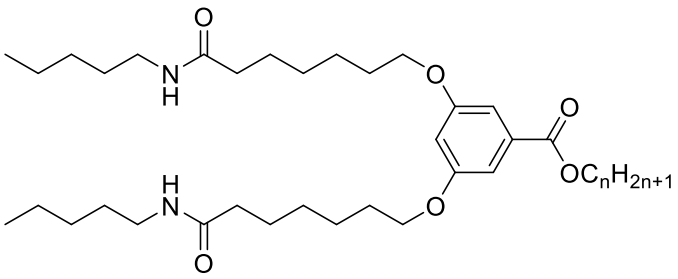

Figure 3.4: Molecular structure of the low molecular weight gelator BHPB-*n* with the alkyl chain length n = 6,10,13.

BHPB-*n* is an organogelator that, depending on its chain length and the solvent, is known to possess different fiber structures. In cyclohexane, for example, the fiber structures from straight ribbons to twisted ribbons and tubes (Figure 3.5).

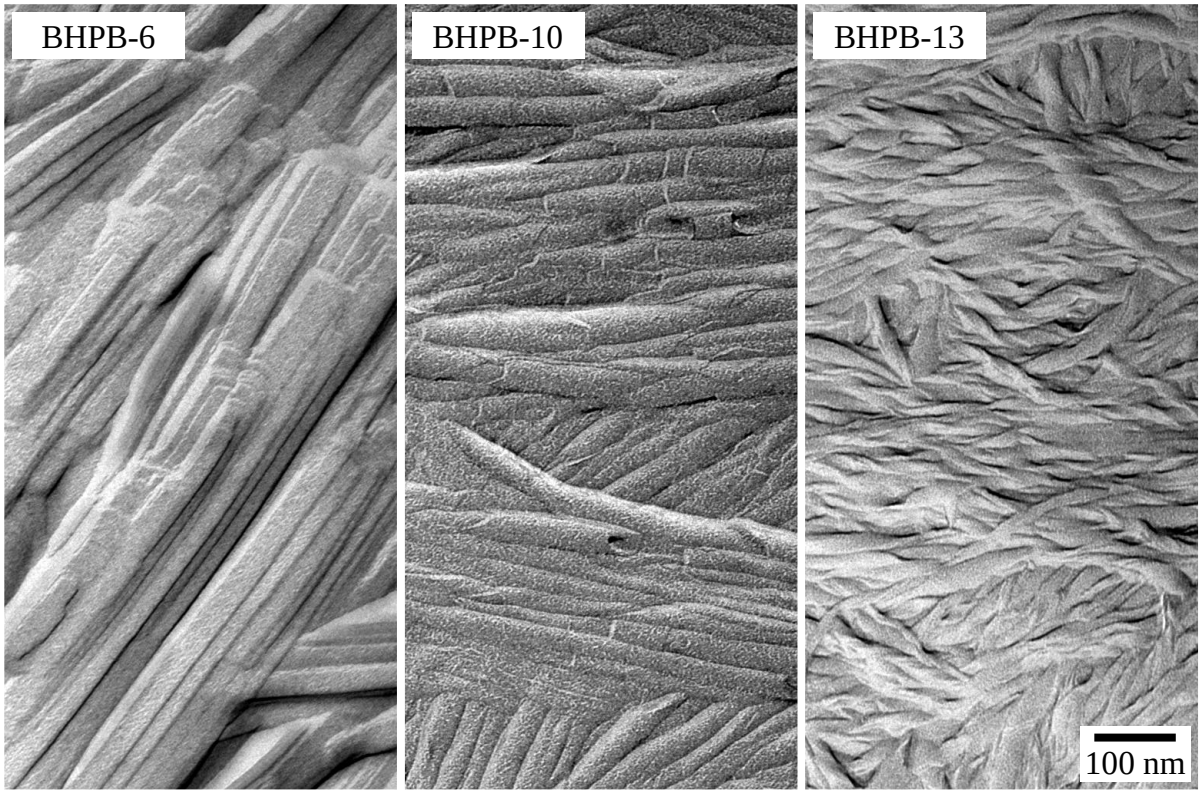

Figure 3.5: Freeze fracture electron microscopy (FFEM) images of binary gels of BHPB-6 (left), BHPB-10 (center), and BHPB-13 (right) in cyclohexane. Each binary gel contains 1 wt% of the respective gelator.

It can be seen that depending on the alkyl chain length the structure of the fiber changes. For BHPB-6 the fibers of the binary gel with cyclohexane are made up of ribbons with widths of up to 100 nm and lengths that can surpass 1 µm. These ribbons also show the tendency to stack on top of each other. The binary gel consisting of BHPB-10 and cyclohexane forms gel fibers that are hollow tubes with a diameter of ~30 nm, while the binary gel consisting of BHPB-13 and cyclohexane possesses fibers of twisted ribbons. To determine which of these gelators is the most suitable to gel the nematic N_C phases, each gelator was used to gel the two N_C phases at a gelator mass fraction of η = 1 wt%. The gelator mass fraction η was calculated according to

$$\eta = \frac{m_{\mathrm{BHPB}-n}}{m_{\mathrm{total}}} \cdot 100\%. \tag{3.4}$$

A vial inversion test was performed for both the binary CDEAB and ternary C_{14}TAB systems with all gelators after an aging time of 1 day. The gels formed by BHPB-6 and BHPB-10 were

strong enough to remain in place after the vial was inverted, whereas the gel formed by BHPB-13 flowed. In addition to the vial inversion test, rheological measurements were performed with all gels (Figure 3.6).

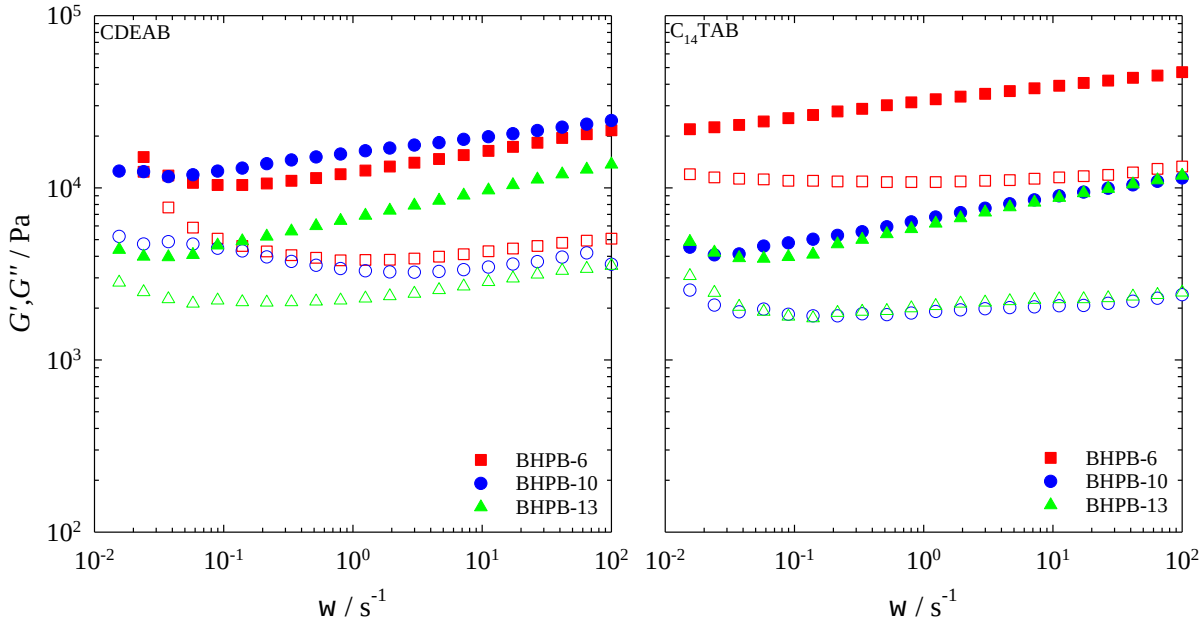

Figure 3.6: Frequency sweeps of the binary LLC (left) and the ternary LLC (right) gelled with BHPB-6 (squares), BHPB-10 (circles), and BHPB-13 (triangles). The storage modules G' is represented by the filled symbols and the loss modulus G'' by the empty symbols. The gelator mass fraction η = 1 wt%, the temperature T = 20°C and the strain γ = 0.5% were kept constant.

Looking at Figure 3.6, one sees that for the binary CDEAB system the gels formed with BHPB-6 and BHPB-10 are of roughly equal strength, while the gel formed by BHPB-13 is weaker. Additionally, the storage modulus G' is higher than the loss modulus G'' over the entire frequency range. In the case of the ternary gel, the gel formed by BHPB-6 is the strongest with the gels formed by BHPB-10 and BHPB-13 being of roughly equal strength. Similar to the binary CDEAB system, the storage modulus G' is higher than the loss modulus G'' over the entire frequency range. Given that some gelators, while able to gel an LLC, induce phase transitions within the LLC [Ste18], we confirmed the existence of the N_C phase in the presence of the gelator with POM (Figure 3.7).

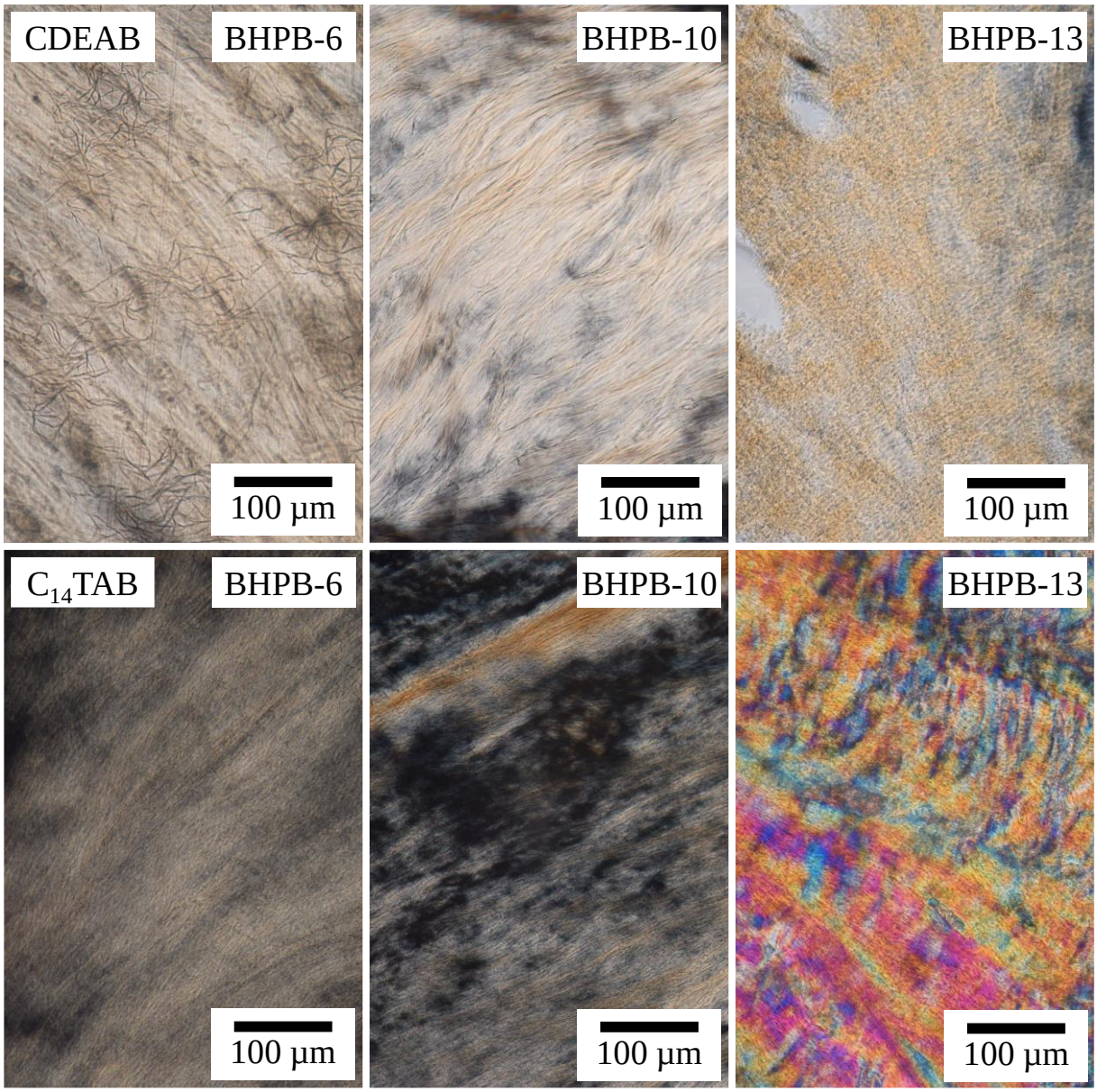

Figure 3.7: POM images between crossed polarizers of the binary CDEAB system (top) and the ternary C_{14}TAB system (bottom) gelled with 1.0 wt% BHPB-6 (left), BHPB-10 (middle), and BHPB-13 (right).

It can be seen that all show birefringence. Given that the N_C phase is bordered by the isotropic L_1 phase and the anisotropic H_1 phase, the observed birefringence and the lack of the characteristic fan-like structure of the H_1 phase indicates that the N_C phase remains stable after the addition of the gelator. Apart from showing that the N_C phase forms in the presence of the gel network, we looked at the structure of the gel network after gelation (Figure 3.8).

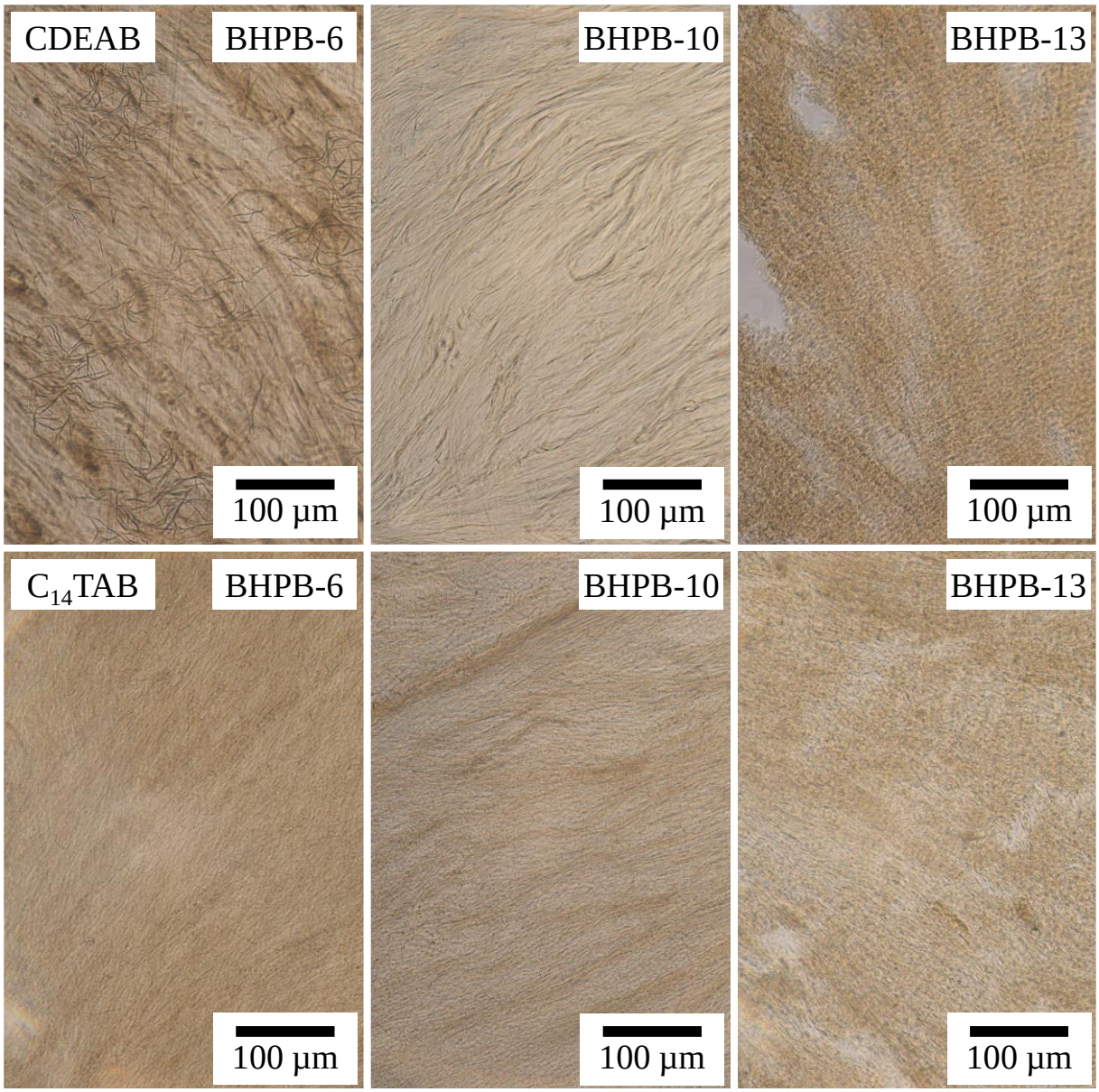

Figure 3.8: POM images with only one polarizer of the binary CDEAB system (top) and the ternary C_{14}TAB system (bottom) gelled with 1.0 wt% BHPB-6 (left), BHPB-10 (middle), and BHPB-13 (right).

To study only the gel structure, we removed one of the polarizers allowing for the fibers to be observed. For the N_C phases gelled with BHPB-6 and BHPB-10 one sees that gel network does not form uniformly but possesses some clusters. In the N_C phases gelled with BHPB-13 we observe additionally the formation of cracks where no gel fibers are visible.

For future studies we decided to only use one of the tested gelators. We chose to use BHPB-6 as our gelator as the formed gels had the highest G' and G'' values. Moreover, the G' and G''

values of the gelled binary CDEAB system and the gelled ternary C_{14}TAB system, respectively, were comparable.

Conclusion

We selected two surfactants as basis for our lyotropic liquid crystal (LLC) gels. First, *N*,*N*-dimethyl-*N*-ethyl-1-hexadecylammonium bromide (CDEAB), which is capable of forming the calamitic nematic N_C phase with water alone, and second, *N*,*N*,*N*-trimethyl-1-tetradecylammonium bromide (C_{14}TAB), which requires the cosurfactant *n*-decanol in addition to water to form the N_C phase. To determine the ideal concentration of the ternary C_{14}TAB system we began by recording its ternary phase diagram. Using the ternary phase diagram we selected the surfactant-to-cosurfactant ratio $\sigma = 0.93$ as here the extension of the N_C phase is the largest. We then measured a temperature dependent phase diagram using polarized optical microscopy (POM) showing that the N_C phase forms at a total concentration (surfactant + cosurfactant) of $\mu_{ter} = 33 - 37$ wt% at $T = 20$°C, with the highest clearing temperature $T_{Cl} = 35$°C observed at $\mu_{ter} = 35$ wt%. For the CDEAB system both the ternary phase diagram [Gör96] and the temperature dependent binary phase diagram [Sch15] were already known. In the binary CDEAB system, the N_C phase forms at a surfactant concentration of $\mu_{bin} = 31 - 35$ wt% at $T = 20$°C, with the highest clearing temperature $T_{Cl} = 28$°C observed at $\mu_{ter} = 31$ wt%. We then tested three homologues of the gelator 3,5-bis-(5-hexylcarbamoyl-pentoxy)-benzoate acid *n*-alkyl ester (BHPB-*n*) with different chain lengths ($n = 6, 10, 13$). Freeze fracture electron microscopy (FFEM) of binary gels formed with cyclohexane and each of the three gelators showed different gel fiber structures. The fibers formed by BHPB-6 are ribbons with widths of up to 100 nm and lengths of up to 1 µm which tended to stack on top of each other. The binary gel of cyclohexane and BHPB-10 formed hollow tubes with a diameter of ~30 nm and the binary gel of cyclohexane and BHPB-13 formed twisted ribbons. We then used rheology to study the gels of our LLCs gelled with BHPB-*n*. In the case of the binary CDEAB system the gels formed with BHPB-6 and BHPB-10 were of approximately equal strength, whereas in the case of the ternary C_{14}TAB system, the gel formed with BHPB-6 was the strongest. For both systems, the gels formed with BHPB-13 were the weakest. We used POM to determine if the gelator disturbed the N_C phase in either system and found that none of the gelators had a negative effect on the N_C phases. We then observed the gel structure using microscopy and found, in gels formed by BHPB-13, some regions where no gel structure was present. Meanwhile, gels formed by BHPB-6 and BHPB-10 were largely homogenous. For our subsequent studies, we decided to only use the gelator BHPB-6 as it was the best performing of the three gelators.

3.2 Rheological Studies

The amount of the gelator BHPB-6 available during the preliminary studies was limited, thus additional batches of the gelator had to be used for future experiments. In total, three distinct batches were used. The first and second batch were generously provided by the group of Mésini, while the third was synthesized following Mésini's procedure [Sim13]. Due to the limited amounts of BHPB-6 of batch 1, we were only able to do frequency sweeps of the samples. We selected a shear strain of $\gamma = 0.5$ %, which we assumed to be within the LVE-region of the gel samples. For batch 2 and 3 we performed amplitude sweeps to locate the LVE-region of the gelled samples (Figure 3.9).

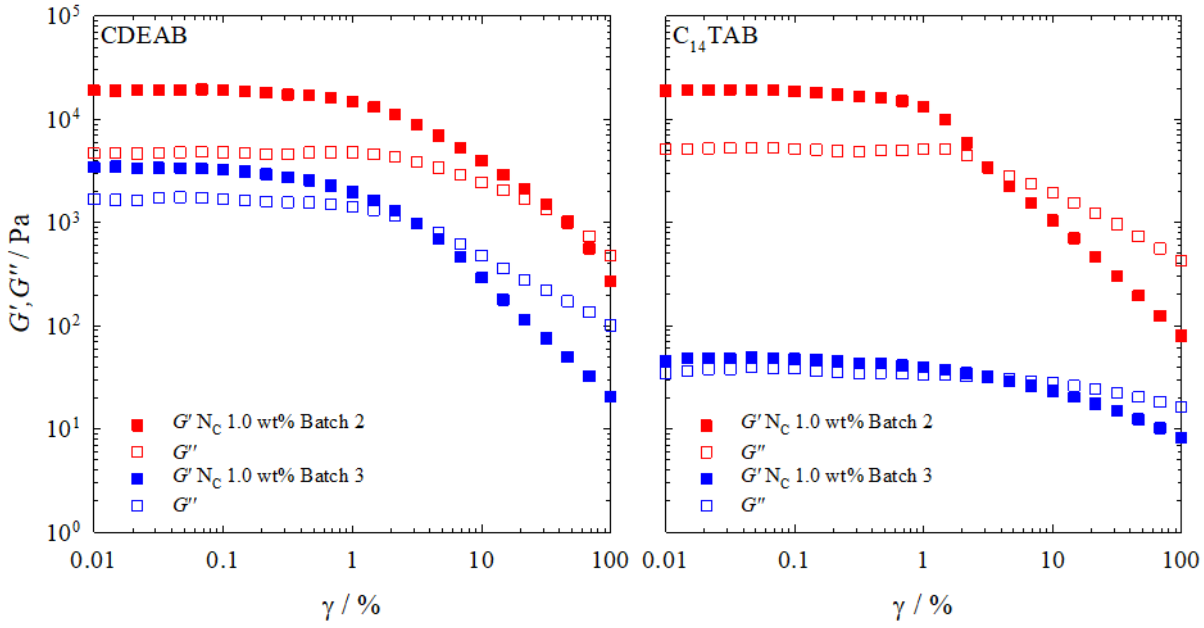

Figure 3.9: Amplitude sweeps of the CDEAB system (left) and the C_{14}TAB system (right) gelled with 1 wt% BHPB-6 from batch 2 (red) or batch 3 (blue). The storage moduli G' (filled boxes) and loss moduli G'' (empty boxes) of the gelled N_C phase are shown. The frequency ω was set to $\omega = 10\ s^{-1}$ for the samples gelled with batch 2 and $\omega = 1\ s^{-1}$ for the samples gelled with batch 3.

It can be seen that there are discrepancies between the gels prepared with different batches, especially between those of the ternary C_{14}TAB system. In both systems the absolute G' and G'' values decreased from batch 2 to 3. However, in the case of the binary CDEAB system, the difference was in the range of one order of magnitude while in the case of the ternary C_{14}TAB system the difference was well over two orders of magnitude. For the subsequent measurements with batch 2 we decided to use a shear stress of $\tau = 30$ Pa, which in this case roughly

corresponds to a shear strain of γ = 0.15 %. In the case of batch 3, which has a smaller LVE-region, a lower shear strain of γ = 0.1 % was chosen instead. We also compared the frequency sweeps of the three gelator batches at a gelator mass fraction of η = 1 wt% (Figure 3.10).

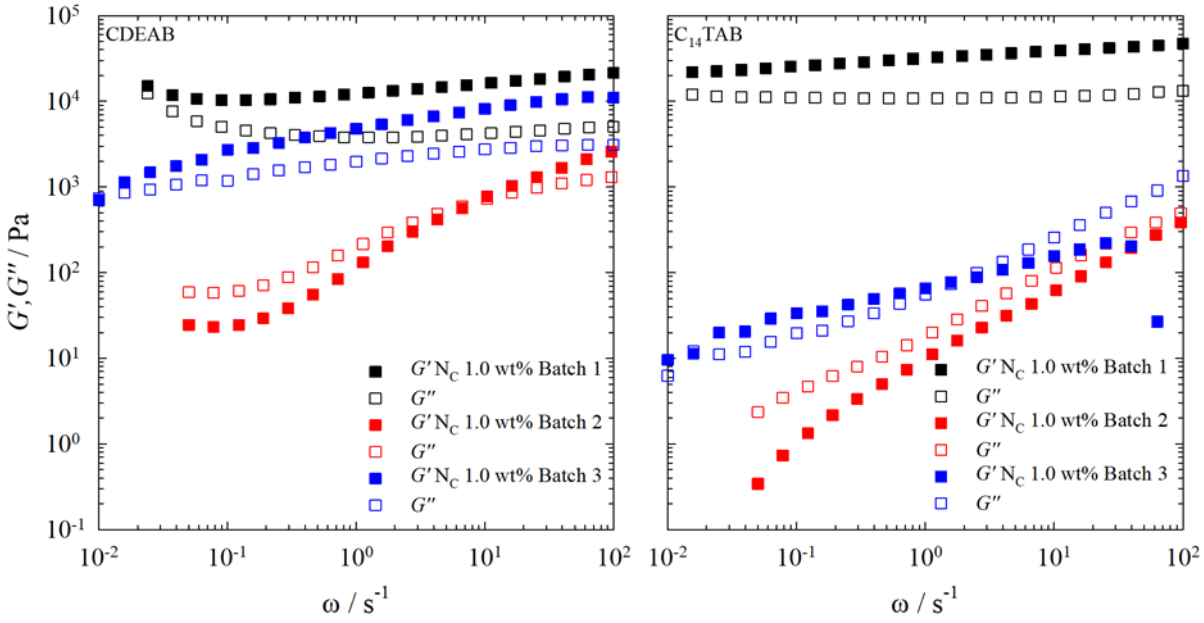

Figure 3.10: Frequency sweeps of the CDEAB system (left) and the C_{14}TAB system (right) gelled with 1 wt% BHPB-6 from batch 1 (black), batch 2 (red) or batch 3 (blue). The storage moduli G' (filled boxes) and loss moduli G'' (empty boxes) of the N_C phase are shown. The constant shear strain was set to γ = 0.5 % for measurements with batch 1 and γ = 0.1 % for measurements with batch 3. In the case of batch 2, a constant shear stress of τ = 30 Pa, which is equivalent to γ = 0.15 %, was used instead.

It can be seen that in the case of batch 1, the storage modulus G' is higher than the loss modulus G'' over the entire frequency range showing a gel-like behavior for both systems. Additionally, the absolute G' and G'' values are quite high. For batch 2, we saw a surprising decrease in the absolute G' and G'' values compared to the amplitude sweep. In addition, in the case of the of the binary gel, we see a crossover at ω = 10 s^{-1}, suggesting a more liquid-like behavior at low frequencies, while for the ternary gel G' and G'' are inversed over the entire frequency range. This shows a drastic change in behavior from batch 1 to batch 2. Batch 3 also differs from its predecessors. In the case of the binary gel, the frequency sweep shows similar but lower absolute G' and G'' values compared to batch 1. In the case of the ternary gel, the frequency sweep again showed G' and G'' much lower than those of batch 1. We also studied the evolution of the gel network within the first 20 hours with batches 2 and 3. The samples were placed on

the rheometer in a liquid state and allowed to gel over the following 20 hours. The results are shown in Figure 3.11.

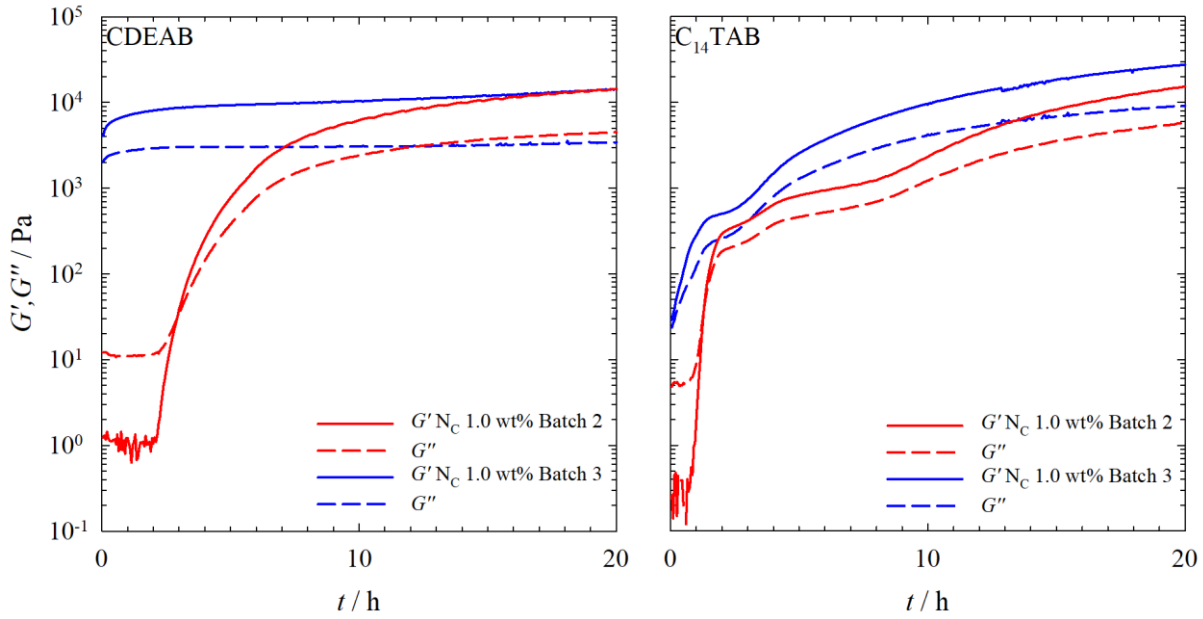

Figure 3.11: Storage modulus $G^{'}$ (straight line) and loss modulus $G^{''}$ (dashed line) of (left) the binary CDEAB system and (right) the ternary C_{14}TAB system measured at a constant temperature of T = 20°C, shear strain γ = 0.1 %, and frequency of ω = 1 s^{-1}. The N_C phases were gelled using 1.0 wt% BHPB-6 from either batch 2 (red) or batch 3 (blue).

It can be observed that for the gels formed with batch 2, some time elapses before the gelation process starts. With batch 3 gelation starts immediately. The absolute $G^{'}$ and $G^{''}$ values are approximately the same for all samples, whether binary or ternary, and whether gelled with batch 2 or batch 3. However, the binary gel formed with batch 3 differs from the other samples by having high $G^{'}$ and $G^{''}$ values from the beginning of the measurements.

The gelator batch obviously has a large influence on the gel strength and the gelation time. Despite the fact that the same procedures were followed during the synthesis and similar purities were determined by NMR measurements, the different batches resulted in different gels. In order to avoid errors due to the different behaviors of the batches, only one batch will be used from now on. The results shown in the following chapters were all obtained with batch 3.

Conclusion

The decision to use the gelator BHPB-6 for all future measurements was based on the results obtained with a small amount of the gelator. For subsequent measurements, two additional batches were prepared that differed significantly from the first batch. Since we had not enough gelator of batch 1 for both amplitude and frequency sweeps, we decided to perform frequency sweeps only, assuming that a shear strain of $\gamma = 0.5$ % is within the LVE-region of the gel. For batch 2 and batch 3, both amplitude and frequency sweeps were performed. Following the amplitude sweeps of batch 2 and batch 3, we chose a shear strain of $\gamma = 0.1$ % for the frequency sweep for batch 2, and a shear stress of $\tau = 30$ Pa, which in this case roughly corresponds to a shear strain of $\gamma = 0.15$ %, for batch 3. We compared the frequency sweeps of both the binary CDEAB system and the ternary C_{14}TAB system gelled with 1 wt% of each gelator batch. In the case of the binary CDEAB system, we found that batch 1 performed the best, with batch 3 a close second. Batch 2, on the other hand, performed much worse, suggesting a more liquid-like behavior at low frequencies. In the case of the ternary C_{14}TAB system, batches 2 and 3 performed much worse than batch 1, with both batches having much lower G' and G'' values than batch 1. In addition, the G'' values are greater than the G' values over the entire frequency range for batch 2, while batch 3 has a crossover point for the G' and G'' values. We also examined the time-dependent evolution of the gel strength of batch 2 and batch 3. We found that while both batches ultimately reach similar G' and G'' values after 20 h, the gelation of gels formed by batch 2 is delayed by 1-2 h, while the gels formed by batch 3 start gelling immediately. The differences between the batches showed the necessity of using only one batch in a series of experiments, as multiple batches would lead to incomparable results. In the following experiments, we only used the gelator of batch 3.

3.3 Time Dependency of Nematic LLC Gel Formation

Having shown that it is possible to gel the calamitic nematic N_C phases of the binary H_2O – *N*,*N*-dimethyl-*N*-ethyl-1-hexadecylammonium bromide (CDEAB) and the ternary H_2O – *N*,*N*,*N*-trimethyl-1-tetradecylammonium bromide (C_{14}TAB) – *n*-decanol systems with the low molecular weight gelators BHPB-6, BHPB-10 and BHPB-13 we studied the time dependence of our gels. In the case of the binary CDEAB system we used a surfactant mass fraction μ_{bin} = 31 wt%. For the ternary C_{14}TAB system we used a surfactant mass fraction μ_{ter} = 31 wt% and a surfactant-to-cosurfactant ratio was set at σ = 0.93. For the following studies, we looked exclusively at gels formed with BHPB-6. First, in the preliminary studies, we looked at gel samples that were generally aged for over 24 hours. This was due to the preparation conditions that saw them aged in glass vials before being either transferred to the rheometer or placed in capillary tubes. The 24 h aging time assured a smooth transfer of the sample, and a sufficiently complete gelation process, however, the exact gelation time was not known. In addition, there were distinct differences in the visual appearance of the two gelled LLC systems (Figure 3.12).

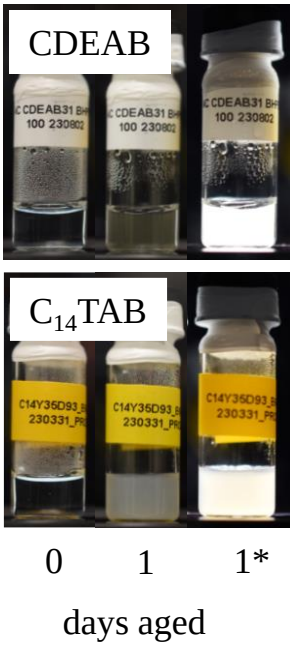

Figure 3.12: Gel aging of the binary CDEAB system (top) and the ternary C_{14}TAB system (bottom) gelled with 1.0 wt% BHPB-6. Images of the samples were taken immediately after preparation and after 1 day. The images of the sample after 1 day were also taken using crossed polarizers (*) to show the existence of the birefringent N_C phase. The image was adapted from [Dom24].

Looking at Figure 3.12, one sees visual differences between the visual appearance of the binary CDEAB and the ternary C_{14}TAB system. In the case of the binary CDEAB system the sample remains clear throughout the first 24 h while the ternary C_{14}TAB system begins to turn turbid after approximately 3 to 4 h, turning fully turbid within 24 h. This difference in behavior is surprising given that both surfactants are very similar, with the major difference between the two surfactant systems being the inclusion of the cosurfactant *n*-decanol in the ternary C_{14}TAB system. *n*-Decanol is a good solvent for BHPB-6 and could allow for different interactions during the gelation process explaining the different visual behavior of the two systems. We decided to more closely study the aging process of the two systems within the first 20 hours using rheology. To study the initial gelation, we measured the rheological behavior of samples heated over the sol-gel transition temperature $T_{sol\text{-}gel}$ ($\geq$ 90°C) and cooled to 20°C between the rheometer plates. The samples were then measured over the course of 20 h. The results can be seen in Figure 3.13.

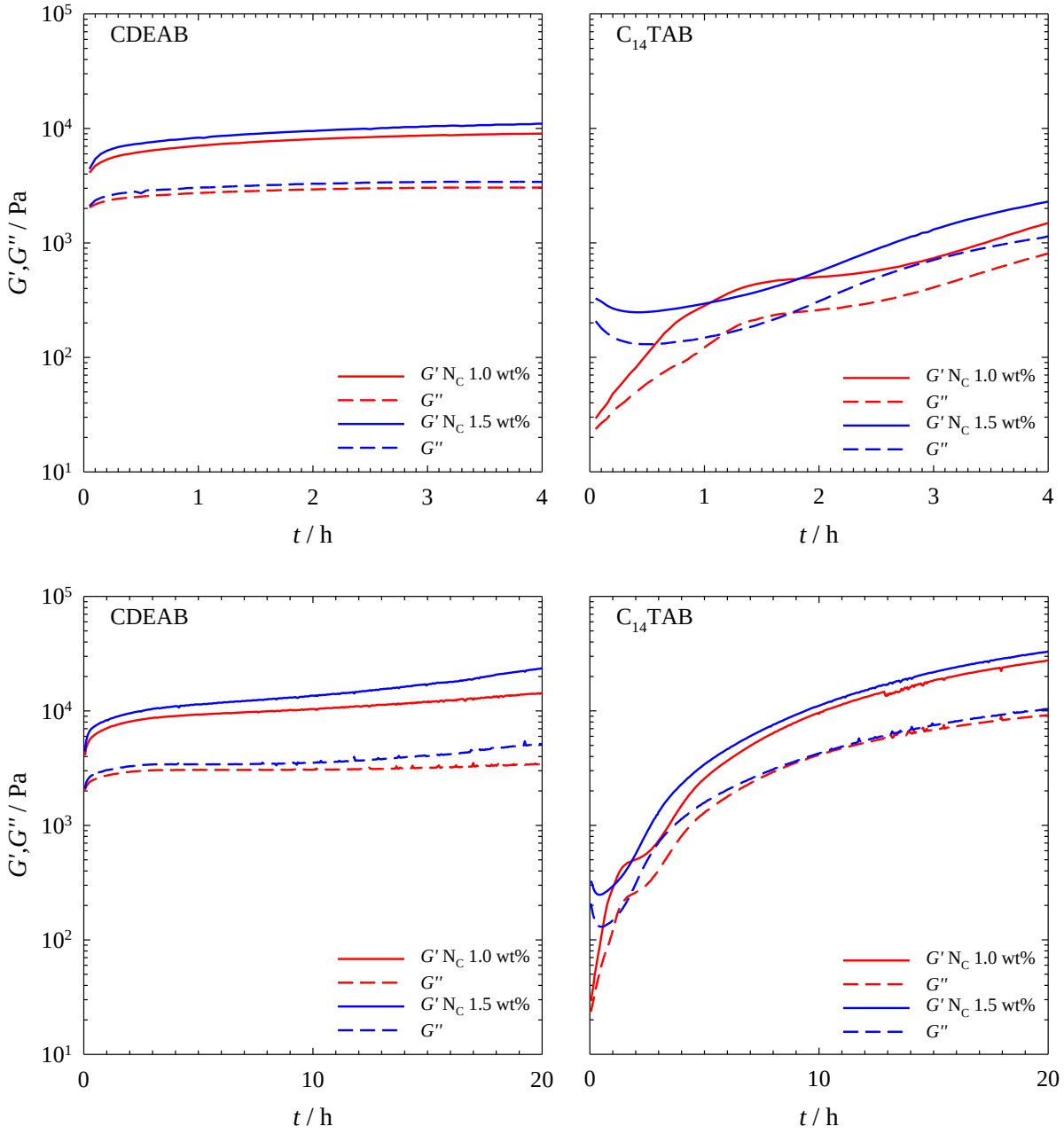

Figure 3.13: Storage modulus $G^{'}$ (straight line) and loss modulus $G^{''}$ (dashed line) of (left) the binary CDEAB system and (right) the ternary C_{14}TAB system measured at a constant temperature of T = 20°C, shear strain γ = 0.1%, and frequency of ω = 1 s^{-1}. The N_C phases were gelled using 1.0 wt% (red) and 1.5 wt% (blue) BHPB-6. The top images cover the first 4 hours, while the bottom images cover the full twenty hours of the measurement. The image was adapted from [Dom24].

We observed different behaviors of the two N_C phases gelled with BHPB-6 at two different gelator concentrations, namely at 1.0 wt% and 1.5 wt%. The gel formed in the binary N_C phase has high $G^{'}$ and $G^{''}$ values, approximately 10^4 and $2 \cdot 10^3$ Pa, respectively, within one hour, which continue to increase slightly over the course of two hours. The gel formed with 1.5 wt% of the

gelator was only marginally stronger than that formed with 1.0 wt%. The gel formed in the ternary N_C phase has much lower G' and G'' values at the beginning and the gelator concentration has a larger influence. The G' and G'' values of the sample gelled with 1.0 wt% BHPB-6 start at about 20 Pa, while those of the sample gelled with 1.5 wt% start at about 300 Pa and 200 Pa, respectively. The final G' and G'' values of the ternary gels eventually exceed those of their binary counterparts, but for the ternary gels it takes several hours to form as opposed to the binary gels which forms within one hour. In addition, the ternary gel containing 1.0 wt% BHPB-6 has a temporary plateau after two hours before the G' and G'' values begin to rise again to reach their final value. This plateau is not observed in the ternary gel gelled with 1.5 wt% BHPB-6, nor in the binary gels at either gelator concentration. We attribute this plateau as well as the general difference in the curves to the presence of *n*-decanol, which is a good solvent for BHPB-6. This, in turn, should affect the formation of the nematic N_C phase as some of the required cosurfactant would be used to keep the gelator dissolved. During the gelation process the cosurfactant would be released allowing for the formation of the nematic N_C phase. To test this theory, we heated the gelled samples of the binary CDEAB and ternary C_{14}TAB systems to 130°C and observed the formation of the nematic N_C phase during cooling. Note that T = 130°C is well above the clearing temperature T_{Cl} of the binary CDEAB system (T_{Cl} = 30°C) and ternary C_{14}TAB system (T_{Cl} = 32°C) as well as the sol-gel transition temperature $T_{sol\text{-}gel}$ of the gelator, to reach the molecular isotropic phase. We then cooled the samples to below their clearing temperatures T_{Cl} and observed the formation of the nematic N_C phase through crossed polarizers (Figure 3.14).

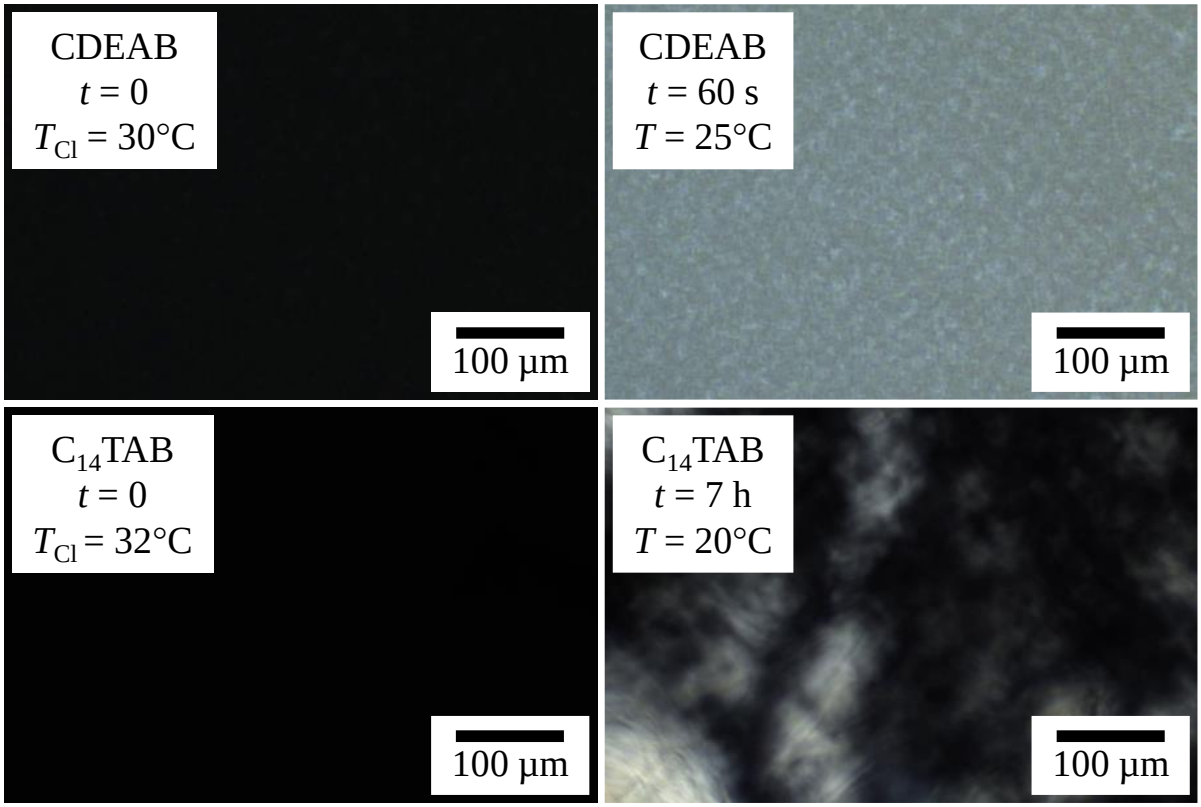

Figure 3.14: POM images between crossed polarizers of the binary CDEAB system (top) and the ternary C_{14}TAB system (top) recorded shortly after reaching the clearing temperatures (left), which for the binary CDEAB system was T_{Cl} = 30°C and for the ternary C_{14}TAB system was T_{Cl} = 32°C, and after the formation of the nematic N_C phase (right). All samples were gelled with 1 wt% BHPB-6. The image was adapted from [Dom24].

In Figure 3.14 we can see that in the binary CDEAB system the N_C phase forms within a minute, while in the ternary C_{14}TAB system the N_C phase takes up to 7-10 hours to form, with some birefringence visible after 1-3 hours. This supports our assumption that the *n*-decanol is not readily available to form the nematic N_C phase after cooling from the molecular isotropic phase (T = 130°C). Furthermore, the delay of 1-3 hours before the first birefringent regions, i.e. the nematic N_C phase, are observed is consistent with the plateau that we observe in Figure 3.13 for the sample gelled with 1.0 wt%. The increase of the G' and G'' values after 1-3 hours can then be attributed to the gelator that becomes available as more and more of the *n*-decanol is incorporated into the micelles. For the sample with the higher gelator concentration of 1.5 wt% we assume that the excess gelator concentration is sufficient to maintain a regular but slower gel growth compared to the binary LLC gel, hence the absence of a plateau. The binary CDEAB system, which has no cosurfactant, obviously has fewer interactions with the gelator. As a consequence, the growth of the fibers is faster. In the case of the ternary gel the stronger

interactions between the gelator and the liquid crystal allow a much faster transition to the more stable turbid gel, which is why we do not observe a clear gel after 24 hours. We can attribute the difference of the two systems to the varying nucleation and growth behavior of the two systems. In the case of the binary CDEAB system the limited interactions of the lyotropic liquid crystal (LLC) and the gelator forces the gelator out of the solubilized state, causing many nucleation seeds to form. For the ternary C_{14}TAB system, however, the favorable interactions of the LLC with the gelator causes fewer gelator molecules to be available, thus leading to fewer nucleation seeds which then form bigger bundles. The amount and length of the fibers is responsible for their visual appearance. In the binary CDEAB system the bigger amount of smaller fibers causes the gel to appear clear, while the fewer bigger fibers of the ternary C_{14}TAB system are able to refract light, rendering the sample turbid.

After studying the first 20 hours of the gel formation we studied the following 14 days in order to observe any changes in the binary CDEAB system and ternary C_{14}TAB system that may or may not be associated with visual changes.

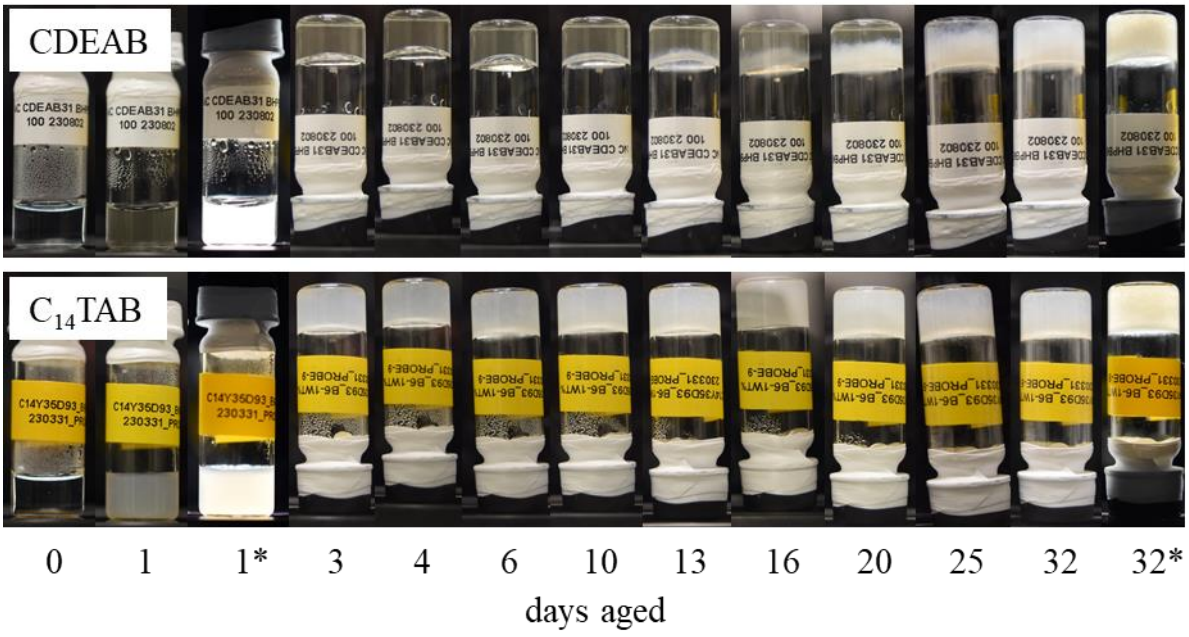

Figure 3.15: Gel aging of the binary CDEAB system (top) and the ternary C_{14}TAB system (bottom) gelled with 1.0 wt% BHPB-6. Images of the samples taken after 1 day and 32 days were also taken using crossed polarizers (*) to show the existence of the birefringent N_C phase. The image was adapted from [Dom24].

Looking at Figure 3.15, one sees that the binary CDEAB system begins to slowly turn turbid after 10 to 13 days. It then took up to 20 additional days for the sample to fully turn turbid. For

the ternary sample visual changes were less apparent although the turbidity did increase over the course of 32 days. We then intended to follow the development of the gel development using rheology, but unlike our experiment in Figure 3.13, we did not gel our samples inside the rheometer for practical reasons. Instead, we chose to gel them outside of the rheometer and to transfer them onto the rheometer plates after selected aging times. The samples were allowed to equilibrate for two hours before starting the measurement. The results are shown in Figure 3.16:

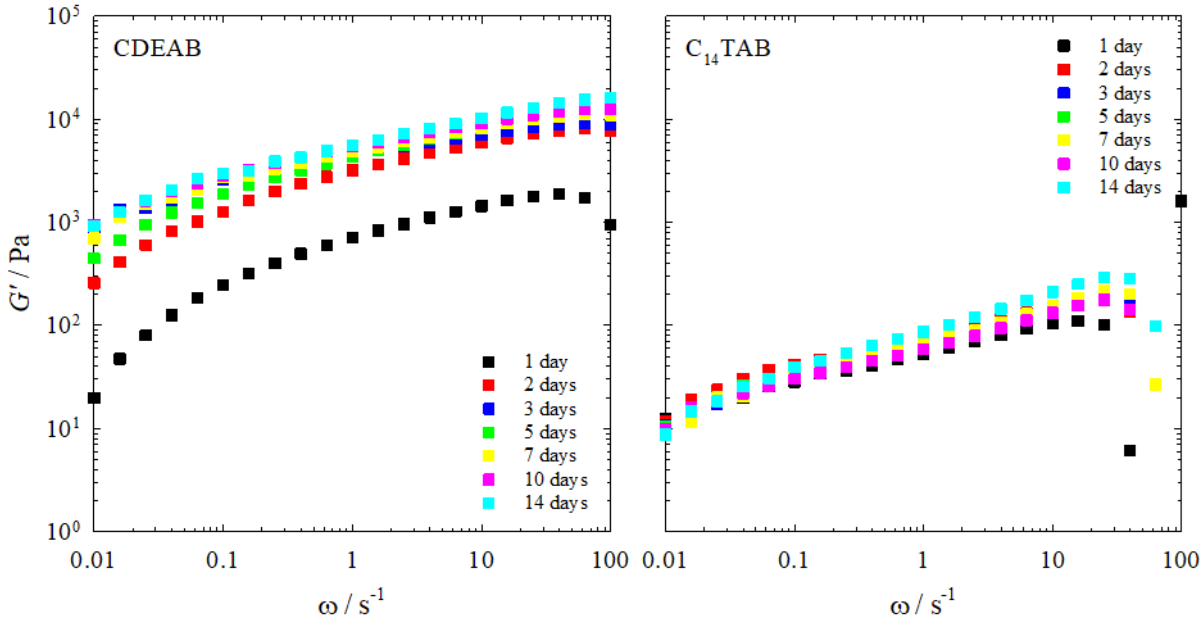

Figure 3.16: Frequency sweeps of the binary LLC (left) and the ternary LLC (right) gelled with a gelator mass fraction η = 1 wt%, temperature T = 20°C and the strain γ = 0.1% and aged for up to 14 days. The loss moduli G'' were omitted for the sake of clarity. The image was adapted from [Dom24].

It can be seen that the samples hardly change over the course of 14 days, the only exception being the sample aged for 1 day of the binary CDEAB system. It is also observed that the G' values are lower in the case of the binary CDEAB system and much lower in the case of the ternary C_{14}TAB system than those observed in Figure 3.13 after 20 hours. We compared the G' and G'' values at ω = 1 s^{-1} of the aged samples of Figure 3.16 with the final values obtained after 20 h in Figure 3.13 and plotted them in Figure 3.17.

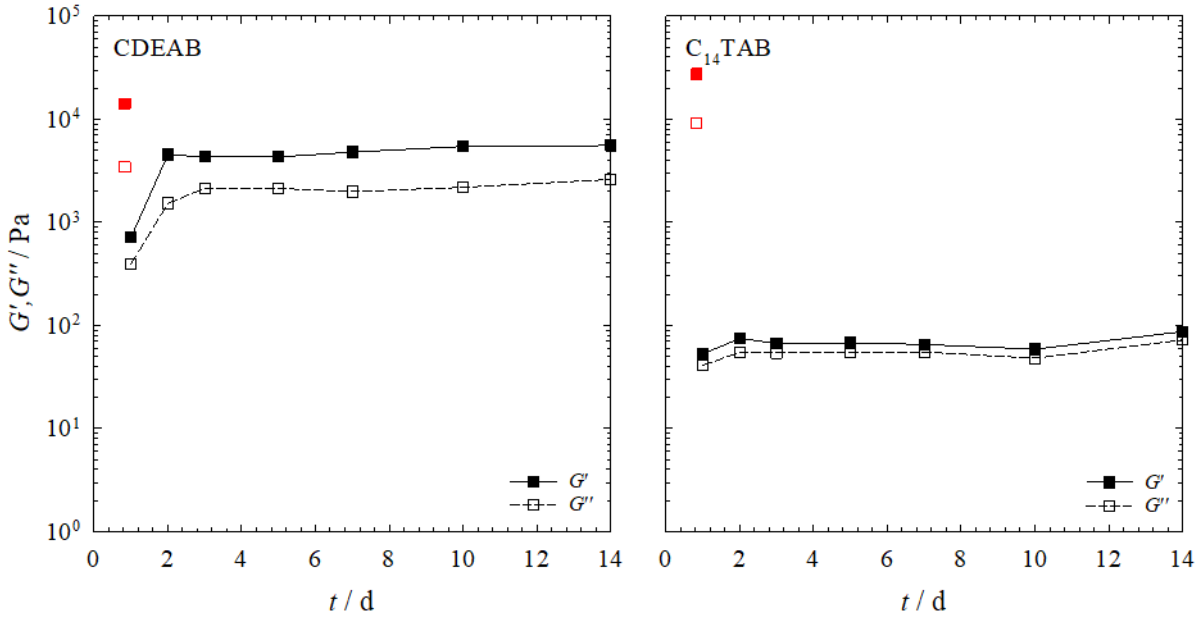

Figure 3.17: Storage modulus $G^{'}$ (filled boxes) and loss modulus $G^{''}$ (empty boxes) of the N_C phase of the binary CDEAB system (left) and the ternary C_{14}TAB system (right), aged for 1-14 days outside of the rheometer (black) and after 20 h of aging within the rheometer (red). All samples were gelled with a gelator mass fraction $\eta = 1.0$ wt%, and measured with at the temperature $T = 20$°C, at a frequency of $\omega = 1\ s^{-1}$ and the strain $\gamma = 0.1$%. The image was adapted from [Dom24].

One sees that the $G^{'}$ and $G^{''}$ values of the samples gelled outside the rheometer do not vary according to their gelation time. Furthermore, one clearly sees the difference between the binary CDEAB system, where apart from the first day only a small decrease in the $G^{'}$ and $G^{''}$ values is observable, and the ternary C_{14}TAB system where the $G^{'}$ and $G^{''}$ values have decreased by two orders of magnitude. We attribute the decrease in gel strength to the transferring process from the glass vial used for aging to the rheometer plate. Furthermore, the gel samples of the binary gel were all clear whereas those of the ternary sample were all turbid. We thus hypothesize that the gel formed by the binary CDEAB systems were much more plastic/elastic than those formed by the ternary C_{14}TAB system which favors more rigid gels. This was in line with visual observations showing the binary gels to be much more plastic/elastic and the ternary gels to be more rigid. We hypothesize that the difference between the ternary gel samples gelled within and without the rheometer is due to the rigidity of the gel network that, in the case of the samples gelled outside the rheometer, is destroyed during the transfer process. The binary gel, however, due to its more plastic nature is less affected. To verify this, we compared the binary and ternary gel samples gelled for 20 h within the rheometer with 1 wt% BHPB-6, as seen in

Figure 3.13, with two samples that were gelled outside the rheometer for 7 days and then measured for 20 h (Figure 3.18).

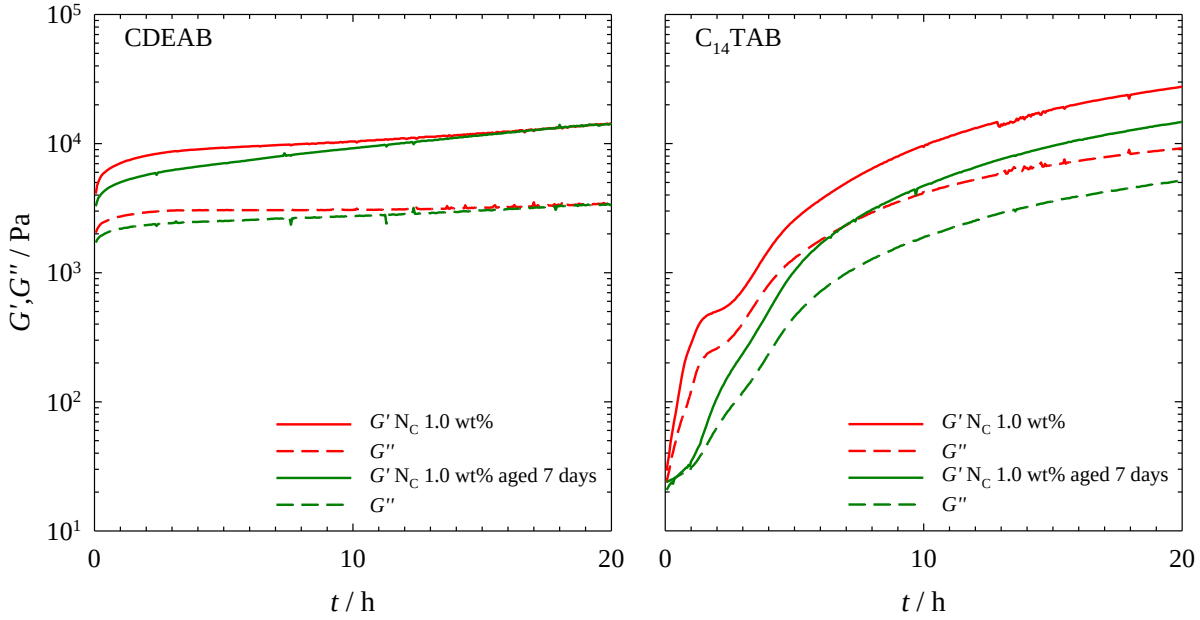

Figure 3.18: Storage modulus G' (straight line) and loss modulus G'' (dashed line) of (left) the binary CDEAB system and (right) the ternary C_{14}TAB system measured at a constant temperature of T = 20°C, shear strain γ = 0.1%, and frequency of ω = 1 s^{-1}. The N_C phases were gelled using 1.0 wt% BHPB-6. The gelation took place within the rheometer for 20 h (red) or outside the rheometer for 7 days, and then the samples were measured within the rheometer for 20 h (green). The image was adapted from [Dom24].

Looking at Figure 3.18, one sees that the G' and G'' values of the samples gelled outside of the rheometer and within follow the same trend. In the case of the binary CDEAB system, the G' and G'' values begin at a high value with the sample gelled outside of the rheometer starting at slightly lower values but reaching the same G' and G'' values of the sample gelled within the rheometer within 20 h. The ternary C_{14}TAB system shows greater differences between the gels formed within or outside the rheometer. The plateau which in the case of the gel formed within the rheometer appears after two hours, and is attributed to the delayed formation of the N_C phase, is not present in the aged sample as the transferal process does not influence the LLC phase. Furthermore, the absolute G' and G'' values of the aged sample do not reach the same values as the sample gelled within the rheometer, as opposed to the binary CDEAB system where the G' and G'' values of the two samples reach the same levels. Despite the fact that the transferal process destroyed the gel structure of the sample gelled outside the rheometer, the

sample regained its gel strength at a rate comparable to the sample gelled within the rheometer, showing self-healing properties.

Finally, we studied the different time-dependent development of the gel network in the binary CDEAB system and the ternary C_{14}TAB system using freeze fracture electron microscopy (FFEM). We studied two samples for each system after differing aging times. In the case of the binary CDEAB system, the first sample was aged for three days, while the second sample was aged for 12 days. The first sample was fully transparent, whereas the second sample turned completely turbid within 12 days. Given that the two binary samples are so visually distinct we intended to see whether a similar difference can be observed using FFEM. In the case of the ternary gel, the samples turn turbid within one day and thus both the younger and older sample were both turbid. The first sample was aged for two days, while the second sample was aged for three months. The FFEM images are shown in Figure 3.19.

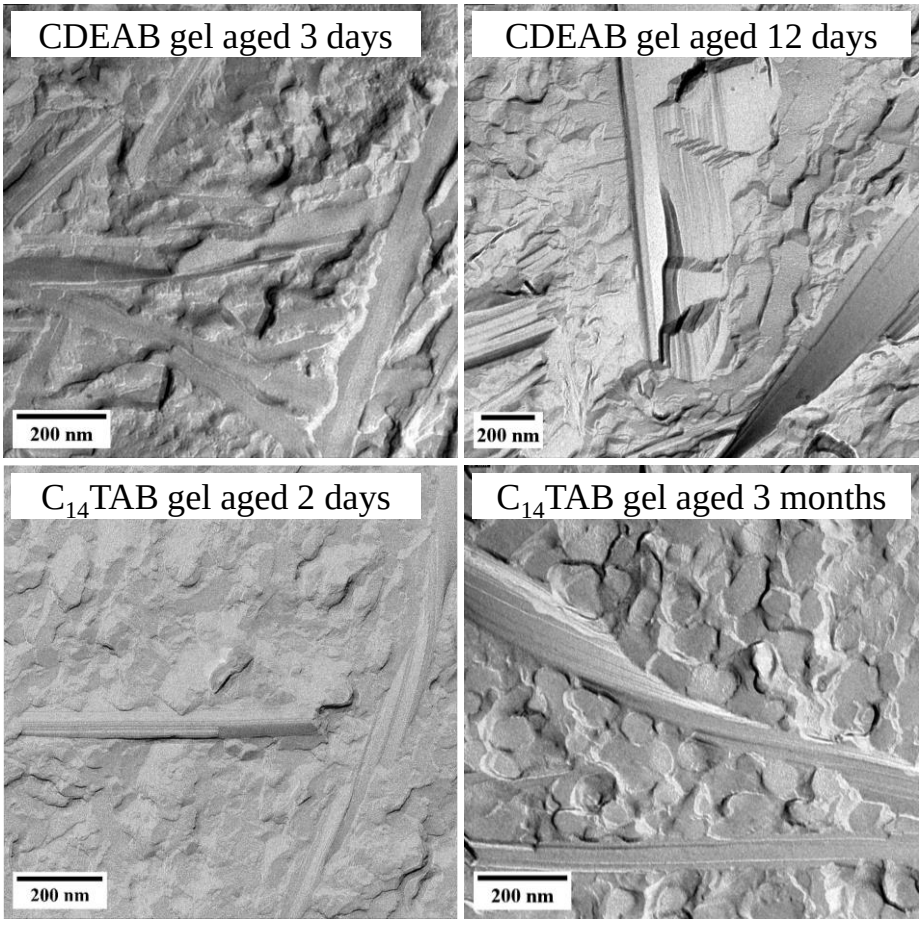

Figure 3.19: FFEM images of the gelled N_C phase of (top) the binary CDEAB system and (bottom) the ternary C_{14}TAB system with different ages gelled with 1.0 wt% BHPB-6. The age of the samples is indicated in the picture. The image was adapted from [Dom24].

It is shown in Figure 3.19 that for the binary CDEAB system a notable difference is visible between the sample gelled for 3 days (top, left) and the sample gelled for 12 days (top, right). For the younger samples we observed either single flat ribbons or small stacks of ribbons. The average width of these ribbons was about 60 nm, with some having widths of up to 125 nm. The shape of the fibers is in line with those observed in binary gels of cyclohexane gelled with BHPB-6 [Her23,Sim13]. For the turbid sample aged for 12 days, we observed significantly broader ribbons width an average width of 220 nm. Additionally, the stack size observed in the turbid samples were vastly greater than those observed in the transparent sample. The thickness of most of the observed stacks were between 100 and 850 nm with some stacks being over 1 µm thick. In most cases the exact thickness of the fibers could not be determined as the preparation of the sample favors fractures at the weakest points. As such the fractures would occur most frequently along the ribbon as opposed to through it. Some smaller fiber bundles showed twisting, however, the thicker stacks did not show any twisting. For the ternary C_{14}TAB system both the sample aged for 2 days (bottom left) and the sample aged for 3 months (bottom right) were turbid and no visual difference between the samples was observable. The FFEM images also only show minor differences between the younger and aged sample. In both we were able to observe stacked ribbons with widths up to 170 nm, in the case of the sample aged for 2 days, and up to 200 nm, in the case of the sample aged for 3 months. We observe some thicker stacks in the aged sample compared to the young sample, however, the thickness of the stacks is much lower compared to those of the binary aged sample. To summarize, the macroscopic visual changes are in line with structural changes of the gel network. In the case of the binary CDEAB system the change from transparent to turbid can be associated to the change from individual fibers or fibers with small stacks to much larger bundles with increased thickness and width. In the case of the ternary C_{14}TAB system, where both samples were turbid, neither significant macroscopic nor microscopic changes could be observed between the younger and aged sample. Furthermore, BHPB-6 forms much larger fibers compared to other gelators used to gel lyotropic liquid crystals [Die19a,Die20b,Ste19a,Ste19b]. Despite the large size of the fibers, when compared to DBS, whose fibers possess a width of 8-18 nm [Ste19a], or 12-HOA, whose fibers possess a width of ~27 nm [Die19a], which can go up to 850 nm, the nematic N_C phase remains intact. This is in contrast to attempts to gel the N_C phase using 12-HOA where the gelator induced a phase transition to the lamellar phase [Die19a].

Conclusion

We studied the time dependence of the gel formation in the binary CDEAB system and the ternary C_{14}TAB system on two time scales. Firstly, we studied the gel formation within the first 20 h. Over the course of the first 20 h, the sample of the binary CDEAB system gels, while remaining transparent. On the other hand, in the same time frame, the ternary C_{14}TAB system becomes completely turbid. We also followed the gelation of both systems, gelled with either 1.0 wt% or 1.5 wt% BHPB-6, using rheology, by applying a constant shear strain of $\gamma = 0.1\%$ and a frequency of $\omega = 1\ s^{-1}$ for 20 h. The results showed that the two systems behave quite differently. To begin, the binary CDEAB system has high G' and G'' values immediately after the start of the measurements at both gelator concentrations. On the other hand, the C_{14}TAB system starts with much lower G' and G'' values that slowly increase over the course of 20 h to finally exceed those of the binary CDEAB system. Furthermore, the sample gelled with 1.0 wt% BHPB-6 has a local plateau at 2-3 h after the start of the gelation. Using polarized optical microscopy (POM), we studied the development of the calamitic nematic N_C phase over the same time scale. We found that, in the case of the binary CDEAB system, the N_C phase starts to form immediately after the phase transition temperature $T = 30°C$ is reached. In the case of the ternary C_{14}TAB system, the formation of the N_C phase is delayed, starting after 1-3 h and taking up to 7-10 h to complete. This time frame is consistent with the plateau we observed in the rheology measurements and could be explained by the interactions between the cosurfactant *n*-decanol and the gelator BHPB-6. *n*-Decanol is a good solvent for BHPB-6, which explains the delayed formation of the N_C phase and the slowed gel formation. The *n*-decanol needed to solubilize BHPB-6 cannot be incorporated into the N_C phase, delaying its formation, while the gel network takes longer to form because some of the gelator remains solubilized. The process of the incorporation of *n*-decanol into the N_C phase is diffusion controlled, which explains the long time frame to form both the N_C phase and subsequently the gel network. Secondly, we studied the gel formation after 20 h up to 32 d. To begin, we continued to observe the macroscopic appearance of the samples of the binary CDEAB system and the ternary C_{14}TAB system. In the case of the binary CDEAB system, we observe that the initially transparent gel sample begins to slowly turn turbid after 10-13 d and becomes completely turbid after 32 d. The ternary C_{14}TAB system became completely turbid within 1 d and continued to become more turbid over the course of 32 d. We intended to follow the aging of the gel using rheology, but since it was not feasible to keep a sample in the rheometer for this extended period, we gelled multiple samples in separate vials for up to 14 d and transferred the gel to the rheometer after sufficient aging. The measurements obtained from the externally

aged samples revealed that their G' and G'' values are lower compared to the samples which were gelled in the rheometer. Here, the values of the externally gelled ternary C_{14}TAB system were much lower than those of the binary CDEAB system. The transfer process from the vial to the rheometer plate damages the sample resulting in lower G' and G'' values compared to the values obtained for the samples that were gelled in the rheometer. We note that the binary CDEAB system was less affected, which we attribute to its higher plasticity compared to the more rigid gel network of the ternary C_{14}TAB system. We verified this claim by comparing the time-dependent development of the gels gelled inside the rheometer for 20 h with that of the gels aged outside the rheometer for 7 d and then placed on the rheometer and also measured for 20 h. In the case of the binary CDEAB system, we found that the sample aged outside the rheometer had slightly lower G' and G'' values than the sample gelled inside the rheometer, following the same general trend. In the case of the ternary C_{14}TAB system, we also see a similar trend between the gel aged inside and outside of the rheometer, with the gel aged outside of the rheometer having slightly lower G' and G'' values. Finally, we used freeze fracture electron microscopy (FFEM) to observe the differences between samples aged for a short time and samples aged for a longer time. In the case of the binary CDEAB system, we compared a sample aged for 2 d, which was fully transparent, to a sample aged for 12 d, which was already turbid. The sample aged for 12 d showed significantly larger and thicker fiber stacks than the sample aged for only 2 d. For the ternary C_{14}TAB system, on the other hand, the differences between a sample aged for 3 d and one aged for 3 months were negligible. This suggests that the change from transparent to turbid in the binary CDEAB system is accompanied by changes in the gel structure, while for the ternary C_{14}TAB system, which is turbid from the beginning, no such significant changes occur.

3.4 Orientation of Nematic LLC Gels

Orientation of Nematic LLC Gels

After having studied the aging of the gelled LLC samples, we turned our attention to the orientation of the gelled LLC samples. Our goal was to find out if oriented LLC gels can be used as actuators. For them to work as actuators, the reversible phase transition of the LLC must lead to a reversible change in the shape of the gel network. We again used two calamitic nematic N_C phases gelled with either 1.5 wt% or 1.0 wt% BHPB-6, namely the binary system H_2O – *N*,*N*-dimethyl-*N*-ethyl-1-hexadecylammonium bromide (CDEAB) and the ternary system H_2O – *N*,*N*,*N*-trimethyl-1-tetradecylammonium bromide (C_{14}TAB) – *n*-decanol. For the binary CDEAB system, a surfactant mass fraction of μ_{bin} = 31 wt% was used. For the ternary C_{14}TAB system, we used a surfactant mass fraction of μ_{ter} = 31 wt% and a surfactant-to-cosurfactant ratio of σ = 0.93. We used a magnetic field with a strength of 1.0 T to align the samples. A small portion of each gel sample was filled into a borosilicate flat capillary, which was flame-sealed. The sample was then heated to T = 130°C in order to homogenize and reverse any orientation that occurred during the filling process. The heated sample was then placed in a magnetic field where it cooled to room temperature and remained exposed to the magnetic field for 24 h. The idea behind the magnetic field alignment was to influence the orientation of the nematic N_C phase so that the gel network, which generally takes longer to form than the N_C phase, grows within the N_C phase. To verify that the magnetic field is able to orient the nematic N_C phase and subsequently the gel network, images were taken with a microscope. To confirm the orientation of the nematic N_C phase, the sample was observed between crossed polarizers. The unaligned nematic N_C phase possesses neither a bright nor a dark position, as multiple polydomains with different orientations in relation to the crossed polarizers exist simultaneously. The gel network within the same sample should also have no orientation. For an oriented nematic sample, a distinct bright and dark position can be expected because the nematic phase should be oriented along the direction of the applied magnetic field, even when the magnetic field is no longer present. If the sample is oriented this way, we can expect a bright position when the sample is placed at a 45° angle with respect to either polarizer and a dark position when the sample is placed parallel to either polarizer. To observe whether the gel network is likewise oriented in the same sample, the polarizers were simply removed. The images of the oriented nematic phase are shown in Figure 3.20 and the images of the oriented gel are shown in Figure 3.21.

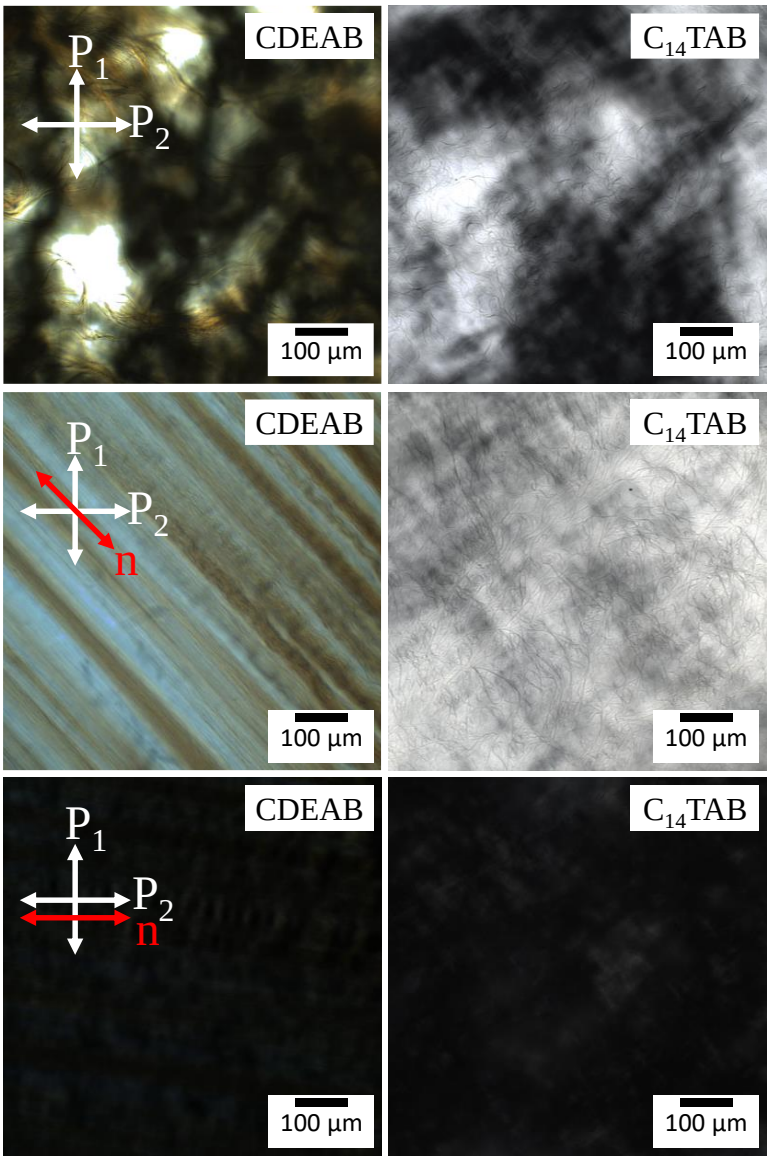

Figure 3.20: Polarized optical microscopy (POM) images of unaligned samples (top) and magnetically aligned samples (middle, bottom) of the binary CDEAB system gelled with 1.5 wt% BHPB-6 (left) and the ternary C_{14}TAB system gelled with 1.0 wt% BHPB-6 (right) between crossed polarizers. The images of the magnetically aligned samples were taken in a manner that the direction of the previously applied magnetic field was either at an angle of 45° (middle) or at an angle of 0°/90° (bottom) to the polarizers. The image was adapted from [Her25].

Looking at Figure 3.20 (left), one sees that the unaligned binary CDEAB sample (top left) between crossed polarizers shows both bright and dark spots. The nematic N_C phase is brightest when the director is at an angle of 45° to the polarizers and at its darkest when the director is parallel to one of the polarizers. The presence of both bright and dark regions indicates that the sample is not aligned and that multiple polydomains are present. In the areas visible due to the

birefringence the fibers of the gel network can also be seen. Like the nematic N_C phase, the gel network does not appear to be oriented. On the other hand, the sample prepared under a magnetic field shows a strong orientation. It can be seen that depending on the orientation of the sample with respect to the polarizers, the sample has a distinct bright position (middle left) and a dark position (bottom left). As mentioned before, when the director of the nematic N_C phase, which follows the direction of the magnetic field during sample preparation, is at an angle of 45° to both polarizers, the birefringence is the strongest. The sample has a bright position, where the entire sample is birefringent, and a dark position, with almost no birefringence when the sample is rotated 45° in either direction. This indicates a high degree of orientation of the N_C phase. Furthermore, in the bright position, the fibers of the gel network are also visible and one can see that they have grown in the same direction as the applied magnetic field. Looking at the unaligned gel sample of the ternary C_{14}TAB system (top right), similarly to the binary CDEAB system, we observe both bright and dark spots, confirming the existence of several polydomains but no overall orientation. In the illuminated position we can also see the gel fibers, which do not appear to be oriented. For the oriented gel sample of the ternary C_{14}TAB system, we again see a bright position (middle right) and dark position (bottom right), i.e. that the N_C phase is oriented. The fibers of the gel network can also be seen, but unlike the gel fibers of the oriented binary CDEAB system, they do not appear to be as oriented as in their binary counterpart. We examined the gel fibers in more detail in the absence of the crossed polarizers. The images are shown in Figure 3.21.

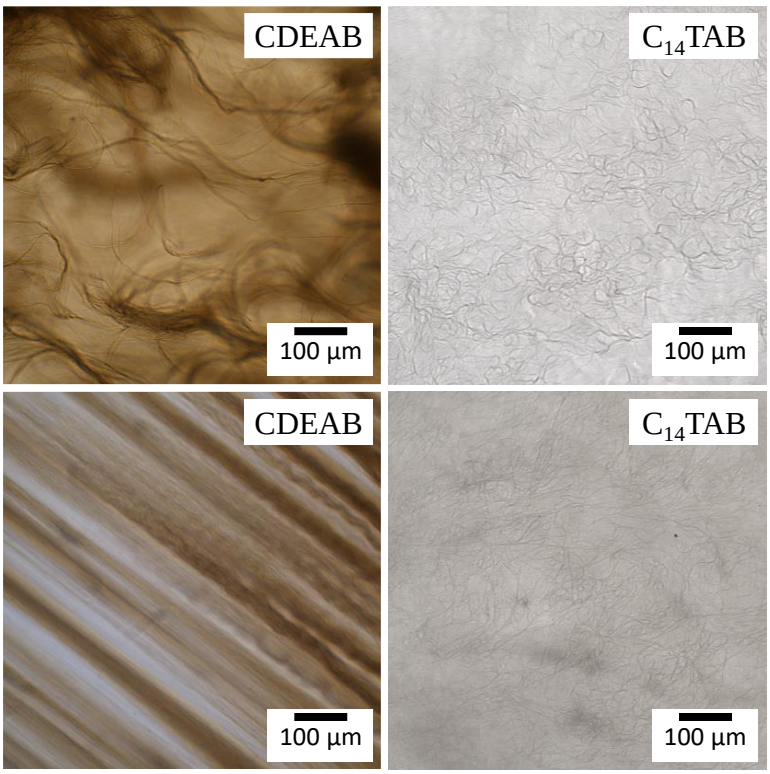

Figure 3.21: Microscopy images of unaligned samples (top) and magnetically aligned samples (bottom) of the binary CDEAB system gelled with 1.5 wt% BHPB-6 (left) and the ternary C_{14}TAB system gelled with 1.0 wt% BHPB-6 (right). The image was adapted from [Her25].

In contrast to the N_C phase in Figure 3.20, we observe differences in the degree of orientation of the gel fibers between the binary CDEAB system and the ternary C_{14}TAB system. In the case of the binary CDEAB system, we see a strong difference in the appearance of the gel fibers of the unaligned sample (top left), which was prepared without a magnetic field, and the aligned sample (bottom left), which was prepared in the presence of a magnetic field. The unaligned gel sample has wavy fibers which are present both as individual fibers and as larger clusters. The aligned gel sample has a high degree of orientation with all fibers being parallel to each other, following the direction of the magnetic field. The fibers also form some bigger bundles which appear darker in the image. In the case of the ternary C_{14}TAB system, the sample prepared without a magnetic field (top right) and the sample prepared in the presence of a magnetic field (bottom right) are indistinguishable. Both have fibers that are wavy and do not appear to be oriented. This is contrary to our expectation since both the nematic N_C phase of the binary CDEAB system and the ternary C_{14}TAB system were aligned using the magnetic

field. Despite the successful alignment of the N_C phases, only the gel network of the binary CDEAB system is visibly aligned, while the gel network of the ternary C_{14}TAB system does not appear to be aligned. We attribute this difference between the two systems to the delayed formation of the nematic N_C phase, as discussed in Section 3.3. In the case of the binary CDEAB system, both the formation of the nematic N_C phase, as well as the formation of the initial gel network, are fast processes. However, the N_C phase, which is formed within minutes after cooling to its clearing temperature T_{Cl} = 30°C, is oriented from the beginning by the magnetic field. This, in turn, allows the N_C phase to act as a template for the gel growth, promoting gel growth in parallel to the direction of the magnetic field. In contrast to the binary CDEAB system, the formation of the N_C phase as well as the gel growth in the ternary C_{14}TAB system takes much longer. The N_C phase can take up to 1-3 hours to start forming, and up to 7-10 hours to fully form. During this time the gel network grows without the templating effect of the N_C phase, i.e. that some parts of the gel network will begin to grow isotropically in the absence of the templating N_C phase. Therefore, the image of the sample gelled without the presence of the magnetic field is almost indistinguishable from the image of the sample gelled within the magnetic field. This gives the impression that the gel network formed in the ternary C_{14}TAB system is not oriented, but further examination of the sample revealed not only its orientation, but also a memory effect of the gel on the N_C phase as will be discussed in the following.

Memory of Nematic LLC Gels

Since our initial intention was to test whether an aligned nematic LLC gel can act as an actuator, we investigated whether the oriented gel acts as a template to maintain the orientation of the N_C phase. To test this, we performed two heating cycles. In the first heating cycle, the aligned gel samples were heated to T = 40°C, well above their respective clearing temperatures, and then cooled them to their initial temperature of T = 20°C. During this heating cycle the LLC undergoes a phase transition from the nematic N_C phase to the isotropic L_1 phase and then back to the nematic N_C phase, while the gel network remains unaffected. If the gel network has templating properties, then even in the absence of a magnetic field, the N_C phase should reform with the same orientation as before the heating cycle. In the second heating cycle, the aligned gel samples were heated to T = 130°C, well above the clearing temperatures of the LLCs and above the sol-gel transition temperature of the gel. This was done to show the effect of the absence of a templating gel network on the orientation of the forming N_C phase. The results of the first and second heating cycles are shown in Figure 3.22 and Figure 3.23, respectively.

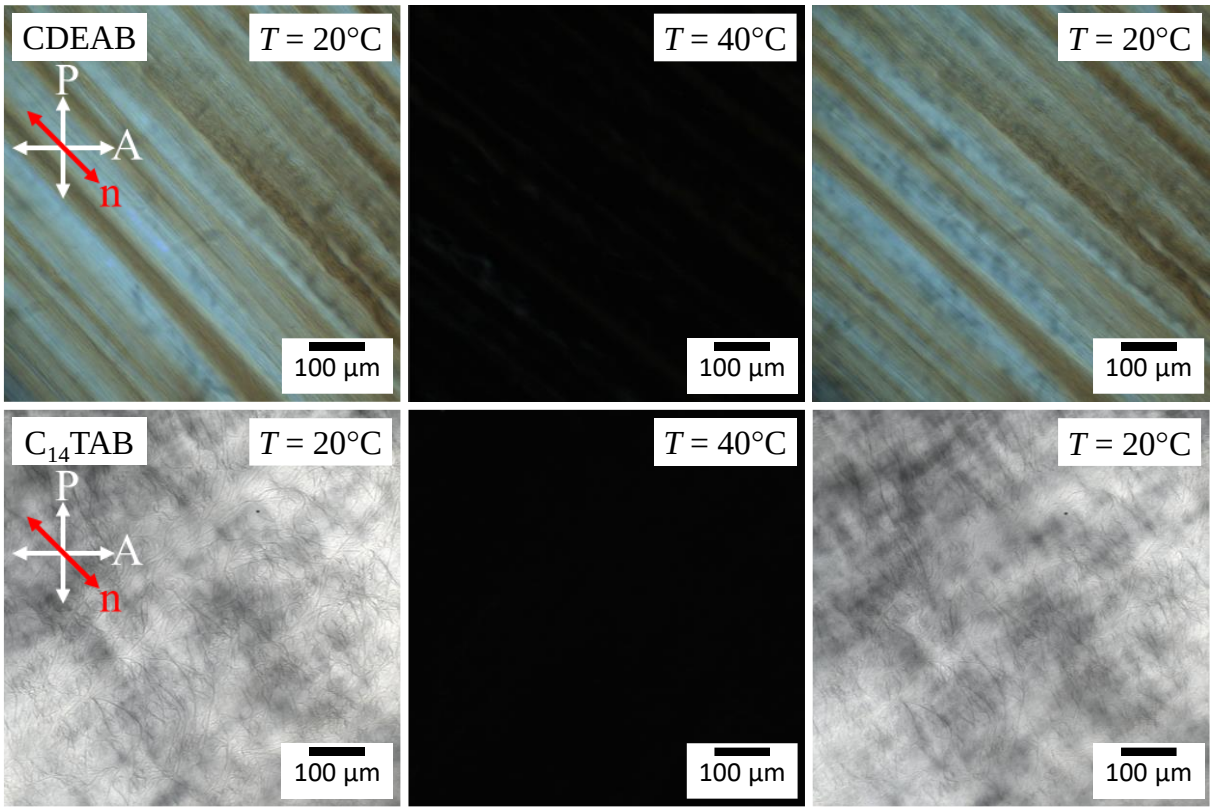

Figure 3.22: POM images of magnetically aligned samples of the binary CDEAB system gelled with 1.5 wt% BHPB-6 (top) and of the ternary C_{14}TAB system gelled with 1.0 wt% BHPB-6 (bottom) between crossed polarizers. The images were taken with the aligned director at a 45° angle relative to the polarizers. The aligned samples were heated from T_1 = 20°C to T_2 = 40°C causing a phase transition from the nematic N_C phase to the isotropic L_1 phase. The samples were then cooled to T_3 = 20°C and the nematic N_C phase formed again with the same orientation as before. The image was adapted from [Her25].

It can be seen that for both the binary CDEAB system and the ternary C_{14}TAB system the N_C phase is reformed after the first heating cycle. When the samples are heated to T = 40°C, the N_C phase undergoes a phase transition to the isotropic L_1 phase, while the gel network remains unaffected as the temperature is well below the sol-gel transition temperature. In the absence of a magnetic field, the reforming N_C phase would normally form without a preferred orientation, with multiple polydomains forming, each with a different director. However, despite the absence of a magnetic field, the reforming N_C phase is oriented in the same direction as before the heating. This can only be explained by the presence of an aligned gel network that acts as a template favoring the formation of the N_C phase in an oriented manner. The presence of an aligned gel network is evident in the case of the binary CDEAB system, as the visible fibers are parallel to each other and oriented in the same direction as the director of the N_C phase. The gel network of the ternary C_{14}TAB system, on the other hand, does not appear to be aligned, but still favors the reformation of the N_C phase in an oriented manner. This shows that, despite the

isotropic appearance, some part of the gel network grew anisotropically. It should also be noted that the reformation of the N_C phase, during the cooling process, occurred within minutes for both systems. This is in contrast to previous observations of the ternary C_{14}TAB system, where the formation of the N_C phase took place over hours. We attribute this difference in the formation time to the temperature from which the sample was cooled and the state of the gel network. In Section 3.3 we described the interactions between the cosurfactant *n*-decanol, which is necessary for the formation of the nematic N_C phase, and BHPB-6. We postulated that *n*-decanol, as a good solvent for BHPB-6, slows gel growth by keeping parts of the gelator solubilized, while also delaying the formation of the N_C phase by using parts of the cosurfactant to keep the gelator solubilized. This explains the slow formation of both the N_C phase and the gel network when cooling from higher temperatures such as T = 130°C used to homogenize the components during sample preparation. It also explains why the N_C phase can reform much faster from T = 40°C, because the gel network is already formed and the cosurfactant is not used to solubilize parts of the gelator. After observing the effect of the aligned gel network on the orientation of the N_C phase during the cooling process from 40°C to 20°C, we observed the reformation of the same sample after cooling from a much higher temperature. In this second heating cycle, the sample was heated to T = 130°C to completely dissolve both the N_C phase and the gel network. The sample was held at this temperature for several minutes to ensure the homogeneity of the sample, as BHPB-6 undergoes a liquid-liquid phase separation before turning into a homogeneous sample [Chr16]. The sample was then cooled to T = 20°C and the orientation of the N_C phase and the gel network was checked. The results are shown in Figure 3.23.

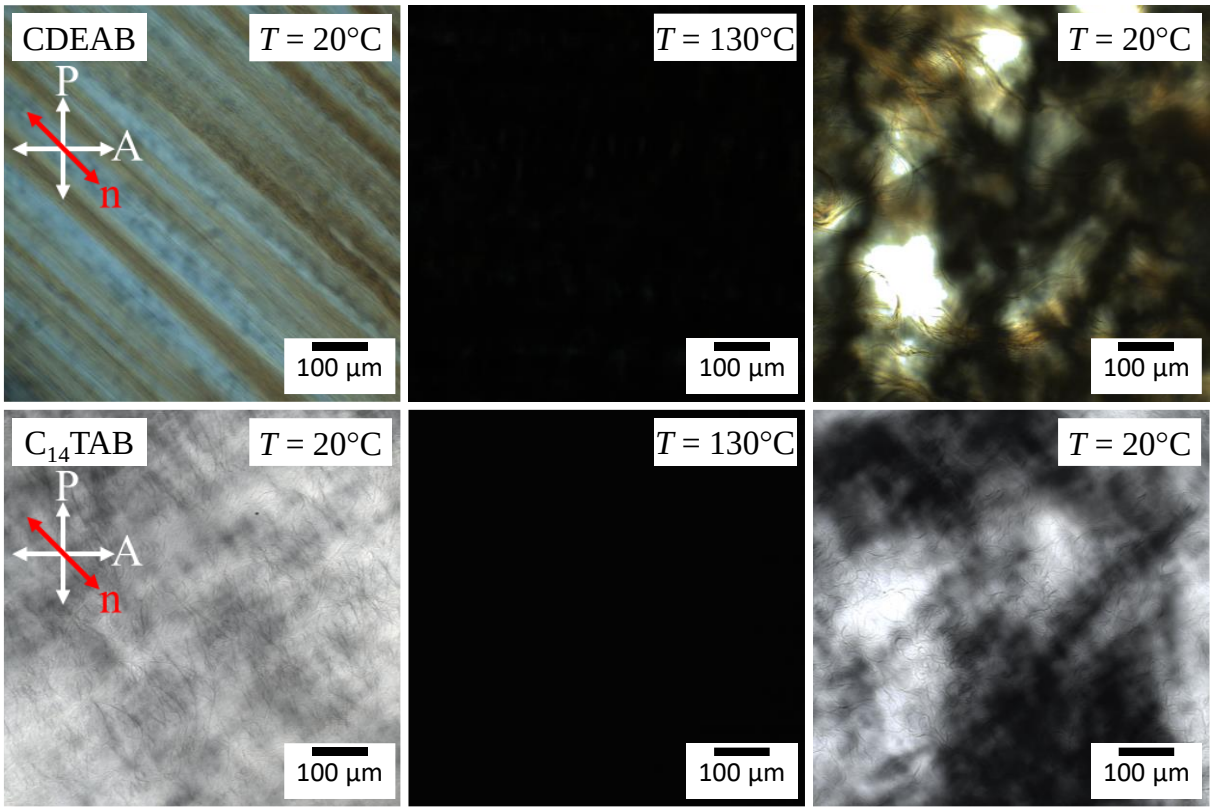

Figure 3.23: POM images of magnetically aligned samples of the binary CDEAB system gelled with 1.5 wt% BHPB-6 (top) and of the ternary C_{14}TAB system gelled with 1.0 wt% BHPB-6 (bottom) between crossed polarizers. Images were taken with the aligned director at a 45° angle relative to the polarizers. The aligned samples were heated from T_3 = 20°C to T_4 = 130°C causing a phase transition from the nematic N_C phase to the isotropic L_1 phase as well as a full dissolution of the gel network. The samples were then cooled to T_5 = 20°C where the N_C phase and the gel network formed without a preferred direction. The image was adapted from [Her25].

It can be seen that the N_C phase of both the binary CDEAB system and the ternary C_{14}TAB system was reformed after the second heating cycle. However, the previous orientation of the N_C phase is lost, as the image shows both bright and dark spots although the sample was completely bright before. Thus, without the aligned gel network the LLC forms multiple polydomains. Similarly, the gel fibers of the binary CDEAB system, visible in the bright spots of the sample, are not oriented as opposed to before. The gel fibers of the ternary C_{14}TAB system are not aligned either after the second heating cycle, having the same visual appearance as before the first heating cycle. The main indicator of alignment of at least some of the ternary C_{14}TAB system is its ability to act as a template for the N_C phase. Since the N_C phase was not uniformly oriented after the second heating cycle, we can assume that the gel network was not uniformly oriented either. Thus, we can conclude that for both systems, the gel network oriented by the magnetically oriented N_C phase is critical to the ability of the samples to reform the N_C

phase in an oriented manner outside of a magnetic field. If the gel network is thermally destroyed, the sample loses this "memory effect". We then changed our focus to the gel network and the changes it undergoes during the two heating cycles. To that end we observed the same samples under the microscope without the polarizers. The images are shown in Figure 3.24 and Figure 3.25, respectively.

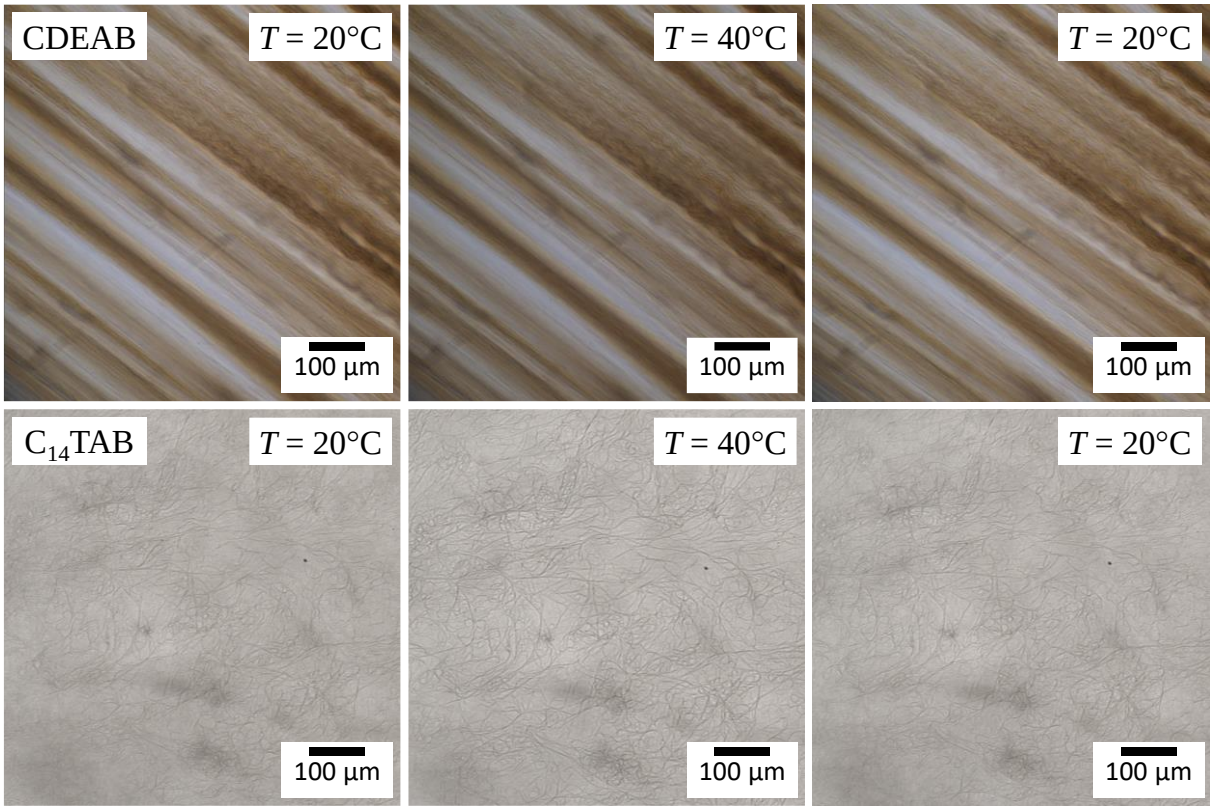

Figure 3.24: Microscopy images of magnetically aligned samples of the binary CDEAB system (top) and of the ternary C_{14}TAB system (bottom). The aligned samples were heated from T_1 = 20°C to T_2 = 40°C, which is above the nematic phase transition temperature but below the sol-gel transition temperature, before being cooled down again to T_3 = 20°C. The gel fibers showed no change after the first heating cycle and retained their original orientation. The image was adapted from [Her25].

It can be seen that there are no changes in the gel structure during the first heating cycle. If the aligned nematic gel is capable of acting as an actuator, as was our original goal, then changes in the LLC should induce changes in the gel structure. Since no changes were observed in this heating cycle, we can assume that the phase transition from the nematic N_C phase to the isotropic L_1 phase does not induce enough force to affect the gel fibers. In contrast to liquid crystal elastomers (LCEs) [Her22], where the liquid crystal is covalently bound to the gel network, our N_C phase is gelled with a low molecular weight gelator (LMWG) and is therefore not covalently bound to the gel network. Additionally, we observed the changes in the gel

network after a heating cycle to T = 130°C to see the gel growth without the guiding forces of the magnetically aligned N_C phase. The results are shown in Figure 3.25.

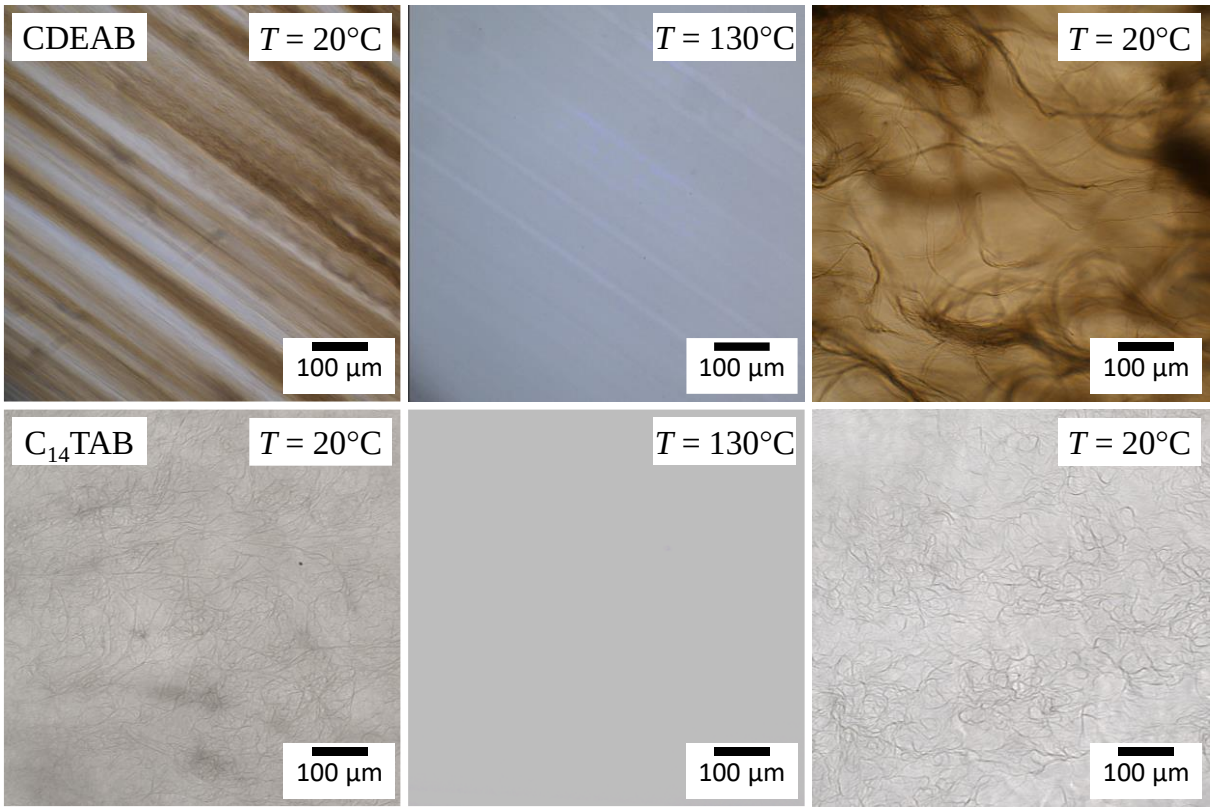

Figure 3.25: Microscopy images of magnetically aligned samples of the binary CDEAB system (top) and ofthe ternary C_{14}TAB system (bottom). The aligned samples were heated from T_3 = 20°C to T_4 = 130°C, which is above the nematic phase transition temperature and the sol-gel transition temperature, before being cooled down again to T_5 = 20°C. The image was adapted from [Her25].

In contrast to the first heating cycle, where no change was observed, the gel network is completely dissolved and reformed in the second heating cycle without the presence of an orienting magnetic field. This results in isotropic gel network formation, which is readily apparent in the case of the binary CDEAB system, where the gel network changes from visibly aligned parallel gel fibers to multiple clusters of fibers pointing in multiple directions. In the case of the ternary C_{14}TAB system the changes in the orientation of the gel network remain imperceptible. As previously described, the delayed formation of the N_C phase as well as the slow gel growth in the ternary C_{14}TAB system leads to the initial formation of an isotropic gel network even in the presence of a magnetic field. This in turn gives the aligned sample an unaligned appearance, although the gel network has a templating effect. After the second heating cycle, this templating effect is no longer present and the gel network is fully isotropic.

However, the appearance of the partially aligned gel network (bottom left) and the unaligned gel network (bottom right) remains virtually indistinguishable.

Conclusion

Firstly, we studied the orientation of the nematic LLC gels formed with two different systems. We used magnetic alignment for the orientation. To do this, we placed a small quantity of our gel samples in borosilicate capillaries, which were then flame-sealed and heated to homogenize them fully. The hot samples were placed in the magnetic field where they cooled to room temperature and remained for 24 hours. We then compared our aligned samples with unaligned samples under a microscope. The orientation of the nematic N_C phase can be determined by observing the sample between crossed polarizers, since the N_C phase is birefringent. For the unaligned samples, we observed the same amount of birefringence regardless of the position of the samples, which is indicative of multiple polydomains without a preferred orientation. For the magnetically aligned samples, however, we observed that the samples became much brighter when placed at an angle of 45° with respect to either polarizer, which confirms the successful alignment of both the binary CDEAB system and the ternary C_{14}TAB system. We also observed the orientation of the gel network by looking at the same samples without polarizers. For the unaligned samples, we observed isotropic gel growth with no clear direction for both systems. For the aligned samples, however, we observed visually a strong alignment in the case of the binary CDEAB system, and no alignment in the case of the ternary C_{14}TAB system. This difference is due to the delayed formation of the N_C phase. The N_C phase takes several hours to form, during which parts of the gel network can grow isotropically. Secondly, we investigated a possible memory effect of the gel network. We hypothesized that within an aligned gel network the reversible phase transition from the nematic N_C phase to the isotropic L_1 phase can be guided to restore the original orientation of the N_C phase. To test this, we heated both samples to $T = 40°C$ to induce the phase transition of the N_C phase before cooling them back down to $T = 20°C$. We followed the heating cycles under a microscope with crossed polarizers and found that the original orientation of the N_C phase was restored in both the binary CDEAB system, with its visibly aligned gel network, and the ternary C_{14}TAB system, with its apparently isotropic gel network. This shows that the gel networks formed under a magnetic field do indeed have a templating effect. Furthermore, in the case of the ternary C_{14}TAB system, the apparently unaligned gel network must have some orientation, otherwise it would not be able to orient the N_C phase. The gel network did not appear to change during this heating cycle.

When the samples were heated to T = 130°C the gel network was completely dissolved and the subsequent gel network and N_C phase were reformed in an unaligned manner.

4 Conclusion and Outlook

The scope of this work was to explore the possibility of using lyotropic liquid crystals (LLCs) gelled with low molecular weight gelators (LMWGs) as stimuli-responsive actuators. For this purpose, suitable LLCs had to be selected and an appropriate LMWG had to be chosen. We chose LLC systems with the calamitic nematic N_C phase as they are the best counterparts to the thermotropic liquid crystals used in liquid crystal elastomers (LCEs) that can function as actuators [Ohm11].

Firstly, we performed preliminary studies with two surfactant systems for which calamitic nematic N_C phases were reported, namely H_2O – *N*,*N*-dimethyl-*N*-ethyl-1-hexadecylammonium bromide (CDEAB) [Gör96, Sch15] and H_2O – *N*,*N*,*N*-trimethyl-1-tetradecylammonium bromide (C_{14}TAB) – *n*-decanol [Sau91]. We recorded the phase diagram of the ternary C_{14}TAB system to determine the surfactant-to-cosurfactant ratio σ at which the extension of the N_C phase is the largest. At σ = 0.93 a temperature dependent phase diagram was recorded to determine the ratio of total surfactant to water at which the system has the highest clearing temperature. Using polarized optical microscopy (POM) we found that in the case of the ternary C_{14}TAB system, the N_C phase forms at a total concentration of surfactant and cosurfactant of μ_{ter} = 33 - 37 wt% at T = 20°C, with the highest clearing temperature of T_{Cl} = 35°C observed at μ_{ter} = 35 wt%. For the CDEAB system both the ternary phase diagram [Gör96] and the temperature dependent binary phase diagram [Sch15] were already known. In the binary CDEAB system, the N_C phase forms at a surfactant concentration of μ_{bin} = 31 - 35 wt% at T = 20°C, with the highest clearing temperature of T_{Cl} = 28°C observed at μ_{ter} = 31 wt%. The concentration with the highest clearing temperature was then used for all subsequent studies. Three homologues of the gelator 3,5-bis-(5-hexylcarbamoyl-pentoxy)-benzoate acid *n*-alkyl ester (BHPB-*n*) with different chain lengths (*n* = 6, 10, 13) were tested for their gelling properties. Freeze fracture electron microscopy (FFEM) of the binary gel of each BHPB-*n* homologue with cyclohexane revealed different fiber structures. The fibers forming in the binary gel of BHPB-6 and cyclohexane are ribbons with widths of up to 100 nm and lengths of up to 1 µm. The ribbons tend to stack on top of each other. The fibers forming in the binary gel of BHPB-10 and cyclohexane have the shape hollow tubes with a diameter of ~30 nm, while those of BHPB-13 and cyclohexane are twisted ribbons. Rheology was performed on gels formed with the binary CDEAB system and the ternary C_{14}TAB system with each gelator homologue. Differences in the gel strength were observed between the binary CDEAB system, where the gels formed with BHPB-6 and BHPB-10 were the strongest, and

the ternary C_{14}TAB system, where the gel formed with BHPB-6 was the strongest. POM was used to verify the coexistence of the N_C phase and the gel network, as previous combinations of LLCs and different gelators led to phase transitions [Ste18]. No phase transitions into either the isoptropic L_1 phase or the hexagonal H_1 phase were observed, demonstrating the coexistence of both the Nc phase and the gel network. The gel network was then observed without polarizers, which showed that the gels formed with BHPB-6 and BHPB-10 were mostly homogeneous, while the gels formed with BHPB-13 had several areas with no gel network. Among the three gelators, BHPB-6 had the best properties and was therefore selected as the only gelator in the following studies.

Secondly, further rheological studies were performed with the LLC gels formed with BHPB-6 since there were multiple batches of BHPB-6. We compared our initial batch with two subsequent batches, named batch 1, batch 2 and batch 3, respectively. In a direct comparison of frequency sweeps, batch 1 performed best with the highest G' and G'' values. Batch 2 was the worst performing of all batches with significantly lower G' and G'' values than batch 1. Batch 3 performed slightly worse than batch 1 in the binary CDEAB system, but significantly worse in the ternary C_{14}TAB system. The evolution of the gel strength over 20 h was also tested with batch 2 and batch 3. For batch 2, a delay of 1-2 hours was observed before the gel network started to grow, while for batch 3 the gel network started to grow immediately. However, the final G' and G'' values were comparable. Due to the different properties of the batches, it was decided to perform further experiments with batch 3 only.

Thirdly, a more detailed study of the time-dependent evolution of gel network was performed. The evolution of the visual appearance of the binary CDEAB system and the ternary C_{14}TAB system was followed for 24 h. For the binary CDEAB system the sample remained completely clear within the first 24 h during gel network formation. For the C_{14}TAB system, on the other hand, the sample began to turn turbid several hours after preparation and became completely turbid within 24 h. The evolution of the gel strength was then followed in the same time frame using rheology, by letting heated samples gel in the rheometer (internally aged). Similar to their different visual appearance, the rheological data of the two systems varied significantly. The G' and G'' values of the binary CDEAB system start at a high value and increase only slightly over the course of 20 h, suggesting a rapid gel formation. For the C_{14}TAB system, the G' and G'' values start at much lower values and increase slowly over the course of 20 h. In addition, a plateau region was observed 2-3 h after the onset of the gelation. The evolution of the N_C phase was then followed using POM. For the binary CDEAB system, the N_C phase was formed

immediately after cooling below the clearing temperature. In the case of the ternary C_{14}TAB system, the N_C phase took much longer to form, with some birefringence visible after 1-3 h and taking up to 7-10 h to fully form. The delay in the formation of the N_C phase is attributed to the slow diffusion process of *n*-decanol into the N_C phase. As long as the *n*-decanol is not incorporated into the N_C phase, it serves as a good solvent for the gelator BHPB-6, which explains the slower formation of the gel network when compared to the binary CDEAB system.

The evolution of the gel was then observed over a longer time frame. Further visual changes in the aging samples of both systems were observed over the course of 32 d. For the binary CDEAB system, which remained completely clear after 24 h, the sample began to become turbid after 10-13 d, with complete turbidity occurring after 32 d. For the ternary C_{14}TAB sample, which was already turbid after 24 h, only a slight increase in turbidity was observed over the course of 32 d. Using rheology, samples aged for up to 14 d were measured. These samples were prepared outside of the rheometer, aged in vials for 1 to 14 d, and then placed on the rheometer (externally aged). The results obtained from the rheological measurements of the externally aged samples suggested that the aging time had no effect on the strength of the gel. However, this was due to the method used to prepare the samples. The externally aged samples experience strong destructive forces when removed from their vials and placed on the rheometer. The G' and G'' values obtained from these measurements were therefore reflections of the destroyed gel network. Notably, the G' and G'' values of the externally gelled binary CDEAB system were only slightly smaller than their internally gelled counterparts. For the ternary C_{14}TAB system, however, we observed a strong decrease in the G' and G'' values of the externally gelled samples compared to the internally gelled ones. The binary CDEAB system was less affected which is due to its higher plasticity as opposed to the more rigid gel network of the C_{14}TAB system. Freeze fracture electron microscopy (FFEM) was used to observe the differences in the gel fibers of new samples compared to those of aged samples. For the binary CDEAB system, a strong increase in the size of the fibers as well as large fiber stacks were observed. For the ternary C_{14}TAB system, the fresh and aged samples, respectively, showed no significant differences in their gel fibers.

Finally, the orientation of the two LLC systems was performed by magnetic field alignment. After the homogenization, the samples were cooled to room temperature and then stored for 24 h in a magnetic field. Observation of the samples using POM revealed a strong birefringence when the sample was placed at an angle of 45° with respect to either polarizer. This shows a strong degree of orientation in both the binary CDEAB system and the ternary C_{14}TAB system.

Observation of the gel network by regular microscopy revealed a strong alignment of the gel network in the binary CDEAB system, while the gel network of the ternary C_{14}TAB system had an unaligned appearance. The unaligned appearance of the gel network of the ternary C_{14}TAB system can be linked to the delayed formation of its N_C phase, which acts as a templating force in the magnetic field. Prior to the formation of the N_C phase, the gel network grows isotropically, and only starts to grow anisotropically after the formation of the N_C phase. The gel network thus has a partially aligned character with an unaligned appearance. Next, the ability of the gel network to act as a template in the absence of a magnetic field was tested. For this purpose, the N_C phase was heated to induce a phase transition to the isotropic L_1 phase and then cooled to reform the N_C phase. The samples were heated to T = 40°C, which induces the phase transition but does not melt the gel network. It was observed that after cooling back to T = 20°C, the N_C phases of both systems reformed with their previous orientation intact. This shows that the oriented gels formed by BHPB-6 in both systems are able to act as templates. The reformation of the N_C phase after heating to T = 130°C and cooling back to T = 20°C was also tested. In this case, the aligned gel network was completely dissolved at the beginning of the cooling process: the subsequently reformed N_C phase was not oriented and the reformed gel network grew isotropically.

To summarize, two LLCs possessing the nematic N_C phase were successfully gelled using the gelator BHPB-*n*. The coexistence of the nematic phase with the gel network was demonstrated and no adverse effects such as phase transitions were observed. Rheology was performed on gelled samples of the N_C phases using three homologues of BHPB-*n* with different chain lengths *n* (*n* = 6, 10, 13). Based on these data, BHPB-6 was chosen as the only gelator for the following experiments. The time evolution of the gel was followed by rheology and visual observation, and two different time periods for gel formation were found. An initial gel formation period that lasts for 20 h and a longer slower process, where the fibers coalesce into larger stacks, which can last up to several weeks. Magnetic field alignment was used to align the N_C phase and the gel network. The aligned gel network was successfully used to reorient the N_C phase after a reversible temperature-dependent phase transition into the L_1 phase.

For future experiments, the recording of phase diagrams in the presence of the gelator could be considered. For this study, we used only the phase diagrams without the gelators and checked whether the N_C phase was still intact after the formation of the gel network. However, it is known that some gelators can alter the phase boundaries of LLC systems [Ste18], and whether and to what extent BHPB-6 alters the phase boundaries is worth further investigating.

Additionally, the swelling response of the aligned LLC gels could be tested. Next to a phase transition induced by the addition of excess water into the N_C phase, the response of the aligned gel network should be studied. The alignment of the gel network could cause the swelling process to be likewise directed, whereas an unaligned gel sample would swell equally in all directions. Finally, the observed memory effect of the LLC gels should be investigated using different gelators with different properties. The gelator BHPB-6 forms relatively thick fibers and stacks compared to other low molecular weight gelators such as DBS and 12-HOA [Ste19a, Die19a]. Furthermore, smaller fibers such as those of DBS (8-18 nm) maybe better suitable for the creation of stimuli-responsive actuators.

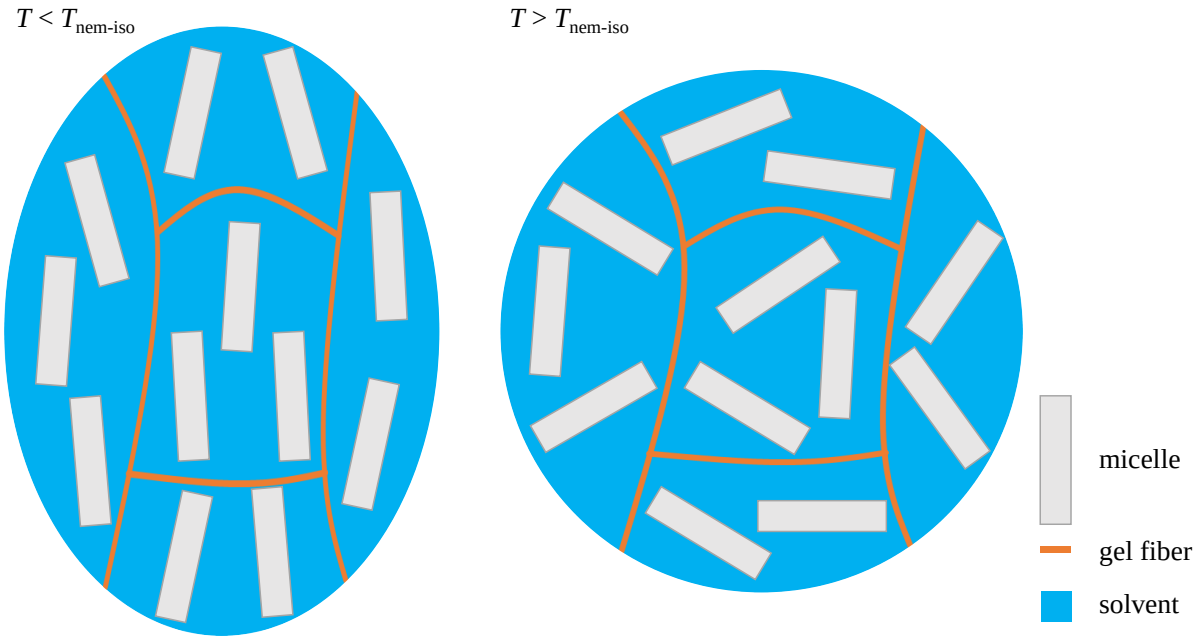

Figure 4.1: Possible actuation principle of lyotropic nematic gels. The fiber network self assembles in the aligned nematic N_C phase in a stretched conformation and the rod-like micelles are largely immobilized in the void between the fibers. Upon a phase-transition from the nematic N_C phase to the isotropic L_1 phase the differing orientation of the micelles could cause a macroscopic shape change in the fiber network.

In Figure 4.1 one can see the possible actuation principle of a nematic LLC gel. When a phase transition occurs from the aligned nematic N_C phase to the isotropic L_1 phase or back the gel fibers should move in conjunction with the orientation of the micelle. However, the fibers formed by BHPB-6 tend to form large stacks which are not very malleable, leading to them not being very suitable for actuation. On the other hand, gelators which form smaller fibers, such as DBS, may be able to be influenced by phase transitions in the LLC and work as an actuator.

5 Experimental

5.1 Chemicals and Sample Preparation

Chemicals

Table 5.1: Chemicals used in this study. The gelators BHPB-6 (batch 1 and batch 2), BHPB-10 and BHPB-13 were prepared by the group of Prof. Mésini following their procedure [Sim13]. Batch 3 of the gelator was synthesized by us following the same procedure.

Name	Abbreviation	Supplier	Purity
water	H_2O		bidistilled
n-decanol		Merck KgaA	≥ 99%
N,*N*-dimethyl-*N*-ethyl-1-hexadecylammonium bromide	CDEAB	Merck KgaA	98%
N,*N*,*N*-trimethyl-1-tetradecylammonium bromide	C_{14}TAB	Thermo Scientific	99%
cyclohexane		Merck KgaA	≥ 99.5%
3,5-bis-(5-hexylcarbamoyl-pentoxy)-benzoate acid hexyl ester	BHPB-6		n/a
3,5-bis-(5-hexylcarbamoyl-pentoxy)-benzoate acid decyl ester	BHPB-10		n/a
3,5-bis-(5-hexylcarbamoyl-pentoxy)-benzoate acid tridecyl ester	BHPB-13		n/a

Sample Preparation

We prepared three different kinds of samples, namely, binary gels of cyclohexane gelled by BHPB-*n*, the ungelled lyotropic liquid crystals and the lyotropic liquid crystals gelled by BHPB-*n*.

The lyotropic liquid crystal samples were prepared using the surfactant mass fraction μ. For the binary CDEAB system. the surfactant mass fraction μ is calculated according to

$$\mu_{\mathrm{bin}} = \frac{m_{\mathrm{surfactant}}}{m_{\mathrm{surfactant}} + m_{\mathrm{H_2O}}} \cdot 100\% = 31\%. \qquad (5.1)$$

For the ternary C_{14}TAB system the equation of the surfactant mass fraction μ_{ter} was modified to include the cosurfactant and is calculated according to

$$\mu_{\mathrm{ter}} = \frac{m_{\mathrm{surfactant}} + m_{\mathrm{cosurfactant}}}{m_{\mathrm{surfactant}} + m_{\mathrm{cosurfactant}} + m_{\mathrm{H_2O}}} \cdot 100\% = 35\%. \tag{5.2}$$

The surfactant-to-cosurfactant ratio σ was kept constant and is calculated according to

$$\sigma = \frac{m_{\mathrm{C_{14}TAB}}}{m_{\mathrm{C_{14}TAB}} + m_{n-\mathrm{decanol}}} = 0.93. \tag{5.3}$$

In gelled samples of the lyotropic liquid crystal and in the binary gel the gelator mass fraction η is calculated according to

$$\eta = \frac{m_{\mathrm{BHPB}-n}}{m_{\mathrm{total}}} \cdot 100\%. \tag{5.4}$$

In general, the samples were prepared by weighing in the individual components, to a total of 1 g, in a glass vial, which was then sealed with a screw cap. The screw cap was then additionally reinforced with Teflon tape to ensure that the vial remained closed during the heating process. The samples were then heated and shaken using a thermoshaker (Hettich MHR-23) until completely solubilized. In the case of the ungelled lyotropic liquid crystals, the sample was heated at 60°C for 45 minutes. The gelled lyotropic liquid crystal samples were heated to 130°C and held at this temperature until complete solubilization (10 min). The binary gels of cyclohexane and BHPB-*n* were heated to 80°C until completely solubilized (10 min).

5.2 Methods

Phase Diagram

A part of the ternary phase diagram of the system H_2O – *N*,*N*,*N*-trimethyl-1-tetradecylammonium bromide (C_{14}TAB) – *n*-decanol was obtained by visual observation of the birefringence of the sample in a temperature-controlled water bath. The temperature was controlled by a thermostat (Thermos Scientific DC30) and a thermometer. Visual changes were observed using two crossed polarizers and a lamp. Binary mixtures of the surfactant C_{14}TAB and water were prepared at surfactant mass concentrations of μ = 20-40 wt% and *n*-decanol was

slowly added. Phase boundaries were determined by observing changes in viscosity, in the case of the transition from the low viscosity calamitic nematic N_C phase to the high viscosity hexagonal H_1 phase, or turbidity, in the case of the transition from the clearer discotic nematic N_D phase to the turbid lamellar L_α phase [Her23]. The temperature dependent phase diagram at a constant surfactant-to-cosurfactant ratio of $\sigma = 0.93$ was recorded using polarized optical microscopy. Several samples with surfactant mass fractions of μ_{ter} = 28-38 wt% were heated from 20°C to 60°C to determine the phase boundaries. In the case of the transition from the nematic N_C phase to the isotropic L_1 phase, the phase transition was observed by a decrease in birefringence up to its complete disappearance. In the case of the transition from the N_C phase to the H_1 phase, the phase transition was characterized by a change in texture.

Rheology

Oscillating shear rheometry was performed using a Physica MCR 501 rheometer from Anton Paar with a plate-plate geometry, using a constant gap size of 1 mm, and an upper plate diameter of 25 mm. The lower stationary plate was thermostatted and the temperature was set at T = 20°C for all measurements. To perform the measurements, the upper plate was raised enough to place the sample (~0.8 g) on the lower plate, either by using a spatula for solid samples or by pouring for liquid samples. The upper plate was then lowered to the measuring position with a gap width of 1 mm. Depending on the measurement, the sample was also allowed to equilibrate for a certain amount of time before starting the measurement. In total three different types of measurements were performed.

Firstly, amplitude sweeps were performed to determine the linear viscoelastic (LVE) range. By slowly increasing the shear strain γ = 0.01-100%, typically 26 logarithmic steps, while applying a constant frequency ω, one obtains the LVE region and can determine the appropriate shear strain γ or shear stress τ for the subsequent frequency sweeps.

Secondly, frequency sweeps were performed using the shear strain γ or shear stress τ obtained from the amplitude sweeps. At constant shear strain γ or shear stress τ, the frequency ω was logarithmically decreased from 100 s^{-1} to 0.01 s^{-1}.

Finally, time-dependent measurements were performed at a constant frequency $\omega = 1\ s^{-1}$ and constant shear strain γ = 0.1% over 20 h.

For the amplitude sweeps and the frequency sweeps the already solid sample was placed between the two rheometer plates with a gap size of 1 mm and equilibrated for 2 h before starting the measurements. For the time-dependent measurements the sample was heated in a

thermoshaker to 90°C and poured onto the rheometer plate. The measurements were started immediately after.

Polarized Optical Microscopy

The optical properties e.g. birefringence of samples were observed using a Leica DMLP polarizing microscope. Samples were filled into borosilicate flat capillaries from Electron Microscopy Sciences with a wall thickness of 0.300 mm, with of 3.0 mm, height of 0.30 mm and varying lengths. The capillaries were flame-sealed and heated to 130°C for 10 minutes and the stored at room temperature for at least 1 day. Images were recorded using a Nikon D5300 camera. For the magnetically aligned samples an electromagnet (Bruker B-E 25v) with a magnetic field strength of 1.0 T was used.

Freeze Fracture Electron Microscopy

A small amount of the sample was placed between two copper grids, in a so-called sandwich, which was then plunged into liquid ethane cooled by liquid nitrogen. The samples were then transferred into liquid nitrogen, fractured and transferred into the vacuum chamber of the Leica EM BAF060 freeze fracture and etching system. The fractured samples were subsequently covered first by a layer of Pt/C with a thickness of ~2 nm at an angle of 45° and second by pure Carbon with a thickness of ~ 20 nm at an angle of 90°. These replicas were cleaned using acetone and ethanol and dried. Images of the replicas were recorded using an EM10 transmission electron microscope from Zeiss at 60 kV.

6 References

[Alm93] K. Almdal, J. Dyre, S. Hvidt, O. Kramer, *Poly. Gels Netw.* **1993**, *1*, 5-17.

[And18] J. L. Andrews, E. Pearson, D. S. Yufit, J. W. Steed, K. Edkins, *Cryst. Growth Des.*, **2018**, *18*, 7690-7700.

[Bal69] R. R. Balmbra, J. S. Clunie, J. F. Goodman, *Nature*, **1969,** *222*, 1159-1160.

[Bar15] A. Baral, S. Basak, K. Basu, A. Dehsorkhi, I. W. Hamley, A. Banerjee, *Soft Matter*, **2015**, *11*, 4944-4951.

[Bri09] A. M. Brizard, M. C. A. Stuart and J. H. van Esch, *Faraday Discuss*., **2009**, *143*, 345–357.

[Chr16] E. Christ, C. Blanc, A. A. Ouahabi, D. Maurin, R. L. Parc, J.-L. Bantignies, J.-M. Guenet, D. Collin, P. J. Mésini, *Langmuir*, **2016**, *32*, 4975-4982.

[Dia05] N. Díaz, F. X. Simon, M. Schmutz, M. Rawiso, G. Decher, J. Jestin, P. J. Mésini, *Angew. Chem. Int. Ed*., **2005**, *44*, 3260-3264.

[Dia15] S. Díaz-Oltra, C. Berdugo, J. F. Miravet, B. Escuder, *New J. Chem*., **2015**, *39*, 3785-3791.

[Die19a] S. Dieterich, T. Sottmann, F. Gießelmann, *Langmuir*, **2019**, *35*, 16793-16802.

[Die19b] I. Dierking, Polymer-modified Liquid Crystals. Royal Society of Chemistry, Cambridge, 2019, 1-16.

[Die20b] S. Dieterich, S. Prévost, C. Dargel, T. Sottmann, F. Gießelmann, *Soft Matter*, **2020**, *16*, 10268-10279.

[Die21] S. Dieterich, F. Stemmler, N. Preisig, F. Gießelmann, *Adv. Mater.*, **2021**, *33*, 2007340.

[DiL19] G. A. DiLisi, An Introduction to Liquid Crystals (Ed.: J. J. DeLuca), Morgan & Claypool, San Rafael, 2019.

[Dja16] M. Djabourov, K. Bouchemal, Disordered Pharmaceutical Materials, Polymer Gels, Hydrogels, and Scaffolds, (Eds.: M. Descamps), Wiley-VCH, Weinheim, 2016, 241-282.

[Dom24] M. Dombrowski, M. Herbst, N. Preisig, F. Giesselmann, C. Stubenrauch, *Gels*, **2024**, *10*, 261.

[Dra15] E. R. Draper, T. O. McDonald, D. J. Adams, *Chem. Commun.*, **2015**, *51*, 6595-6597.

[Dra17] E. R. Draper, D. J. Adams, *Chem*, **2017**, *3*, 390–410.

[Du15] X. Du, J. Zhou, J. Shi, B. Xu, *Chem. Rev.*, **2015**, *115*, 13165−13307.

[Dut17] S. Dutt, P. F. Siril, S. Remita, *RSC Adv.*, **2017**, *7*, 5733-5750.

[Fer80] J. D. Ferry, Viscoelastic Properties of Polymers, John Wiley & Sons, 1980, 486-544.

[Flo74] P. J. Flory, *Faraday Discuss. Chem. Soc.*, **1974**, *57*, 7-18.

[Gör96] C. Görgens, Dissertation, **1996**, University of Dresden.

[Hen84] Y. Hendrikx, J. Charvolin, M. J. Rawiso, *Colloid Interface Sci.*, **1984**, *100*, 597-600.

[Her22] K. M. Herbert, H. E. Fowler, J. M. McCracken, K. R. Schlafmann, J. A. Koch, T. J. White, *Nature Reviews Materials*, **2022**, *7*, 23-38.

[Her23] M. Herbst, M. Dombrowski, N. Preisig, S. Dieterich, F. Gießelmann, P. Mésini, C. Stubenrauch, *Liq. Cryst.*, **2023**, *50*, 1090-1100.

[Her25] M. Herbst, M. Dombrowski, C. Stubenrauch, F. Gießelmann, submitted.

[Hof05] H. Hofmeier, U. S. Schubert, *Chem. Commun.*, **2005**, 2423–2432.

[Hu14] X. Hu, T. Xiao, C. Lin, F. Huang, L. Wang, *Acc. Chem. Res.* **2014**, *47*, 2041-2051.

[Ily17] M. Ilyas, Md. Anamul Haque, Y. Yue, T. Kurokawa, T. Nakajima, T. Nonoyama, J. P. Gong, *Macromolecules*, **2017**, *50 (20)*, 8169-8177.

[Isr76] J. N. Israelachvili, D. J. Mitchell, B. W. Ninham, *J. Chem. Soc., Faraday Trans. 2, 1976, 72*, 1525-1568.

[Kum14] D. K. Kumar, J. W. Steed, *Chem. Soc. Rev.* **2014**, *43*, 2080-2088.

[Lai89] P. E. Laibinis, J. J. Hickman, M. S. Wrighton, G. M. Whitesides, *Science*, **1989**, *245*, 845-847.

[Lau15] M. Laupheimer, N. Preisig and C. Stubenrauch, *Colloids Surf. A: Physicochem. Eng. Asp.*, **2015**, *469*, 315–325.

[Mez06] T. G. Mezger, The Rheology Handbook 2nd Edition, Vincentz Network, Hannover, 2006.

[Moh03] S. Mohanty, *Resonance*, **2003**, *8 (11)*, 52-70.

[Net05] A. M. Figueiredo Neto, S. R. A. Salinas, The Physics of Lyotropic Liquid Crystals, Phase Transitions and Structural Properties, Oxford, New York, 2005, 1-68.

[Ohm11] C. Ohm, N. Kapernaum, D. Nonnenmacher, F. Gießelmann, C. Serra, R. Zentel, *J. Am. Chem. Soc.*, **2011**, *133*, 5305 – 5311.

[San10] P. S. Santos, M. G. Abiad, M. A. Carignano, O. H. Campanella, *Rheol Acta*, **2012**, *51*, 3–11.

[Sau91] A. Saupe, S. Plumley, Y. K. Zhu, P. Photinos, *Physica A: Statistical Mechanics and its Applications*, **1991**, *174*, 195-207.

[Sch15] F. Schörg, Dissertation, **2015**, University of Stuttgart.

[Sim13] F. X. Simon, T. T. T. Nguyen, N. Díaz, M. Schmutz, B. Demé, J. Jestin, J. Combet, P. J. Mésini, *Soft Matter*, **2013**, *9*, 8483-8493.

[Smi24] D. K. Smith, *Soft Matter*, **2024**, *20*, 10-70.

[Ste18] K. Steck, C. Schmidt, C. Stubenrauch, *Gels*, **2018**, *4*, 78.

[Ste19a] K. Steck, C. Stubenrauch, *Langmuir*, **2019**, *35*, 17132-17141.

[Ste19b] K. Steck, N. Preisig, C. Stubenrauch, *Langmuir*, **2019**, *35*, 17142-17149.

[Ste20] K. Steck, S. Dieterich, C. Stubenrauch, F. Gießelmann, *J. Mater. Chem. C*, **2020**, *8*, 5335-5348.

[Stu16] C. Stubenrauch, F. Gießelmann, *Angew. Chem. Int. Ed.* **2016**, *55*, 3268-3275.

[Tan16] F. Tantakitti, J. Boekhoven, X. Wang, R. V. Kazantsev, T. Yu, J. Li, E. Zhuang, R. Zandi, J. H. Ortony, C. J. Newcomb, L. C. Palmer, G. S. Shekhawat, M. Olvera de la Cruz, G. C. Schatz, S. I. Stupp, *Nature Mater*, **2016**, *15*, 469-476.

[Wan10] H. Wang, C. Ren, Z. Song, L. Wang, X. Chen, Z. Yang, *Nanotechnology*, **2010**, *21*, 225606.

[Wie06] R. G. Weiss, P. Terech, Molecular Gels, Materials with Self-Assembled Fibrillar Networks (Eds.: R. G. Weiss, P. Terech), Springer, Dordrecht, 2006, 1- 13.

[www01] https://wiki.anton-paar.com/en/basics-of-rheology/#viscoelastic-behavior (12.11.2024)

[www02] https://www.degruyter.com/document/doi/10.1515/cti-2022-0010/html (12.11.2024)

[Xu12] Y. Xu, C. Kang, Y. Chen, Z. Bian, X. Qiu, L. Gao, Q. Meng, *Chem. Eur. J.*, **2012**, *18*, 16955- 16961.

[Xu15] Y. Xu, M. Laupheimer, N. Preisig, T. Sottmann, C. Schmidt, C. Stubenrauch, *Langmuir*, **2015**, *31*, 8589-8598.

[Yil23] S. Yilmazer, D. Schwaller, P. J. Mésini, *Gels*, **2023**, *9*, 273.

[Zha18] J. Zhang, Y. Hu, Y. Li, Gel Chemistry Interactions, Structures and Properties, Springer, Singapore, 2018, 1-51.

Declaration of Authorship

I hereby certify that the dissertation entitled

Rheological Studies, Time Dependency and Orientation of Nematic Lyotropic Liquid Crystal Gels

is entirely my own work except where otherwise indicated. Passages and ideas from other sources have been clearly indicated.

Name: Max Dombrowski

Signed: 

Date: 27.05.2025

Curriculum Vitae

Max Dombrowski

born 14th June 1996 in Rosenheim, Germany

Education

Since 2021	PhD student at the University of Stuttgart
	Topic: "Rheological Properties and Thermo-mechanical Response of Lyotropic Liquid Crystal Gels"
2018-2020	M.Sc Chemistry at the University of Regensburg
	Thesis title: "Solubilization of the novel UV-filter Cyclohexenyliden Ethoxyethylcyanoacetate (S87)"
2015-2018	B.Sc Chemistry at the University of Regensburg
	Thesis title: "Synthesis and Characterization of Supramolecular aggregates containing Pn-ligand complexes, coinage metals and organic linkers"
2007-2015	Karolinen-Gymnasium Rosenheim, Rosenheim Germany
	General Higher Qualification for University Entrance